



The Hebrew University of Jerusalem  
Faculty of Science  
Racah Institute of Physics

# Hybrid Logical-Physical Qubit Interaction for Quantum Metrology

אינטראקציה היברידית לוגית-פיזית עבור  
חישה קוונטית

**Nadav Carmel**

Thesis submitted in partial fulfillment of the requirements  
for the Master of Sciences degree  
in Physics

Under the supervision of **Prof. Nadav Katz**

**August 2021**



האוניברסיטה העברית בירושלים  
הפקולטה למתמטיקה ולמדעי הטבע  
מכון רקח

## Hybrid Logical-Physical Qubit Interaction for Quantum Metrology

אינטראקציה היברידית לוגית-פיזית עבור  
חישה קוונטית

מוגש על ידי  
נדב כרמל

עבודת גמר לתואר מוסמך בפיזיקה

עבודה זו הונחתה על ידי  
פרופ' נדב כץ

אלול, ה'תשפ"א

# תקציר

השימוש במערכות קוונטיות עבור חישוב קוונטי וחישה קוונטית הוא תחום מחקר יחסית חדש. מדידת אופרטורים היא התכלית של תיאוריה שנקראת חישה קוונטית, שהוקрат את היכולת שלנו להשתמש במערכות קוונטיות למטרות חישה מדוקפת.

מחשב קוונטי מורכב מביטים קוונטיים (קיובייטים), מערכות בעלות שתי רמות אנרגיה שניתן לשאור ולתפעל לפי רצונו וכאן מאפשרות את ההרצה של אלגוריתמים מורכבים. משפהה של אלגוריתמים שימושים אותן למטרות חישה קוונטיות נקבעת הערכת פאזה קוונטית, והיא מאפשרת את המדידה של ערך עצמי של אופרטור בהינתן המצב העצמי המתאים.

בעזרת גרסאות איטרטיביות של הערכת פאזה קוונטית, ניתן למדוד בדיק ארביטרاري את הערך העצמי המדובר, לפחות בתיאוריה. אך בעולם האמתי ישנן שגיאות (מדידה, שגיאות בשערים, או שגיאות שנובעות מחשיאה של הקיובייטים לעולם החיצון) שמכבילות את היכולת שלנו למדוד ערכים בדיק גבוה. תיקון שגיאות קוונטי הוא תחום של מחשב קוונטי (תחום מדעי המחשב) שספק שיטות כלליות להתגבר על שגיאות ורעים, ממש כמו תיקון שגיאות במחשבים קלאסיים. משפט הסוף עבור חישוב קוונטי מצין שבבhinתן שהרעיון בשערים קוונטיים הוא מתחתי לשף מסוים, ניתן לבצע ביעילות חישובים גדולים כרצוננו במחשב קוונטי בעזרת שיטות חישוב עמידות לשגיאות. הרעיון של שיטות חישוב עמידות אלה הוא לעצב שערים בצורה

כזו שומרת את המצב הקונטני בקוד, וגם מבטיחה שם קرتה לכל היותר שגיאת אחת בהפעלת שער, אז יהיה לכל היותר קיוביט אחד שיש בו שגיאה בסוף החישוב, אפילו אם השער יוצר שגיאה.

בחירה-בדיעבד היא שיטה נוספת המשמשת להתרמודדות עם שגיאות בחישוב קוונטי, שבה אני בוחרים בדיעבד את המידע שמתאים לציפויו שלנו.

במחקר זה אנחנו מציגים רעיונות חדשים שימושיים את התהומות של חישה קוונטיות, תיקון שגיאות קוונטי ובחירה-בדיעבד, בנסיבות רעש חיצוני, ע"י שימוש בקוד חמוץ הקיובייטים, שהוא הקוד הכי קטן שמאפשר תיקון של כל סוג של שגיאות:

- אנחנו מציגים אלגוריתם הערכת פאזה איטרטיבי חדש, שמאפשר מדיודה של מספר ספרות בכל איטרציה. האלגוריתם הזה הוא למעשה מעשה הכללה של אלגוריתם קיים.
- אנחנו חוקרים ומסבירים איך בבחירה-בדיעבד על החישון יכולה להועיל למטרות חישה קוונטיות באlgorigitmic הערכת פאזה.
- אנחנו מגדירים את הקונספט שלבחירה-בדיעבד לוגית, ומספקים פיתוח תיאורטי שסביר את התפקיד שלו נגד שגיאות כלליות.
- אנחנו מגדירים תכוונה של קודים קוונטיים לתקן שגיאות שמאפשרת את האינטראקציה בין קיובייטים משכבות שונות, ומוצאים את הנسبות הכלליות שבין האינטראקציה כזו לנוכנת יתרון.
- לבסוף, אנחנו מדגימים את השימוש בבחירה-בדיעבד לוגית עבור שני אלגוריתמים של הערכת פאזה קוונטי, ומוסיפים את הסף הרלוונטי שבו השימוש בשיטה הנ"ל משפר את התוצאות.

# Abstract

The use of quantum systems for quantum computing and quantum sensing is a relatively new area of research, both theoretically and experimentally. Measuring an operator is the purpose of a theory called Quantum Sensing, exploring our ability of using quantum systems for accurate sensing.

A quantum computer is made of quantum bits (qubits), two-level quantum systems that can be controlled and entangled at will, and thus can perform algorithms. One family of algorithms used for quantum sensing is called Quantum Phase Estimation (QPE), enabling the measurement of an eigenvalue of an operator, given it's corresponding eigenstate.

The eigenvalue can, in theory, be measured to arbitrary accuracy using a small number of qubits, with iterative versions of QPE. But in the real world, there are errors (measurement errors, gate errors, qubit decoherence...) limiting our ability of precise measurement. Quantum Error Correction (QEC) is a field of quantum computing (computer science) that gives general methods for overcoming errors and noise, much like the classical field of error correction in classical computers. The threshold theorem for quantum computations states that provided the noise in individual quantum gates is below a certain constant threshold it is possible to

efficiently perform an arbitrarily large quantum computation using methods of fault tolerance quantum computation. The idea of fault-tolerant quantum computation is to design the gates acted on the quantum state, in a way that keeps the state in the code and assures that if one error occurred in the process of applying the gate, then we have at most one faulty qubit in each code block at the end, even if the gate creates entanglement.

Post selection is another technique used for coping with errors, in which we choose to work only with the portion of the data that fits our expectations.

In this work we present some new ideas in the field of quantum sensing, quantum error correction and post selection, in the presence of T1,T2 qubit relaxation, using the five-qubit code (the smallest error correcting code):

- We present a new QPE algorithm, which is a generalization of IPEA, enabling the measurement of more than one digit in each iteration.
- We explore and explain how Sensor Post Selection (SPS) may be effective for quantum sensing with QPE algorithms.
- We define the notion of Logical Post Selection (LPS) and give theoretical derivation of it's advantage against the depolarizing channel.
- We define a property of quantum codes enabling an interaction between qubits of different logical layers, and find under which circumstances it gives an advantage.
- Finally, we demonstrate the use of logical ancilla and physical sensor qubits for QPE and find the relevant threshold for quantum sensing.

# Acknowledgements

This work has been a most meaningful experience for me in the last year - a journey of self-revelation, development as a researcher and as a person. I owe the success of that journey to quite a few people, primarily of course to my advisor, Prof. Nadav Katz. Growing up, asked who is a role-model for me, I always had a hard time finding the right people to answer that definition. Over the years I have gathered a small collection of individuals who can be role models for me, and Nadav is definitely one of them. In my initial acquaintance with Nadav, I was amazed at how much a person can be professional in his field. Nadav is a physicist with very broad knowledge, sharp intuition and plenty of interesting ideas. In time I got to know him better, and I saw a man who was not only full of passion for research, but also for practical work - his investment in the development of the quantum field at the Hebrew University and in Israel has served as an example for a person who cares, on a large scale. Most of all I enjoyed the conversations with Nadav at the meta level, as he instilled in me motivation and explained to me the true meaning of being a researcher. In addition to being a professional, caring and passionate person, he is also an excellent teacher, always looking for opportunities to enrich his students and broaden their knowledge and understanding. I thank him

mainly for actively developing my research abilities, which will definitely serve me in the future.

I also wish to thank Prof. Michael Ben-Or for his help in understanding the field of quantum error correction, and to Dr. Tuvia Gefen for two fruitful discussions on quantum sensing.

I'd like to thank my friends from Talpiot, helping me to continue through a lot of struggles and reminding me about passion and hard work.

My commanding officers from the program over the years had a large influence on me, pushing me towards being a researcher. I'd especially like to thank two of them, to Omer Deutsch who fought to give me the appropriate conditions to carry out my research and to Daniel Yaron, my personal commanding officer over the last year, who was very understanding and cared a lot of my improvement as a researcher and as a person.

# Contents

<b>1</b>	<b>Introduction</b>	<b>1</b>
1.1	Wait, But What Is A Qubit? . . . . .	1
1.1.1	The Bloch Sphere . . . . .	2
1.1.2	Quamtum Gates . . . . .	3
1.1.3	Physical Implementations . . . . .	6
1.2	Quantum Noise . . . . .	8
1.2.1	Shot Noise . . . . .	8
1.2.2	Decoherence . . . . .	9
1.3	Distance Measures for Quantum Information . . . . .	12
1.4	Quamtum Sensing . . . . .	14
1.4.1	The Quamtum Sensing Protocol . . . . .	15
1.4.2	Fisher Information & Quantum Cramer Rao Bound .	19
1.4.3	Algorithmic Quantum Sensing . . . . .	22
1.5	Quantum Error Correction . . . . .	29
1.5.1	Stabilizer Formalism . . . . .	29

1.5.2	Fault-Tolerant Quantum Computation . . . . .	31
1.5.3	Quantum Error Correction for Quantum Metrology .	34
<b>2</b>	<b>Research Question</b>	<b>35</b>
<b>3</b>	<b>Methods &amp; Theoretical Derivations</b>	<b>37</b>
3.1	n-Iterative Phase Estimation Algorithm . . . . .	37
3.2	The Simulation . . . . .	38
3.2.1	Gate-Based Evolution . . . . .	41
3.2.2	Krauss-Based Decoherence . . . . .	41
3.2.3	Measurements . . . . .	43
3.3	Sensor Post Selection . . . . .	45
3.3.1	The Potential of Sensor Post Selection . . . . .	45
3.3.2	SPS Simulation Methods . . . . .	46
3.4	Logical Post Selection . . . . .	48
3.4.1	Scaling of the Error Probability . . . . .	50
3.4.2	Hybrid Logical-Physical Entanglement . . . . .	52
3.5	Logical Post Selection for Quantum Metrology . . . . .	56
3.5.1	Gate Implementations . . . . .	56
3.5.2	LPS Simulation Methods . . . . .	62
3.6	Measurement Errors . . . . .	67
<b>4</b>	<b>Results</b>	<b>68</b>
4.1	Sanity Checks for the Simulation . . . . .	68

<i>CONTENTS</i>	ix
4.1.1 $T_1$ & $T_2$ Extractions . . . . .	68
4.1.2 Ramsey Experiment . . . . .	70
4.1.3 From Decoherence to Gate Fidelity . . . . .	71
4.2 Sensor Post Selection for Quantum Sensing . . . . .	72
4.2.1 Target: Accuracy . . . . .	72
4.2.2 Resource: Minimal Number of Trials . . . . .	73
4.3 Logical-Physical Interaction - General Numeric Exploration	75
4.4 Logical Post Selection for Quantum Metrology . . . . .	80
4.4.1 Gate Selection . . . . .	80
4.4.2 Kitaev's Approach - with Accelerated Hamiltonians .	83
4.4.3 IPEA - without Accelerated Hamiltonians . . . . .	89
<b>5 Conclusion &amp; Outlook</b>	<b>93</b>
<b>A Code Guide</b>	<b>95</b>
A.1 About . . . . .	95
A.2 Installation . . . . .	95
A.2.1 required packages . . . . .	95
A.2.2 Download . . . . .	96
A.3 The Simulators . . . . .	96
A.3.1 Creating a Quantum Register . . . . .	97
A.3.2 Simulating a Quantum Circuit . . . . .	100
A.3.3 Visualizing The State History of a Qubit . . . . .	101

# List of Figures

1.1	Bloch Sphere Representation of a Qubit . . . . .	2
1.2	Basic Gates on Bloch Sphere . . . . .	4
1.3	Frequently Used Gates . . . . .	5
1.4	Models of Closed and Open Quantum Systems . . . . .	9
1.5	Basic Steps of Quantum Sensing . . . . .	17
1.6	Standard Quantum Phase Estimation . . . . .	24
1.7	AQFT Implementation . . . . .	25
1.8	Iterative Phase Estimation Algorithm . . . . .	26
1.9	Kitaev's Iterative Quantum Phase Estimation . . . . .	28
1.10	CZ Gadget . . . . .	33
3.1	n-Iterative Phase Estimation Algorithm . . . . .	37
3.2	General Circuit Simulation . . . . .	39
3.3	SPS Simulations - Circuit-Level . . . . .	47
3.4	Logical-Physical Entangling Gate for the 5-Qubit Code . . . . .	54
3.5	Logical State Preparation . . . . .	58

*LIST OF FIGURES* xi

3.6	Logical Hadamard . . . . .	58
3.7	Logically Controlled Rotation . . . . .	59
3.8	Logical-Physical Entangling Gate for Quantum Sensing . . .	59
3.9	Logical $R_z(\theta)$ Rotation . . . . .	60
3.10	Syndrome Extraction Circuits . . . . .	61
4.1	Verifying Decoherence . . . . .	69
4.2	Ramsey with Dephasing . . . . .	70
4.3	Map from $T_1, T_2$ to gate fidelity . . . . .	71
4.4	SPS for Accuracy . . . . .	73
4.5	SPS for Minimal Number of Trials . . . . .	74
4.6	Logical-Physical Entanglement with Constant Gate Fidelity	77
4.7	Logical-Physical Entanglement with Constant Circuit Depth	78
4.8	Logical-Physical Entanglement . . . . .	79
4.9	Gate Selection for State Preparation . . . . .	82
4.10	LPS for Accuracy . . . . .	84
4.11	LPS for Minimal Number of Trials . . . . .	86
4.12	Confirming Error Probability Scaling . . . . .	88
4.13	IPEA - Good Sensor Noisy Ancilla . . . . .	91
4.14	IPEA - Dephasing Sensor $ +\rangle$ Good Ancilla . . . . .	91
4.15	IPEA - Relaxing Sensor $ +\rangle$ Good Ancilla . . . . .	92
4.16	IPEA - Relaxing Sensor $ 1\rangle$ Good Ancilla . . . . .	92

A.1	The Bell State . . . . .	101
A.2	Verifying Decoherence . . . . .	105
A.3	All Defined Gates . . . . .	107

# List of Tables

1.1	Generator Table for the 5-Qubit Code . . . . .	32
1.2	Recovery Table for the 5-Qubit Code . . . . .	32
3.1	Gate-Hamiltonian for Simulation . . . . .	41
3.2	Logical Post Selection - Error Probability Scaling . . . . .	52
4.1	Thresholds Accelerated Hamiltonian . . . . .	85
4.2	Assumptions for IPEA . . . . .	90

# 1 Introduction

## 1.1 Wait, But What Is A Qubit?

The *bit* is the fundamental unit of classical information. It can be in one of two states - 0 or 1. The bit can be thought of as a pure mathematical concept, and it has numerous physical realizations, usually two distinct values of voltage, current, light intensity, magnetization or polarization, etc. Quantum information theory is built upon an analogous fundamental unit - the *qubit*.

In this section we introduce the concept of a qubit, discuss its mathematical properties and give examples for a few of its physical implementations.

In contrast with the bit which has to be in one of its two states, a qubit can be in a normalized complex superposition of the states:

$$|\psi\rangle = \alpha|0\rangle + \beta|1\rangle$$

With  $\alpha, \beta \in \mathbb{C}$ ,  $|\alpha|^2 + |\beta|^2 = 1$ . However, when we 'read' (measure) the qubit we can read only one of our two computational basis states -  $|0\rangle$  with probability  $|\alpha|^2$  and  $|1\rangle$  with probability  $|\beta|^2$ . Thus if we have a global phase  $e^{i\theta}$  multiplying the state, it has no physical measurable effect.

### 1.1.1 The Bloch Sphere

One particularly useful way to think of qubits is the following geometrical interpretation: The qubit's has two degrees of freedom, and thus it can be represented as a point and a unit sphere:

$$|\psi\rangle = \cos \frac{\theta}{2} |0\rangle + e^{i\varphi} \sin \frac{\theta}{2} |1\rangle$$

Up to a global phase.

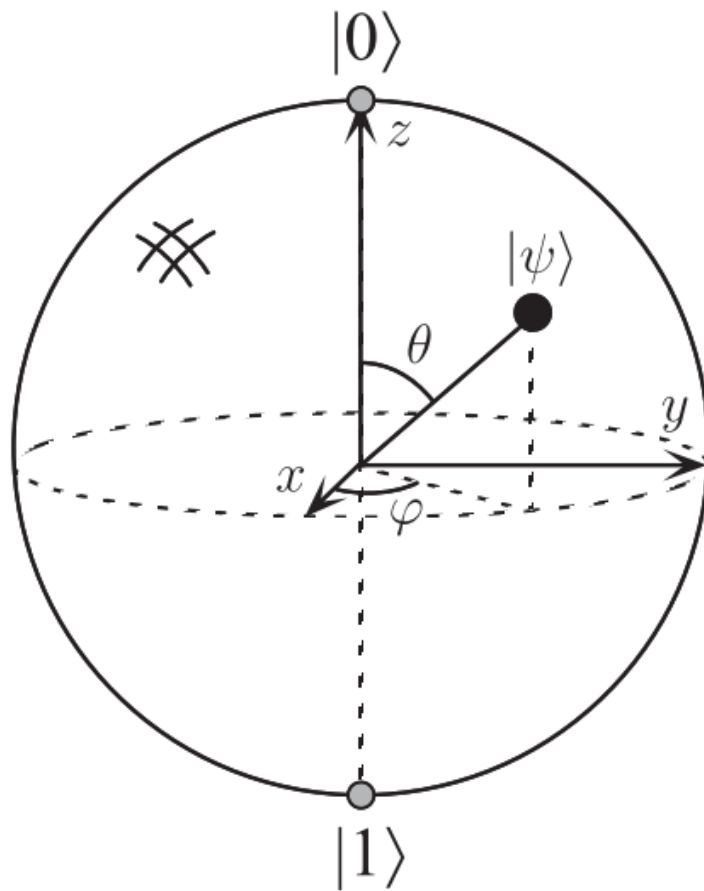


Figure 1.1: Bloch sphere representation of a qubit.

We can also represent the density matrix  $\rho$  as a function of the point it creates on Bloch sphere:

$$\rho = \frac{I + \vec{r} \cdot \vec{\sigma}}{2} = \frac{1}{2} \begin{bmatrix} 1 + r_z & r_x - ir_y \\ r_x + ir_y & 1 - r_z \end{bmatrix}$$

### 1.1.2 Quantum Gates

In perfect analogy to the classical logic gates, there are quantum logic gates. While the only classical single bit gate is the NOT gate, there are a continuum of single qubit gates moving the qubit from one point on the Bloch sphere to another. This is true for two qubit gates as well, and in this section we introduce the most frequently used quantum gates. All frequently used gates are defined in figure 1.3.

In addition to the defined gates of figure 1.3 we define the useful gates

$$R_x(\theta) = e^{-i\frac{\theta}{2}\sigma_x}, R_y(\theta) = e^{-i\frac{\theta}{2}\sigma_y}, R_z(\theta) = e^{-i\frac{\theta}{2}\sigma_z} \quad (1.1)$$

They are particularly useful since all single qubit gates can be described as rotations on the Bloch sphere. Bloch Representation of some of them are in figure 1.2.

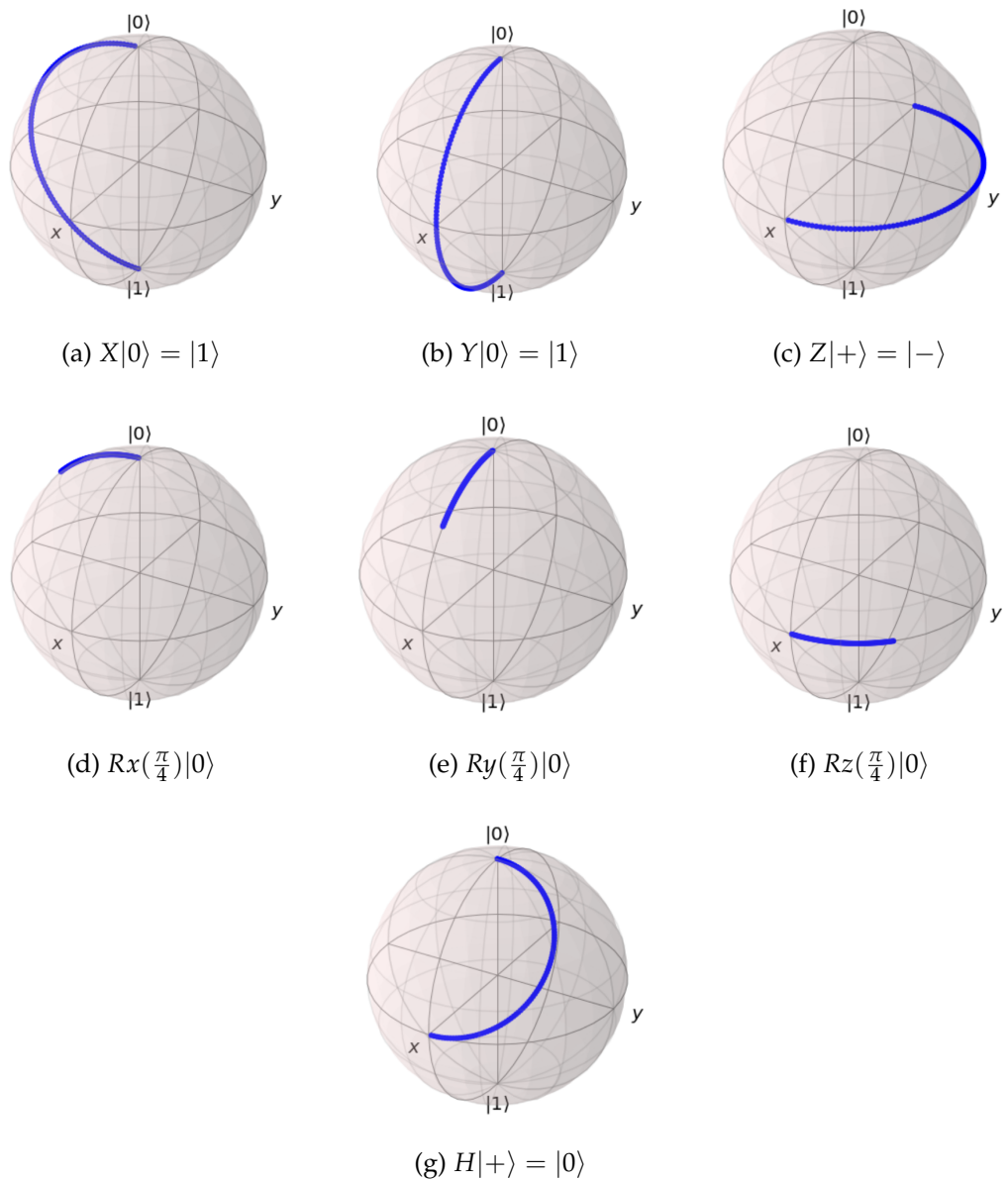


Figure 1.2: Basic gates on Bloch sphere

Hadamard		$\frac{1}{\sqrt{2}} \begin{bmatrix} 1 & 1 \\ 1 & -1 \end{bmatrix}$
Pauli-X		$\begin{bmatrix} 0 & 1 \\ 1 & 0 \end{bmatrix}$
Pauli-Y		$\begin{bmatrix} 0 & -i \\ i & 0 \end{bmatrix}$
Pauli-Z		$\begin{bmatrix} 1 & 0 \\ 0 & -1 \end{bmatrix}$
Phase		$\begin{bmatrix} 1 & 0 \\ 0 & i \end{bmatrix}$
$\pi/8$		$\begin{bmatrix} 1 & 0 \\ 0 & e^{i\pi/4} \end{bmatrix}$
controlled-NOT		$\begin{bmatrix} 1 & 0 & 0 & 0 \\ 0 & 1 & 0 & 0 \\ 0 & 0 & 0 & 1 \\ 0 & 0 & 1 & 0 \end{bmatrix}$
swap		$\begin{bmatrix} 1 & 0 & 0 & 0 \\ 0 & 0 & 1 & 0 \\ 0 & 1 & 0 & 0 \\ 0 & 0 & 0 & 1 \end{bmatrix}$
controlled-Z		$\begin{bmatrix} 1 & 0 & 0 & 0 \\ 0 & 1 & 0 & 0 \\ 0 & 0 & 1 & 0 \\ 0 & 0 & 0 & -1 \end{bmatrix}$

Figure 1.3: Gates are defined in the basis  $(0,1)$  for single qubit gates and in the basis  $(00,01,10,11)$  for two qubit gates

### 1.1.3 Physical Implementations

In order to realize a physical qubit one needs to satisfy four basic requirements:

- The quantum system at stake should have two distinct state (possibly degenerate) which are easily separated from other energy levels or states of the system.
- Controllable unitary evolution should be possible, allowing the implementation of quantum gates.
- One has to be able to prepare an initial state.
- One has to be able to measure the qubits.

In this section we discuss two leading implementations of qubits: Superconducting circuits and Ion traps.

#### Superconducting Circuits

One prominent platform for constructing a multi-qubit quantum processor involves superconducting qubits [26, 27, 43], in which information is stored in the quantum degrees of freedom of nanofabricated, anharmonic oscillators constructed from superconducting circuit elements. In contrast to other platforms, superconducting qubits are macroscopic in size and are thus easier to work with.

One remarkable feature of superconducting qubits is that their energy-level spectra are governed by circuit element parameters and thus are configurable; they can be designed to exhibit “atom-like” energy spectra with

desired properties. Therefore, superconducting qubits are also often referred to as artificial atoms, offering a rich parameter space of possible qubit properties and operation regimes, with predictable performance in terms of transition frequencies, anharmonicity, and complexity.

## **Ion Traps**

Spins provide potentially good representations for qubits [31]. Spin is a strange (but very real!) concept but since the energy difference between different spin states is typically very small compared with other energy scales (such as the kinetic energy of typical atoms at room temperature), the spin states of an atom are usually difficult to observe, and even more difficult to control. In carefully crafted environments, however, exquisite control is possible. Such circumstances are provided by isolating and trapping small numbers of charged atoms in electromagnetic traps, then cooling the atoms until their kinetic energy is much lower than the spin energy contribution. After doing this, incident monochromatic light can be tuned to selectively cause transitions which change certain spin states depending on other spin states. This is the essence of how trapped ions can be made to perform quantum computation. A quantum register made up of trapped ions is comprised of the spin states of the quits, and one extra qubit is represented by the collective motional state of the trapped ions, enabling qubit-qubit entangled interaction.

## 1.2 Quantum Noise

Up until now we have discussed the mathematical properties of a qubit and more importantly, we have mentioned some of its physical implementations. In this section we describe two types of noise, one is the famous *shot noise* due to the discrete nature of quantum systems, and one is related to the fact that a qubit can not be perfectly isolated from the environment.

### 1.2.1 Shot Noise

Shot noise is the most fundamental limitation on our ability to extract information from a quantum system. Suppose a qubit is in some unknown state, and our goal is to assess the state in our computational basis. Measuring the qubit will collapse it to one of our computational basis vectors, with some probability. When we refer to shot noise, we usually mean to refer to the fundamental uncertainty of assessing the right probabilities: We will always deal with some standard deviation due to the fact our experiment results have some probability distribution. By the law of large numbers, this standard deviation is equal to the square root of the number of measurements, and thus the relative error will approach zero as the inverse square of the number of measurements. We use shot noise to write the corrected error due to lost information, in equation 3.8.

### 1.2.2 Decoherence

Another kind of noise is arising from the fact our principal quantum system (say, a qubit) couples to the environment in some unknown way. There are two complementary ways to describe this quantum noise: The discrete description, called the *operator-sum representation* of the noise, and the continuous description with *master equations*. We use the discrete description of noise to write our simulations, and so we will focus on the operator-sum representation of noise. For more information on master equations, please consult ref. [38].

A natural way to describe the dynamics of an open quantum system (our principal system) is to describe the dynamics of the closed quantum system, comprised of our principal system and the environment. Suppose our principal system is sent to a black-box  $U$  operating on the system and the environment, as in figure 1.4. For the purpose of this short derivation we assume the input state for this black-box is a tensor product state (a more detailed derivation could be found in ref. [31]) and we define the quantum operation acting on the system as

$$\mathcal{E}(\rho) = \text{Tr}_{\text{env}}[U(\rho \otimes \rho_{\text{env}})U^\dagger] \quad (1.2)$$



Figure 1.4: Models of closed (left) and open (right) quantum systems. An open quantum system consists of two parts, the principal quantum system and the environment.

The *operator-sum representation* of equation 1.2 is just writing the same equation in terms of the operators of the principal system's Hilbert space alone. Let  $|e_k\rangle$  be an orthonormal basis for the Hilbert space of the environment, and suppose the environment starts from a pure state  $\rho_{env} = |e_0\rangle\langle e_0|$ . Equation 1.2 can thus be rewritten as

$$\begin{aligned}\mathcal{E}(\rho) &= \sum_k \langle e_k | U[\rho \otimes |e_0\rangle\langle e_0|]U^\dagger | e_k \rangle \\ &= \sum_k E_k \rho E_k^\dagger\end{aligned}\tag{1.3}$$

Where  $E_k = \langle e_k | U | e_0 \rangle$  is an operator on the state space of the principal system. This is the operator sum representation. We now describe three noise processes using the operator sum representation, focusing on dephasing and amplitude damping. We sometimes refer to the operation elements  $E_k$  as the **Krauss operators** of the noise process.

### The Depolarizing Channel

The depolarizing channel is of use to us for performing the error probability analysis of section 3.4.1, because the ability to error-correct the depolarizing channel automatically implies the ability to error-correct an arbitrary single qubit quantum operation. It is defined as applying each of the Pauli operators with probability  $p/3$ :

$$\mathcal{E}(\rho) = (1 - p)\rho + \frac{p}{3}(X\rho X + Y\rho Y + Z\rho Z)$$

### Amplitude Damping

Amplitude damping, which we sometimes refer to as energy dissipation, energy relaxation,  $T_1$  process, or just relaxation, is the effect due to loss

of energy from the system to the environment. The Krauss operators for energy relaxation are as follows:

$$E_0 = \begin{bmatrix} 1 & 0 \\ 0 & \sqrt{1-p} \end{bmatrix}, E_1 = \begin{bmatrix} 0 & \sqrt{p} \\ 0 & 0 \end{bmatrix} \quad (1.4)$$

$E_1$  is the lowering operator multiplied with the probability to lose a photon.  $E_0$  leaves  $|0\rangle$  unchanged but reduces the population of  $|1\rangle$  by a factor of  $1 - p$ . Physically it means that no energy was lost to the environment and so the environment believes it is more likely that the system is in the ground state rather than the excited state. Replacing  $p$  with something time-dependent, like  $p = 1 - e^{-t/T_1}$  (thus defining  $T_1$ ) and applying on the quantum state  $\rho = \begin{pmatrix} a & b \\ b^* & c \end{pmatrix}$  gives:

$$\mathcal{E}(\rho) = \begin{bmatrix} 1 - (1-p)(1-a) & b\sqrt{1-p} \\ b^*\sqrt{1-p} & c(1-p) \end{bmatrix} = \begin{bmatrix} 1 - e^{-t/T_1}(1-a) & be^{-t/2T_1} \\ b^*e^{-t/2T_1} & ce^{-t/T_1} \end{bmatrix} \quad (1.5)$$

### Phase Damping

Phase damping is a purely quantum mechanical process, which describes the loss of information without the loss of energy. The energy eigenstates of a quantum system do not change as a function of time, but rather accumulate phase proportional to the energy eigenvalue. When an eigenvector evolves in time for a not precisely known amount of time, partial information about this quantum phase - relative phase between energy eigenstates - is lost. We sometimes refer to phase damping as dephasing, or  $T_2$  process.

Here we describe a simple model for this noise process. Suppose we have a qubit  $|\psi\rangle = a|0\rangle + |1\rangle$  upon which a random phase kick  $R_z(\theta)$  is acted, where  $\theta$  being a random variable which has a Gaussian distribution with

mean 0 and variance  $2\lambda$ . The output density matrix from this process is given from averaging over  $\theta$ :

$$\begin{aligned}\rho &= \frac{1}{\sqrt{4\pi\lambda}} \int_{-\infty}^{\infty} R_z(\theta) |\psi\rangle\langle\psi| R_z^\dagger(\theta) e^{-\theta^2/4\lambda} d\theta \\ &= \begin{bmatrix} |a|^2 & ab^* e^{-\lambda} \\ a^* b e^{-\lambda} & |b|^2 \end{bmatrix}\end{aligned}$$

We define the rate at which the coherences are lost as  $t/T_2$ . This process will make the following transformation to the point on Bloch's sphere:

$$(r_x, r_y, r_z) \rightarrow (\sqrt{1-\lambda}r_x, \sqrt{1-\lambda}r_y, r_z)$$

meaning the point will just get closer to the Z axis. Choosing the probability  $p = 1 - e^{-t/T_2}$  gives the following possible representation to the Krauss operators:

$$K_0 = \sqrt{p} \begin{bmatrix} 1 & 0 \\ 0 & 0 \end{bmatrix}, K_1 = \sqrt{p} \begin{bmatrix} 0 & 0 \\ 0 & 1 \end{bmatrix}, K_2 = \sqrt{1-p} \begin{bmatrix} 1 & 0 \\ 0 & 1 \end{bmatrix} \quad (1.6)$$

Such that

$$\mathcal{E}(\rho) = \begin{bmatrix} a & (1-p)b \\ b^*(1-p) & c \end{bmatrix} = \begin{bmatrix} a & be^{-t/T_2} \\ b^*e^{-t/T_2} & c \end{bmatrix} \quad (1.7)$$

### 1.3 Distance Measures for Quantum Information

How close are two quantum states? For this purpose we have to define a distance measure, a metric, which has to satisfy three ground rules:

- $D(x, y) = D(y, x)$
- $D(x, y) = 0 \rightarrow x = y$

- $D(x, z) \leq D(x, y) + D(y, z)$

In this section we try to answer this question, defining the two distance measures widely used in this work - the *Distance*, a variation to *Trace Distance* of ref.[31], which gives us information of the possible outcomes of a measurement, and the *Fidelity* which is not precisely a metric but a more quantum measure, which approaches 1 for similar states and 0 for distant states.

### **Distance**

We define the Distance between two quantum states  $\rho, \sigma$  to be

$$D(\rho, \sigma) = \text{Tr}|\rho - \sigma|^2 \quad (1.8)$$

With  $|A| = \sqrt{A^\dagger A}$  the positive square root of  $A^\dagger A$ . It is possible to prove that our definition of *Distance* behaves the same as the widely used *Trace Distance* defined as  $\frac{1}{2}\text{Tr}|\rho - \sigma|$  [31].

A useful interpretation to the above definition is given using the geometrical picture of the Bloch sphere: Suppose

$$\rho = \frac{I + \vec{r} \cdot \vec{\sigma}}{2}, \sigma = \frac{I + \vec{s} \cdot \vec{\sigma}}{2}$$

Using our definition the distance is  $D(\rho, \sigma) = \frac{1}{2}|\vec{r} - \vec{s}|^2$ , just half the square of the ordinary Euclidean distance.

### **Fidelity**

We use the regular definition of *Fidelity*,

$$F(\rho, \sigma) = \text{Tr}\sqrt{\rho^{1/2}\sigma\rho^{1/2}} \quad (1.9)$$

The fidelity of two quantum states is, as mentioned, not a metric. It resembles an inner product between two quantum states, and it is indeed defined in such a way:

$$F(|\psi\rangle, \rho) = \sqrt{\langle\psi|\rho|\psi\rangle}, F(|\psi\rangle, |\varphi\rangle) = \langle\psi|\varphi\rangle$$

We can see it approaches 1 as the states are closer and approaches 0 when they are not.

## 1.4 Quamtum Sensing

Quantum sensing is one of the few areas of study intended to have real-world consequences in the NISQ era. [30, 34]. "Quantum Sensing" is typically used to describe one of the following [15]:

- Use of a quantum object to measure a physical quantity (classical or quantum). The quantum object is characterized by quantized energy levels.
- Use of quantum coherence to measure a physical quantity.
- Use of quantum entanglement to improve the sensitivity or precision of a measurement, beyond what is possible classically ("Quantum Metrology").

In this study, we mainly focus on quantum metrology.

The Hamiltonian of the quantum sensor consists of three parts: The internal Hamiltonian of the probe, the signal Hamiltonian and the control Hamiltonian used to manipulate the probe and read out the data:

$$\hat{H}(t) = \hat{H}_0 + \hat{H}_V(t) + \hat{H}_{control}(t)$$

Typically, and in our scenarios, the internal Hamiltonian  $\hat{H}_0$  describes approximately (up to higher energy levels) the energy eigenstates  $|0\rangle, |1\rangle$ :

$$\hat{H}_0 = E_0|0\rangle\langle 0| + E_1|1\rangle\langle 1| = \frac{1}{2}\hbar\omega_0\sigma_z$$

With  $\hbar\omega_0$  being the energy difference. Note that it is not strictly necessary that  $\omega_0 \neq 0$  but it will be the case in most scenarios.

The signal Hamiltonian is a function of some external parameter  $V$  that causes a change in the internal energy  $\hbar\omega_0$  of the form  $\gamma =^q E / \partial V^q$  usually with  $q = 1$  or  $q = 2$ . The signal Hamiltonian is a sum of two qualitatively different contributions, the parallel (commuting with the internal Hamiltonian) part  $\hat{H}_{V\parallel}(t)$  and the transverse (non-commuting) component  $\hat{H}_{V\perp}(t)$ . We can write these two parts as:

$$\begin{aligned} \hat{H}_{V\parallel}(t) &= \frac{1}{2}\gamma V_{\parallel}(t)\{|1\rangle\langle 1| - |0\rangle\langle 0|\} \\ \hat{H}_{V\perp}(t) &= \frac{1}{2}\gamma\{V_{\perp}(t)|1\rangle\langle 0| + V_{\perp}^{\dagger}(t)|0\rangle\langle 1|\} \end{aligned} \quad (1.10)$$

These contributions have different effects on the probe: The parallel one leads to shifts in the energy levels and an associated change in the transition frequency  $\omega_0$  and the transverse one can cause transitions between energy levels, thus changing the transition rate.

### 1.4.1 The Quamtum Sensing Protocol

In this subsection we describe the basic methodology for performing measurements with quantum systems. This methodology always consists of three elementary steps: initialization of the sensor, interaction with the signal and readout of the final state. The key quantity is the *quantum phase* picked up by the quantum sensor due to the interaction. After that ba-

sic protocol, algorithmic quantum sensing may be applied to recover the measured quantity.

The basic steps for the quantum sensing protocol appears in figure 1.5. Here we elaborate on the steps:

1. The quantum sensor is initialized to some initial state, usually  $|0\rangle$ .
2. The quantum sensor is initialized to the sensing state.
3. The probe accumulates phase according to the interaction with the signal.
4. the state of the probe is transformed to one that is informatively measured in the readout basis, which is usually the computational basis.
5. The final state is measured.
6. We repeat steps 1 through 5 and average for the probabilities.
7. We usually repeat steps 1 through 6 for a set of different scenarios, and estimate the wanted information of the signal from them.

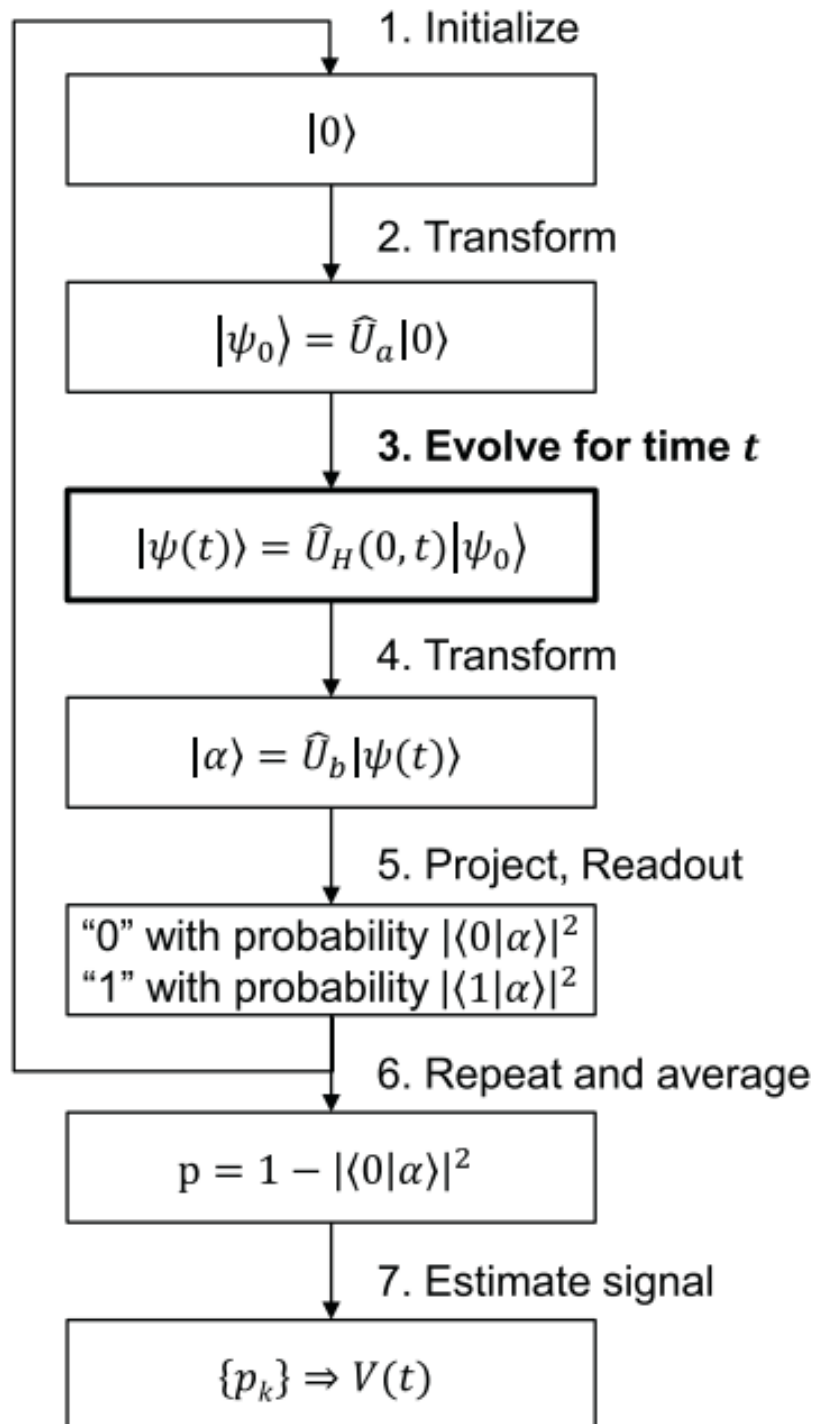


Figure 1.5: Basic steps of the quantum sensing protocol.

A good example for using this scheme is the Ramsey experiment.

### Ramsey Measurement

The Ramsey experiment is used to estimate the static energy splitting  $\hbar\omega_0$ , or  $T_2$  in noisy experiments. Here we discuss the ideal case with no noise. We discuss the noisy version at section 4.1.2.

The steps for the Ramsey experiment are as follows:

1. The quantum sensor is initialized to the ground state,  $|0\rangle$ .
2. Using a  $\pi/2$  pulse, or Hadamard gate, the quantum sensor is transformed to the superposition state

$$|\psi(0)\rangle = |+\rangle = \frac{1}{\sqrt{2}}(|0\rangle + |1\rangle)$$

3. The sensor evolves under the internal Hamiltonian  $\hat{H}_0$  for time  $t$  and accumulates a relative phase,

$$|\psi(t)\rangle = \frac{1}{\sqrt{2}}(|0\rangle + e^{-i\omega_0 t}|1\rangle)$$

4. Using another  $\pi/2$  pulse, or Hadamard gate, the state  $|\psi(t)\rangle$  is converted to a measurable state

$$|\alpha\rangle = \frac{1}{2}(1 + e^{-i\omega_0 t})|0\rangle + \frac{1}{2}(1 - e^{-i\omega_0 t})|1\rangle$$

5. The final state is read-out, giving the transition probability

$$p = 1 - |\langle 0|\alpha\rangle|^2 = \sin^2(\omega_0 t/2)$$

Recording  $p$  as a function of  $t$  enables us to estimate the energy splitting  $\hbar\omega_0$ .

### 1.4.2 Fisher Information & Quantum Cramer Rao Bound

For detailed explanation on Fisher information and Quantum Fisher Information, please consult ref. [30]. Fisher information is all about estimating the amount of information a probability distribution holds. For us, the Fisher information is some quantity that helps us to quantify how precise we can get measuring another quantity.

To quantify the distinguishability of two neighboring probability distributions, the Fisher information is defined by [48]:

$$F(\{P_x(\theta)\}) = \sum_x \frac{1}{P_x(\theta)} \left( \frac{\partial P_x(\theta)}{\partial \theta} \right)^2$$

where  $x$  is the label of measurement results,  $P_x(\theta)$  is the probability of obtaining  $x$  when the parameter is equal to  $\theta$ , satisfying  $P_x(\theta) \geq 0$  and  $\sum_x P_x(\theta) = 1$ . The Fisher information satisfies

$$F(\{P_x(\theta)\}) \leq \text{Tr}[\rho_\theta L_\theta^2] = J(\rho_\theta)$$

Here,  $L_\theta$  is the Symmetric Logarithmic Derivative, defined by  $\partial_\theta \rho_\theta = \frac{1}{2}(L_\theta \rho_\theta + \rho_\theta L_\theta)$  and  $J(\rho_\theta)$  is the quantum Fisher information.

Another way to calculate the Fisher information, theoretically, is given the density matrix  $\rho$  and an observable  $A$  which generates a unitary rotation of the state with parameter  $\theta$ ,  $\rho(\theta) = e^{-i\theta A} \rho_0 e^{i\theta A}$ , the quantum Fisher information is defined to be:

$$J(\rho, A) = 2 \sum_{k,l} \frac{(\lambda_k - \lambda_l)^2}{(\lambda_k + \lambda_l)} |\langle k | A | l \rangle|^2$$

Where  $\lambda_k$  and  $|k\rangle$  are the eigenvalues and eigenvectors of the density matrix  $\rho$ , respectively.

Using the notion of quantum Fisher information and pure mathematical considerations, one can write down the Quantum Cramer-Rao Bound:

$$\delta\theta \geq \frac{1}{\sqrt{N}J(\rho_\theta)} \quad (1.11)$$

Where  $N$  is the number of repetitions.

### Using Entanglement to Saturate QCRB

The (quantum) Cramer-Rao bound contains a factor  $1/\sqrt{N}$  which accounts for the fact that we can simply decrease the standard deviation of our estimates by averaging over  $N$  independent repetitions of the same experiment. The scaling

$$\delta\theta \propto \frac{1}{\sqrt{N}}$$

is called the standard quantum limit (SQL) or shot-noise limit. But the approach of just performing independent repetitions of the same experiment does not make use of one of the most crucial properties of quantum mechanics, namely *entanglement*. Here we repeat the Ramsey measurement, with  $N$  entangled probes:

1. The quantum sensor is initialized to the ground state,  $|0..0\rangle$ .
2. The quantum sensor is transformed to the GHZ state

$$|\psi(0)\rangle = \frac{1}{\sqrt{2}}(|0..0\rangle + |1..1\rangle)$$

3. The sensor evolves under the internal Hamiltonian  $\hat{H}_0$  for time  $t$  and accumulates an enhanced relative phase,

$$|\psi(t)\rangle = \frac{1}{\sqrt{2}}(|0..0\rangle + e^{-iN\omega_0 t}|1..1\rangle)$$

4. The state  $|\psi(t)\rangle$  is converted to a measurable state

$$|\alpha\rangle = \left[ \frac{1}{2}(1 + e^{-iN\omega_0 t})|0_1\rangle + \frac{1}{2}(1 - e^{-iN\omega_0 t})|1_1\rangle \right] |0..0\rangle_{2,N}$$

5. The final state is read-out, giving the transition probability

$$p = 1 - |\langle 0|\alpha\rangle|^2 = \sin^2(N\omega_0 t/2)$$

This factor of  $N$  enhancement lies at the heart of quantum advantage in sensing. You might rightfully ask why this is the case, because we also got a factor  $N$  enhancement from just performing  $N$  separate repetitions. But it turns out that the fact that we enhanced the signal by a factor of  $N$  actually gives us a factor  $N^2$  improvement in the Fisher information! By enhancing the signal by a factor of  $N$  we actually changed the rate with which it changes – the derivative with respect to  $\theta$  – by a factor of  $N$  compared to a single repetition. Because the Fisher information contains the square of the derivative, this effectively gives us the enhancement by a factor of  $N^2$ , leading to the new scaling of the standard deviation:

$$\delta\theta \propto \frac{1}{N}$$

Which is actually the most fundamental limit attainable when exploiting quantum mechanical effects and is called the *Heisenberg limit*.

It is important to note that this scaling is achievable if the probability distribution is not biased, according to [15]. **In this work we see that this is not the case - in the presence of noise the probability distribution is biased, and we give a way of making it less biased, thus approaching to the Heisenberg limit.**

### 1.4.3 Algorithmic Quantum Sensing

Degen *et al.* [15] defines quantitatively the Dynamic Range of a quantum sensor, and finds it scales as the square root of the measurement time. This is where algorithmic quantum sensing is important - It gives a way to enlarge the dynamic range of a quantum sensor to scale as the measurement time by giving an appropriate weighting to different quantum measurements, thus approaching the Heisenberg limit. Here we give a detailed explanation on the most fundamental family of algorithmic sensing protocols, called Quantum Phase Estimation (QPE). Most algorithmic sensing protocols are variations of this family of algorithms, and QPE has numerous applications in other areas of study [13, 32, Santagati et al., Kais], the most famous one being Shor's algorithm.

In the following section we define the problem of quantum phase estimation and give the textbook algorithm, and in the subsequent three sections we give detailed explanation on an implementation of QPE and the two iterative versions of quantum phase estimation that we use - iterative phase estimation algorithm (IPEA) and Kitaev's iterative approach.

#### Quantum Phase Estimation

Quantum phase estimation is a family of algorithms. Suppose a unitary operator  $U$  has an eigenvector  $|u\rangle$  with eigenvalue  $e^{2\pi i\phi}$ , where the value of  $\phi$  is unknown. The goal of the phase estimation algorithm is to estimate  $\phi$ . To perform the estimation, we assume we have available black boxes capable of preparing the state  $|u\rangle$  and performing controlled- $U^{2^j}$  operations for some positive integer  $j$ . The algorithm uses two quantum registers,

one for the measured operator  $U$  and one for ancilla qubits needed for the computation. Phase estimation was first introduced by Kitaev [25]. The standard approach, based on inverse QFT, is depicted in figure 1.6 [31].

It can be realized in many different ways, starting with Kitaev's original approach, using Quantum Fourier Transform (QFT) or using approximate QFT (AQFT). Here we will present three different approaches for doing QPE: an approach using multiple qubits, with constant precision phase shift operators [3], Kitaev's original approach [25], and an approach called Iterative Phase Estimation Algorithm (IPEA) [17].

**Algorithm: Quantum phase estimation**

**Inputs:** (1) A black box which performs a controlled- $U^j$  operation, for integer  $j$ ,  
 (2) an eigenstate  $|u\rangle$  of  $U$  with eigenvalue  $e^{2\pi i \varphi_u}$ , and (3)  $t = n + \lceil \log(2 + \frac{1}{2\epsilon}) \rceil$  qubits initialized to  $|0\rangle$ .

**Outputs:** An  $n$ -bit approximation  $\tilde{\varphi}_u$  to  $\varphi_u$ .

**Runtime:**  $O(t^2)$  operations and one call to controlled- $U^j$  black box. Succeeds with probability at least  $1 - \epsilon$ .

**Procedure:**

1.  $|0\rangle|u\rangle$  initial state
2.  $\rightarrow \frac{1}{\sqrt{2^t}} \sum_{j=0}^{2^t-1} |j\rangle|u\rangle$  create superposition
3.  $\rightarrow \frac{1}{\sqrt{2^t}} \sum_{j=0}^{2^t-1} |j\rangle U^j |u\rangle$  apply black box  
 $= \frac{1}{\sqrt{2^t}} \sum_{j=0}^{2^t-1} e^{2\pi i j \varphi_u} |j\rangle|u\rangle$  result of black box
4.  $\rightarrow |\tilde{\varphi}_u\rangle|u\rangle$  apply inverse Fourier transform
5.  $\rightarrow \tilde{\varphi}_u$  measure first register

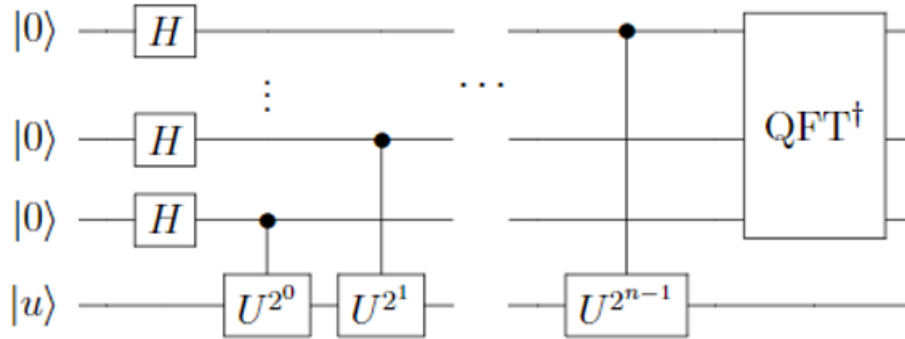


Figure 1.6: the standard QPE procedure, based on inverse QFT. Each digit of the phase is measured separately.

### Quantum Phase Estimation with Constant Precision Phase Shift Operators

The standard QPE method does not use post processing and so is more resilient to noise in the measurement. Its disadvantage is that it uses a large number of qubits and a large number of gates, thus increasing the level of noise. The standard procedure is given in figure 1.6. The constant precision phase shift operators approach has the same advantages and disadvantages as the previous one, but Ahmadi [3] has shown that it can be implemented using a reduced number of gates, and thus it is more resilient to noise. The inverse QFT implemented in this approach is given in figure 1.7, with  $R_k^{-1}$  being  $\begin{pmatrix} 1 & 0 \\ 0 & e^{2\pi i/2^k} \end{pmatrix}$ .

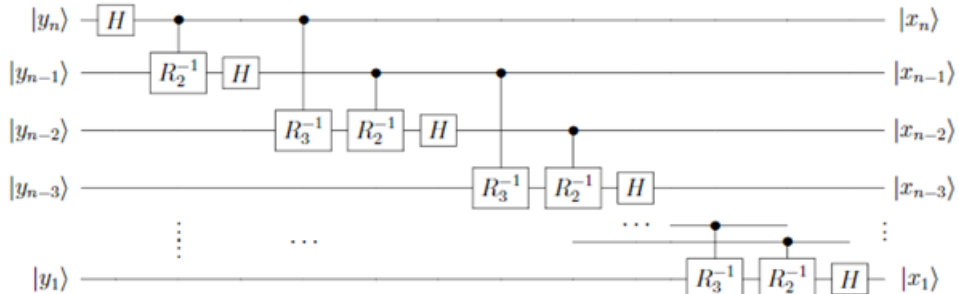


Figure 1.7: QPE with only two controlled phase shift operations, replaces inverse QFT part.

### Iterative Phase Estimation Algorithm

Iterative Phase Estimation [17] uses only one ancilla qubit to perform the phase estimation, and so it has great importance in the age of Noisy Intermediate Scale Quantum (NISQ) computers, since we cannot currently use many qubits simultaneously. (Note that quantum error correction in-

creases the number of qubits at least 5 times fold). Its disadvantage is that it is a dynamic quantum algorithm, in which future states depend on outcomes of measurements that happen during the circuit. Implementing this kind of circuit is hard, and relatively new work [39] has demonstrated that it is possible. This kind of circuit is not yet available on IBM's or Amazon's quantum clouds.

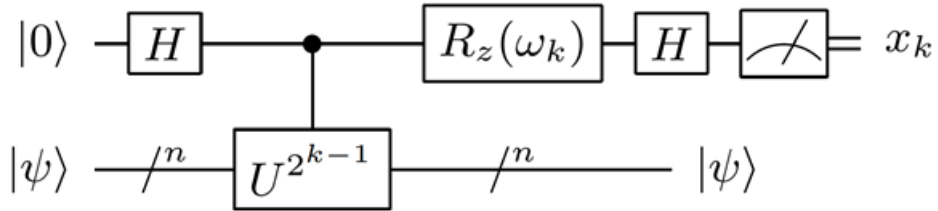


Figure 1.8: The  $k$ 'th iteration of the iterative phase estimation algorithm. The feedback angle depends on the previously measured bits through  $\omega_k = -2\pi(0.0x_{k+1}x_{k+2}\dots x_m)$ , and  $\omega_m = 0$

So how does it work? The circuit for iterative phase estimation is given in figure 1.8. First, suppose we want to measure a phase  $\phi$  that has no more than  $m$  bits,  $\phi = (\phi_1\phi_2\dots\phi_m000\dots)$ . Then, if we label the system's state after the action of the  $j$ 'th gate by  $|\psi_j\rangle$ : After the first Hadamard gate

$$|\psi_1\rangle = \frac{1}{\sqrt{2}}(|0\rangle + |1\rangle)|\psi\rangle$$

. Then we apply the controlled- $U^{2^j}$  operation and we get

$$|\psi_2\rangle = \frac{1}{\sqrt{2}}(|0\rangle + e^{2\pi i 2^{k-1}(\phi_1\phi_2\dots\phi_m000\dots)}|1\rangle)|\psi\rangle$$

. Then we rotate the  $|1\rangle$  state by  $\omega_k = -2\pi(0.0x_{k+1}x_{k+2}\dots x_m)$ , and

$$|\psi_3\rangle = \frac{1}{\sqrt{2}}(|0\rangle + e^{2i(2^{k-1}(0.\phi_1\phi_2\dots\phi_m000\dots)-(0.0\phi_{k+1}\dots\phi_m))}|1\rangle)|\psi\rangle = \frac{1}{\sqrt{2}}(|0\rangle + e^{2i(0.\phi_k)}|1\rangle)|\psi\rangle$$

. finally, after performing the last Hadamard

$$|\psi_4\rangle = \frac{1}{2}(\cos(\pi(0.\phi_k)|0\rangle + (\sin(\pi(0.\phi_k)|1\rangle))|\psi\rangle$$

up to a global phase. So, in the measurement, if  $\phi_k = 0$  we get  $|0\rangle$  with probability 1, and if  $\phi_k = 1$  we get  $|1\rangle$  with probability 1. This means that the whole measurement is deterministic. Now, suppose we want to measure only up to the  $n$ 'th digit, Dobsicek [17] has shown that this procedure does that with an error probability  $\epsilon < 1 - 8/\pi^2$  which is independent of  $n$ . How does that work? Suppose we want to measure  $\phi$  to a precision of  $m$  digits,  $\tilde{\phi} = (\phi_1\phi_2\dots\phi_m)$ . Both answers  $\tilde{\phi}$  and  $\tilde{\phi} + 2^{-m}$  are considered valid. Defining the general remainder  $0 \leq \delta < 1$  as  $\phi = \tilde{\phi} + \delta 2^{-m}$ , the probability to measure  $\phi_m$  correctly is  $\cos^2(\frac{\pi\delta}{2})$ , and if  $\phi_m$  was measured correctly the probability to measure  $\phi_{m-1}$  correctly is  $\cos^2(\frac{\pi\delta}{4})$ . Note that with some remainders ( $\delta \rightarrow 1$ ), the ‘right’ digits may actually be measured with probability  $P = 0$ . The conditional probability to measure the  $k$ 'th bit correctly is  $\cos^2(\pi\delta 2^{k-m-1})$ . Thus the probability to extract  $\tilde{\phi}$  is

$$P(\delta) = \frac{\sin^2(\pi\delta)}{2^{2m} \sin^2(\frac{\pi\delta}{2^m})}$$

and the probability to extract  $\tilde{\phi} + \delta 2^{-m}$  is  $P(1 - \delta)$ , so the overall success probability of the ideal algorithm is  $P(\delta) + P(1 - \delta) > \frac{8}{\pi^2}$ , which is independent of the precision  $m$ .

### Kitaev's Quantum Phase Estimation

Defining  $\alpha_k = 2^{k-1}\tilde{\phi}$  and using the circuit from figure 1.9 we get for using  $K = I$  the relation  $\cos(2\pi\alpha_k) = 2P(0|k) - 1$  and for using  $K = S$  the relation  $\sin(2\pi\alpha_k) = 1 - 2P(0|k)$ . We have enough information to extract  $\alpha_k$ . Once we obtain all the  $\alpha_k$  for  $k$  from 1 to  $m$ , we can retrieve  $\tilde{\phi}$  using the

following algorithm:

---

**Algorithm 1:** Kitaev Estimator
 

---

**Result:**  $\tilde{\phi} = 0.\phi_1\phi_2\dots\phi_{m+2}$  the  $(m+2)$ -bit approximation to the phase  $\phi$

- 1 Estimate all  $\alpha_k$  using the circuit in figure 1.9;
  - 2 Set  $\beta_m = 0.\phi_m\phi_{m+1}\phi_{m+2}$  where  $\beta_m$  is the closest octant  $\{\frac{0}{8}, \frac{1}{8}, \dots, \frac{7}{8}\}$  to  $\alpha_m$ ;
  - 3 **for**  $j = m - 1$  **to** 1 **do**
  - 4      $\phi_j = \begin{cases} 0 & \text{if } |0.0\phi_{j+1}\phi_{j+2} - \alpha_j|_{mod1} < 1/4 \\ 1 & \text{if } |0.1\phi_{j+1}\phi_{j+2} - \alpha_j|_{mod1} < 1/4 \end{cases}$  ;
  - 5 **end**
- 

This algorithm can be used today on Amazon's and IBM's quantum computers – the tasks are independent, the algorithm is built for the ability to estimate probabilities, and tasks can be launched in parallel.

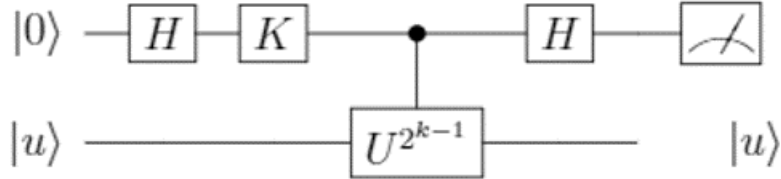


Figure 1.9: Measuring the  $k$ 'th digit using Kitaev's iterative approach. Get measurement histograms for  $K = S$  and  $K = I$ , and then extract the digit using classical computation as described in the text

## 1.5 Quantum Error Correction

Generally, the purpose of quantum error correction is to do quantum information processing reliably – protecting quantum information from noise. The threshold theorem for quantum computations states that provided the noise in individual quantum gates is below a certain constant threshold it is possible to efficiently perform an arbitrarily large quantum computation using methods of fault tolerance quantum computation.

The basic idea of the theory of quantum error correction is to encode quantum states by a unitary operation into a *quantum error correcting code* (QECC), formally defined as a subspace  $C$  of some larger Hilbert space. After encoding the code is subjected to noise, following which a syndrome measurement is performed to diagnose the type of error which occurred, that is, the *error syndrome*. Once this has been determined, a *recovery* operation is performed, to return the quantum system to the original state of the code [31].

### 1.5.1 Stabilizer Formalism

The stabilizer formalism [31] is ideally suited to the description of quantum codes. In this section we describe how this may be done and use it to introduce the five qubit code which is the smallest code that can be used to protect against the effects of arbitrary errors on a single qubit.

First, we define the pauli group  $G_n$  on  $n$  qubits: For a single qubit, we define  $G_1 \equiv \{\pm I, \pm iI, \pm X, \pm iX, \pm Y, \pm iY, \pm Z, \pm iZ\}$ . This set of matrices forms a group under the operation of matrix multiplication. The Pauli group on  $n$  qubits,  $G_n$ , is the group generated by the operators described

above applied to each of the  $n$  qubits in the tensor product Hilbert space  $(\mathbb{C}^2)^{\otimes n}$ . We can now define stabilizers a little more precisely. Suppose  $S$  is a subgroup of  $G_n$  and define  $V_S$  to be the set of  $n$  qubit states which are fixed by every element of  $S$  (for arbitrary operator  $O \in S$  and state  $|\psi\rangle \in V_S$  we have  $O|\psi\rangle = |\psi\rangle$ ).  $V_S$  is the vector space stabilized by  $S$ , and  $S$  is said to be the stabilizer of the space  $V_S$ , since every element of  $V_S$  is stable under the action of elements in  $S$ . Now, every group may be described by its *generators*. A set of elements  $g_1, \dots, g_l$  in a group  $G$  is said to generate the group  $G$  if every element of  $G$  can be written as a product of elements from the list  $g_1, \dots, g_l$ , and we write  $G = \langle g_1, \dots, g_l \rangle$ .

The basic idea is very simple: an  $[n, k]$  stabilizer code is the code that encodes  $k$  logical qubits onto  $n$  physical qubits. It is defined to be the vector space  $V_S$  stabilized by a subgroup  $S$  of  $G_n$  such that  $-I \notin S$  and  $S$  has  $n - k$  independent and commuting generators,  $S = \langle g_1, \dots, g_{n-k} \rangle$ . A method for measuring generators for the 5 qubit code is given in the Methods Chapter. For now, suppose we can measure a generator  $g$  with the result denoted by '0' indicating a state stabilized by  $g$  and a result denoted by '1' indicating a state such that  $g|\psi\rangle = -|\psi\rangle$ . The idea is that any Error  $E$  on a single qubit (we have  $4n$  such errors, for the single qubit errors  $X, Y, Z, I$ ) can be detected (collapsing the state to a state with that error) and corrected by using a code-specific table with (error-syndrome, recovery operation) pairs.

As mentioned earlier, the 5 qubit code is the smallest QECC possible. It's

basis states are:

$$\begin{aligned}
 |0_L\rangle = & \frac{1}{4} [|00000\rangle + |10010\rangle + |01001\rangle + |10100\rangle \\
 & + |01010\rangle - |11011\rangle - |00110\rangle - |11000\rangle \\
 & - |11101\rangle - |00011\rangle - |11110\rangle - |01111\rangle \\
 & - |10001\rangle - |01100\rangle - |10111\rangle + |00101\rangle] \\
 |1_L\rangle = & \frac{1}{4} [|11111\rangle + |01101\rangle + |10110\rangle + |01011\rangle \\
 & + |10101\rangle - |00100\rangle - |11001\rangle - |00111\rangle \\
 & - |00010\rangle - |11100\rangle - |00001\rangle - |10000\rangle \\
 & - |01110\rangle - |10011\rangle - |01000\rangle + |11010\rangle]
 \end{aligned}$$

It's generator are in table 1.1 on page 32 And the Recovery Table 1.2 on page 32.

### 1.5.2 Fault-Tolerant Quantum Computation

A perfect quantum code  $[|n, k, d|]$  encodes  $k$  logical qubits into  $n$  physical qubits, and it can detect and correct errors in at most  $\lfloor (d - 1)/2 \rfloor$  qubits. Let us look at a simple code, with  $k = 1$ : one logical qubit is encoded in  $n$  physical qubits. The 5-qubit code and the 7-qubit code are such codes, with  $d = 3$ . They can correct errors occurring in at most one physical qubit. The idea of Fault-Tolerant quantum computation is to design the gates acted on the quantum state, in a way that keeps the state in the code and assures that if one error occurred in the process of applying the gate, then we have at most one faulty physical qubit at the end, even if the gate creates entanglement. One can answer this challenge using two approaches. One approach is to design the gates transversely (acting on each

Generator Table for the 5-Qubit Code	
$g_1$	$X_1Z_2Z_3X_4$
$g_2$	$X_2Z_3Z_4X_5$
$g_3$	$X_1X_3Z_4Z_5$
$g_4$	$Z_1X_2X_4Z_5$

Table 1.1: Generator Table for the 5-Qubit Code

Error Syndrome $\langle g_1, g_2, g_3, g_4 \rangle$	Recovery Operator
0000	$I$
0001	$X_1$
0010	$Z_3$
0011	$X_5$
0100	$Z_5$
0101	$Z_2$
0110	$X_4$
0111	$Y_5$
1000	$X_2$
1001	$Z_4$
1010	$Z_1$
1011	$Y_1$
1100	$X_3$
1101	$Y_2$
1110	$Y_3$
1111	$Y_4$

Table 1.2: Recovery Table for the 5-Qubit Code

qubit independently), or in any other way that promises a fault tolerant application of the gate in one try [31]. The second approach is trying to know when errors propagate from one qubit to another, and if one such error did propagate – start over, again and again until you have a successful implementation of the gate with error in at most one physical qubit at the end. The second approach is relatively new, and is called ‘flag Fault-Tolerance’ [8] , because we use additional ‘flag’ qubits that indicate us if there was some uncorrectable error. Measuring the flags collapses the state to some subspace of the Hilbert space in which there was no error.

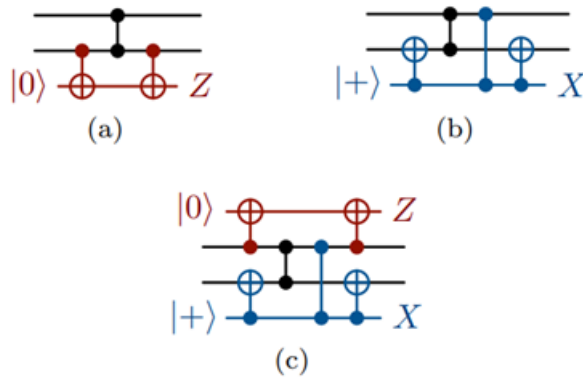


Figure 1.10: CZ gadgets to catch correlated faults. (a) An extra qubit can be used to catch  $XX$ ,  $XY$ ,  $YX$  and  $YY$  faults after the CZ gate. (b) A similar circuit catches  $ZZ$  faults. (c) In combination, these gadgets can catch all two-qubit correlated faults

Implementing the relevant gates fault-tolerantly in the 5-qubit code remains an open problem for future work. Our approach for this future work is to use the second approach (flag fault-tolerance) and a trick introduced by Chao and Reichardt [8]. They call this trick a *CZ gadget*: Adding two flag qubits that indicate for correlated errors. Nielsen had proved [31]

that any entangling gate can be implemented using only CNOTs and single qubit gates, and note that we can use the circuit identity  $\hat{\phi} = \hat{u}_+ \hat{u}_-$  to use only CZs and single qubit gates. The CZ gadget is depicted in figure 1.10, and by Chao and Reichardt's theorem 1, it caches all single qubit correlated errors XX,XY,YX,YY,ZZ.

### 1.5.3 Quantum Error Correction for Quantum Metrology

Much effort has been made to recover the Heisenberg-limit scaling using quantum error correction [4, 7, 19, 29, 36, 48, Unden et al.]. All those efforts focus on sequential quantum metrology, encoding the sensor as a logical qubit and using smart ways to correct errors and not correcting the signal itself. In the next section we introduce our research question, giving a new approach of using quantum error correction for quantum metrology.

## 2 Research Question

In the field of quantum metrology, we are most interested in finding ways to recover the Heisenberg-limit scaling, promising that the error in estimating our observable scales as one over the number of measurements, probing time or number of probes [48]. Recent results indicate that this limit cannot be recovered in the presence of general Markovian noise if the Hamiltonian lies in the span of the noise operators.[28, 47]. Much effort has been made to recover the Heisenberg-limit scaling using quantum error correction [4, 7, 19, 29, 36, 48, Unden et al.]. All those efforts focus on sequential quantum metrology. Recently the use of algorithmic quantum sensing had caught the attention of the community [23, 39], and improving the performance of Quantum Phase Estimation (QPE) for quantum sensing can lead to breakthroughs in other fields, as a result of the algorithm being the basis for an enormous number other uses [13, 32, Santagati et al., Kais], Shor's algorithm is one of them. Thus a lot of study has been done on how QPE performs under the presence of noise [10, 17, 18].

This Heisenberg-limit scaling is achievable if the probability distribution is not biased, according to [15]. In this work we see that this is not the case - in the presence of decoherence the probability distribution is biased, and we give a way of making it less biased, thus approaching to the Heisenberg

limit.

The existence of ancilla qubits opens a new realm to study - doing error correction or error detection on the ancillas instead of on the sensor. The will of making only the ancilla logical, while letting the sensor remain a physical sensor, enforces the need of hybrid logical-physical interaction, which is a new idea to our knowledge. Although we could focus on making this interaction fault-tolerant [Aharonov], for the purpose of quantum sensing we do not need the ability of computing endlessly - we only need one successful run. Thus it is possible to apply only error detection on the ancillas, and post selecting the results [5]. This way we essentially encode some of the noise in redundant degrees of freedom of the Hilbert space, enabling us to get rid of more of it. To our knowledge, we are the first ones approaching the problem this way.

# 3 Methods & Theoretical Derivations

## 3.1 n-Iterative Phase Estimation Algorithm

This section has no direct relation to my work right now - it shows our idea for a slight modification to the IPEA, enabling it to measure few digits at a time. We call it the n-IPEA (see figure 3.1) and it is based on the textbook approach and on the IPEA. This algorithm gives a way to measure the next  $n$  digits of the phase,  $x_k, \dots, x_{k+n-1}$ , given the previous digits  $x_{k+n}, \dots, x_m$  where  $m$  is the desired precision. This version enables to measure a varying number of digits in each iteration, using  $n + r$  qubits with  $r$  the number of sensor qubits.

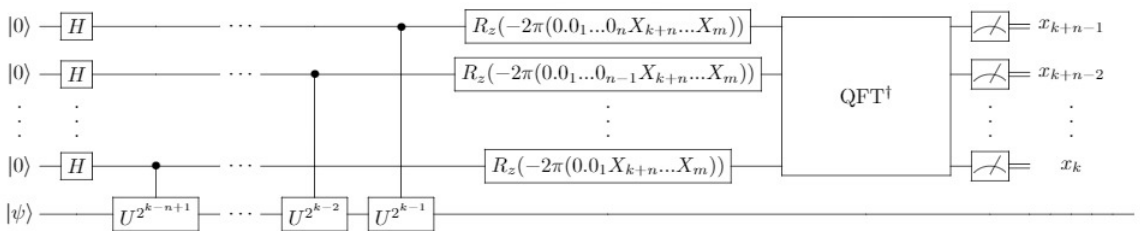


Figure 3.1: n-Iterative Phase Estimation Algorithm. The first few digits may be measured as described in the IPEA, with one ancilla.

The Idea is this: Suppose we want to measure the digits  $x_k, \dots, x_{k+n-1}$ , given  $x_{k+n}, \dots, x_m$ , when the eigenvalue of  $|\psi\rangle$  with the operator  $U$  is  $e^{2i\pi\phi}$ . Using  $n$  ancilla qubits the system's state after the first Hadamards is

$$|\phi\rangle = \frac{1}{2^{n/2}}(|0\rangle + |1\rangle)^{\otimes n} \otimes |\psi\rangle$$

And after the controlled operators sequence, the state becomes

$$|\phi\rangle = \frac{1}{2^{n/2}}\left(\sum_{j=0}^{2^n-1} e^{2i\pi\phi j}|j\rangle\right) \otimes |\psi\rangle$$

Continuing the analysis for the simple  $n = 2$  case, this is exactly

$$\frac{1}{2}(|00\rangle + e^{2i\pi(0.\phi_k\dots\phi_m)}|01\rangle + e^{2i\pi(0.\phi_{k+1}\dots\phi_m)}|10\rangle + e^{2i\pi(0.\phi_k\phi_{k+1}\dots\phi_m+0.\phi_{k+1}\dots\phi_m)}|11\rangle) \otimes |\psi\rangle$$

After the rotations, the state becomes

$$|\phi\rangle = \frac{1}{2}(|00\rangle + e^{2i\pi(0.\phi_k\phi_{k+1})}|01\rangle + e^{2i\pi(0.\phi_{k+1})}|10\rangle + e^{2i\pi(0.\phi_k\phi_{k+1}+0.\phi_{k+1})}|11\rangle) \otimes |\psi\rangle$$

which is exactly the system state for a textbook QPE before the reverse QFT stage. The generalization to  $n$ -digit case is trivial, and so we have a functional n-IPEA.

## 3.2 The Simulation

For a full documentation on the code package see appendix A.

In this Work, we use a full density matrix simulation, similar to Ref.[11]. We save the quantum state of  $n$  qubit register as a 2-d matrix of dimensions  $[2^n, 2^n]$ . Operators are saved as a  $[2^n, 2^n]$  matrix, and if the quantum state was initially  $\rho$  then performing the operation  $U$  on the density matrix is equivalent to updating the density matrix  $\rho \rightarrow U\rho U^\dagger$ .

The noise in the simulation is based on Krauss operators (more of them in section 3.2.2). The simulation is thus made up of many small time steps, with repeated application of Krauss based decoherence in one small time-step and gate-based evolution in the next small time-step. A description of the simulation is given in figure 3.2 along with algorithm 2. In the algorithm, we take the generator of each unitary gate  $G_i$  to be  $H_i$ , such that  $G_i = e^{i \frac{dt}{T} H_i}$ .

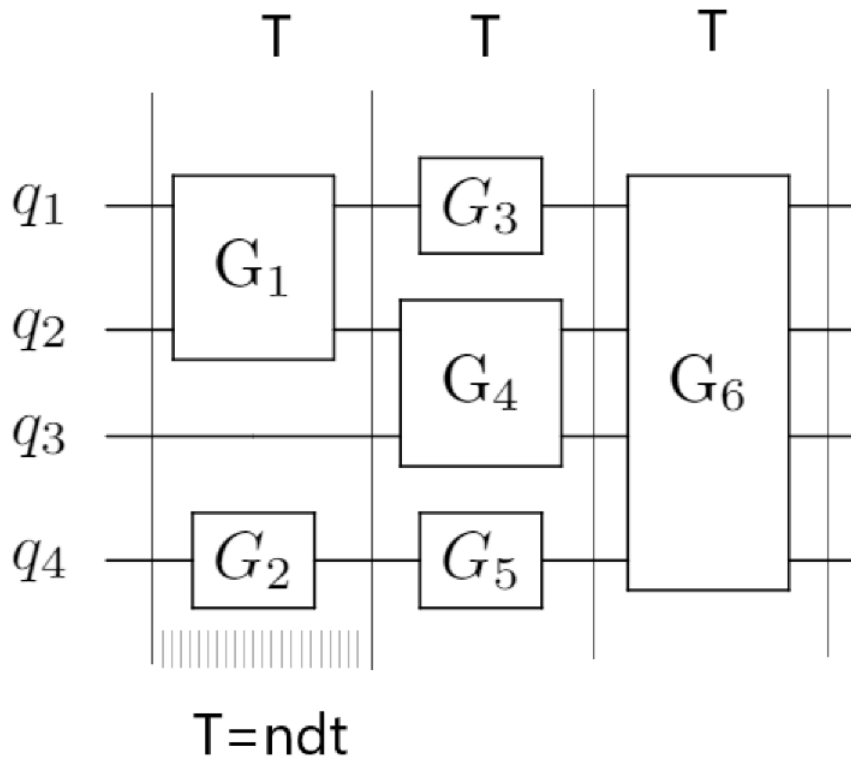


Figure 3.2: Simulation of a general circuit. Each gate-step  $T$  has length  $T_{gate}$  and is made up of  $n = 20$  small time-steps of size  $T_{gate}/n$ .

---

**Algorithm 2:** Noisy Circuit Simulation

---

**Result:** Density matrix of the register after a noisy quantum circuit.

```

1 for gate-step  $T$  do
2    $U_{dt}^T = e^{i \frac{dt}{T} \sum_i H_i}$  ;
3   for  $t$  do
4      $\rho_{t+1} = U_{dt}^T \rho_t (U_{dt}^T)^\dagger$  ;
5     for qubit do
6       amplitude damping ;
7       dephasing ;
8     end
9   end
10 end

```

---

**Main Parameters**

The main parameters used in each simulation are the number of qubits  $N$ , the time  $T_{gate} = n \cdot dt$  ( $n = 20$ ) of each gate-step, the dephasing time of qubit  $q$ ,  $T_2^q$  and the energy relaxation time  $T_1^q$  of the same qubit. From these parameters we define the error rates for each process and qubit:

$$p_{decay}^q = 1 - e^{-\frac{dt}{T_1^q}}, \text{ and } p_{dephase}^q = 1 - e^{-\frac{dt}{T_2^q}}$$

Defining the pauli operator  $\sigma_i^q$  acting on qubit  $q$  as a tensor product of  $\sigma_i$  in the  $q$  index and Identity operators in all other indexes, we take the base Hamiltonian  $H_0 = \bigotimes_{q=1}^N \frac{\hbar\omega_{01}}{2} \sigma_z^q$  to represent the free evolution of the quantum register, with  $\omega_{01} = 6[\text{GHZ}]$ . Practically  $\hbar$  is so small that the computer takes the time evolution operator to be the identity, but defining different, large enough  $\omega_{01}$  for each qubit will result in the mentioned base Hamiltonian.

### 3.2.1 Gate-Based Evolution

In each gate-step, possibly many gates act upon the register. Thus, we start with the base Hamiltonian  $H = H_0$  and for each gate  $G$  in the gate-step we find its corresponding Hamiltonian  $H_G$  using table 3.1 and update the Hamiltonian to be  $H \rightarrow H + H_G$ .

Now, we define the evolution operator  $U$  to be  $e^{iH\frac{dt}{T_{gate}}}$ , and we apply this evolution as in step 4 of algorithm 2 for a total of  $T_{gate}/dt$  times with decoherence step between each application of  $U$ .

Gate	Hamiltonian
$P^q$	$-\frac{\pi}{2}\sigma_P^q$
$R_P^q(\theta)$	$-\frac{\theta}{2}\sigma_P^q$
$H^q$	$\frac{\pi}{2} \cdot \frac{\sigma_X^q + \sigma_Z^q}{\sqrt{2}}$
$CNOT(q_1, q_2)$ - $q_2$ is control	$\ln(\frac{1}{2} \cdot ((I - \sigma_Z^{q_2})\sigma_X^{q_1} + I + \sigma_Z^{q_2}))$
$CZ(q_1, q_2)$ - $q_2$ is control	$\ln(\frac{1}{2} \cdot ((I - \sigma_Z^{q_2})\sigma_Z^{q_1} + I + \sigma_Z^{q_2}))$
$\begin{pmatrix} a & b \\ c & d \end{pmatrix}$ - single qubit ( $q$ ) gate	$\ln(\frac{a+d}{2}I + \frac{a-d}{2}\sigma_Z^q + \frac{c+b}{2}\sigma_X^q + \frac{c-b}{2i}\sigma_Y^q)$

Table 3.1: Gate and Gate Hamiltonian table for the simulation, with  $P \in \{X, Y, Z\}$

### 3.2.2 Krauss-Based Decoherence

In each small time-step  $dt$  we do the Krauss-based decoherence on every qubit in the register. There are three options:

- We are given only decay time  $T_1^q$ , assuming the pure dephasing time  $(T_2^q)^*$  is infinite, for each qubit  $q$ .

- We are given only pure dephasing time  $T_2^q$ , assuming the decay time  $T_1^q$  is infinite, for each qubit  $q$ .
- We are given both the decay time  $T_1$  and the pure dephasing time  $T_2$  for each qubit  $q$ .

Using the relation between the decay time  $T_1$ , the dephasing time  $T_2$  and the pure dephasing time  $T_2^*$ ,  $T_2 = (\frac{1}{2T_1} + \frac{1}{T_2^*})^{-1}$ , we can see that if the pure dephasing time is assumed to be infinite then we have  $T_2 = 2T_1$ . This is embedded in the amplitude damping process, with it's Kraus operators.

So, for the second option (given  $T_2^q$  (pure dephasing time) assuming  $T_1^q$  is infinite) we iterate over the qubit  $q$  and update the register state to be:

$$\rho \rightarrow (1 - \frac{P_{dephase}^q}{2})\rho + \frac{P_{dephase}^q}{2}\sigma_Z^q\rho\sigma_Z^q$$

This is true because if we take the Krauss operators of the phase damping (=phase flip) channel,  $K_1 = \sqrt{p}(\begin{smallmatrix} 1 & 0 \\ 0 & 0 \end{smallmatrix})$ ,  $K_2 = \sqrt{p}(\begin{smallmatrix} 0 & 0 \\ 0 & 1 \end{smallmatrix})$ ,  $K_3 = \sqrt{1-p}(\begin{smallmatrix} 1 & 0 \\ 0 & 1 \end{smallmatrix})$ . We get  $\sum_i K_i \rho K_i^\dagger = (1 - \frac{p}{2})\rho + \frac{p}{2}\sigma_Z\rho\sigma_Z$ .

For the first option (given  $T_1^q$  assuming  $(T_2^q)^*$  is infinite) we define the Krauss operators of the amplitude damping channel  $M_1 = (\begin{smallmatrix} 1 & 0 \\ 0 & \sqrt{1-p} \end{smallmatrix})$ ,  $M_2 = (\begin{smallmatrix} 0 & \sqrt{p} \\ 0 & 0 \end{smallmatrix})$  Which, expressed by pauli operators, look like

$$M_1^q = \frac{\sqrt{1-P_{decay}^q}}{2}(I - \sigma_Z^q) + \frac{1}{2}(I + \sigma_Z^q),$$

$$M_2^q = \frac{\sqrt{P_{decay}^q}}{2}(\sigma_X^q + i\sigma_Y^q)$$

And we iterate over the qubit  $q$ , updating the register to be:

$$\rho = M_1^q \rho (M_1^q)^\dagger + M_2^q \rho (M_2^q)^\dagger$$

Finally, for the third option - given both pure dephasing rate and energy

relaxation rate, we update the state of the register as follows:

$$\rho_{temp} = M_1^q \rho (M_1^q)^\dagger + M_2^q \rho (M_2^q)^\dagger$$

$$\rho = (1 - \frac{P_{dephase}^q}{2})\rho_{temp} + \frac{P_{dephase}^q}{2}\sigma_Z^q \rho_{temp} \sigma_Z^q$$

### 3.2.3 Measurements

There are two kinds of measurements we perform - post selection measurements and probabilistic measurements. Here, we first refer to the post selection measurements.

Post selection measurements are done on the sensor qubit for SPS, on flag qubits for fault-tolerance, and once again on the sensor qubit (that acts as an ancilla qubit for syndrome measurement) for LPS. To perform post selection measurements, we collapse the register state as defined below according to the preferred measurement outcomes. One could say we choose the system's trajectory.

First, to add flag qubits to the simulation, we expand the register state with a tensor product to the two additional qubit sub-spaces. Next, we perform the entangling operations with the flags, and finally project on the trivial flag state  $|0..0\rangle$  using the operator defined below.

For probabilistic measurements (e.g. Error correction measurements), to decide measurement outcome on the qubit group  $A = \{q_{k_1}, \dots, q_{k_n}\}$ , renaming with  $B = \{q_1, \dots, q_N\}/A$ , we trace out B to get  $\rho^A = Tr_B(\rho)$ . Then, we define P as the diagonal of  $\rho^A$  and P' as the cumulative sum of P. we take a random number  $0 < x < 1$  and find the first index  $i$  such that  $x < P'[i]$ . The result of the measurement is the binary string of  $i - 1$ .

To collapse the quantum state to a state after measuring qubits in the group A, we use the following projector:

$$P_m = \bigotimes_{q=1}^N \begin{cases} I_2 & \text{if } q \notin A \\ \frac{I+\sigma_Z^q}{2} & \text{if } q \in A \text{ and measurement result is } |0\rangle \\ \frac{I-\sigma_Z^q}{2} & \text{if } q \in A \text{ and measurement result is } |1\rangle \end{cases}$$

And after this projection operation  $\rho \rightarrow P_m \rho P_m^\dagger$  we trace out the flag qubits.

The procedure described above can cause numeric errors when the state decohere for a long time, because the projection operation as described is not trace preserving. To have a valid density matrix, for each projection, say the  $k$ 'th projection, we first save the state's trace as  $Ps_k$  and then normalize the state. To calculate the portion of information that have been lost due to post selection, we use the following reasoning:

- after one projection, we have lost  $1 - Ps_1$  information and remain with a state with trace  $Ps_1$ .
- after the second projection, we have lost  $Ps_1 \cdot (1 - Ps_2)$  more information.
- after the third projection, we have lost  $Ps_1 \cdot Ps_2 \cdot (1 - Ps_3)$  more information.
- after the  $k$ 'th projection, we have lost  $Ps_1 \cdot \dots \cdot Ps_{k-1} \cdot (1 - Ps_k)$  more information.

Overall, this is the amount of *lost information*:

$$l_i = \sum_i \left( \left( \prod_{k=1}^{i-1} Ps_k \right) \cdot (1 - Ps_i) \right) \quad (3.1)$$

### 3.3 Sensor Post Selection

Up until now we have introduced general background, and discussed technical details of the simulation. In this section and the next two we discuss more thoroughly the core concept we use to improve algorithmic quantum metrology - Post Selection (PS). Post selection is a technique used for coping with errors, in which we choose to work only with the portion of the data that fits our expectations. According to ref.[5], post-selected metrology could, counter-intuitively, give more Fisher information than using the best input state. We begin by presenting the possible advantages of performing post selection on the sensor qubit, or as we call it - Sensor Post Selection (SPS). We then discuss in detail the simulation done for checking SPS performance, in the theoretic circuit-level.

#### 3.3.1 The Potential of Sensor Post Selection

Suppose we have the measured operator  $U = \begin{pmatrix} 1 & 0 \\ 0 & e^{i\theta} \end{pmatrix}$  with eigenvectors  $|u\rangle$  and  $|v\rangle$ , 1 being the eigenvalue of  $|u\rangle$ . Define some error in  $U$  by  $U \rightarrow U + \vec{\Delta} \cdot \vec{\sigma} \stackrel{\text{def}}{=} U'$  with  $\vec{\sigma} = (\sigma_x, \sigma_y, \sigma_z)$ . In this case, we have:

$$U'|u\rangle = (e^{i\theta} - \Delta_z)|u\rangle + (\Delta_x - i\Delta_y)|v\rangle$$

Measuring the sensor qubit and post selecting the measured eigenstate, we can thus eradicate  $\Delta_x$  and  $\Delta_y$  errors. Since  $\Delta_z$  is defined in the eigenbasis of the operator, it translates to a rotation with some different angle  $\theta$  - this is noise in the signal. In real experiments we have some finite precision for the angle in which we rotate the eigenstate, and thus we accept this error  $\Delta_z$  as a part of  $U$  that we do not need to correct, under the assumption this is a random noise with zero mean.

Perhaps the biggest challenge in QPE algorithms is the high power of the measured operator. Doing the naive thing and applying the operator again again is not practical, because we will have to apply the operator for times larger than the qubit's decoherence time. To overcome this challenge one can think of experimental ways (for example, applying a measured magnetic field with different angles) or use VFF [12] as a mean to accelerate the Hamiltonian. Those methods can cause constant errors in  $U$ . Take again the same faulty  $U \rightarrow U + \vec{\Delta} \cdot \vec{\sigma} \stackrel{\text{def}}{=} U'$ , and suppose the ideal operator has two eigenvalues  $\lambda_0$  for  $|0\rangle$  and  $\lambda_1$  for  $|1\rangle$ . We have the two equations:

$$U'|1\rangle = (\lambda_1 - \Delta_z)|1\rangle + (\Delta_x - i\Delta_y)|0\rangle$$

$$U'|0\rangle = (\lambda_0 + \Delta_z)|0\rangle + (\Delta_x + i\Delta_y)|1\rangle$$

Doing QPE and post selecting the sensor for each one, we get the results  $\tilde{\lambda}_1, \tilde{\lambda}_0$  and we can use the following relations to extract the real eigenvalues:

$$\tilde{\lambda}_1 + \tilde{\lambda}_0 = \lambda_1 + \lambda_0$$

$$2 = \lambda_1^2 + \lambda_0^2$$

Where the second equation is a result of normalizing  $U \otimes U|+\rangle$ .

### 3.3.2 SPS Simulation Methods

In this work, we check the affect SPS has on a noisy register running the Kitaev Iterative Phase Estimation 1.4.3, with  $T_2/T_{gate} = 10^{15} \approx \infty$  on the two qubits and  $T_1^{ancilla}/T_{gate} = 10^{15} \approx \infty$  on the control qubit. Since it is interesting to find the efficiency of SPS for the worst case possible put the sensor in the excited eigenstate of  $R_z - |1\rangle$  and allow it to have bit-flip errors. Meaning - We assume only  $T_1$  relaxation on the sensor qubit, and

change the value  $T_1^{sensor} / T_{gate}$  in the range  $[10, 10^3]$ . This translates to the worst case single gate fidelity as described in ?? by applying the identity gate on the excited state and calculating the fidelity of the result with the excited state. We average the results on 10 different evenly spaced phases  $\phi$  in the range  $[0, 2\pi)$ .

We compare three algorithms:

- *Traditional* - The simple, two-qubit Kitaev Iterative Phase Estimation as in figure 1.9, without acceleration.
- *Single SPS* - The simple, two-qubit Kitaev Iterative Phase Estimation, with Sensor Post Selection after all of the applications of the controlled operator, as in figure 3.3 (a).
- *Multiple SPS* - The simple, two-qubit Kitaev Iterative QPE, with Sensor Post Selection after the each application of the controlled operator, as in figure 3.3 (b).

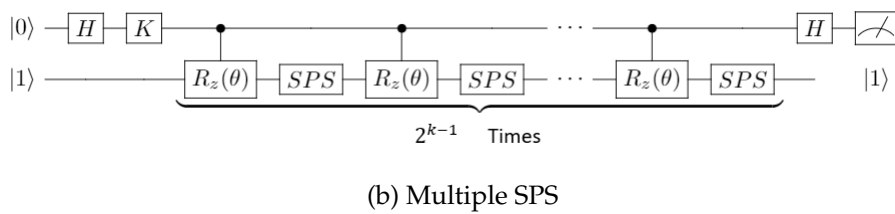
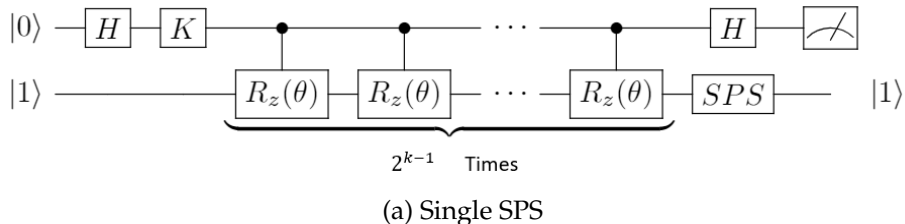


Figure 3.3: Kitaev Iterative QPE as in figure 1.9, without operator acceleration. (a) Single Sensor Post Selection, (b) Multiple Sensor Post Selection.

### 3.4 Logical Post Selection

In the previous section we have introduced the idea of using post selection on the sensor to improve sensing sensitivity. In this section and the next we define the notion of Logical Post Selection (LPS), discuss the scaling of the error probability after performing LPS and develop insights on the subject of hybrid logical-physical entanglement. In the next section we describe briefly the implementation of logical post selection for quantum metrology.

Here we develop a new point of view on post selection. In the act of sensor post selection, we select only the fraction of the data that indicates that the sensor was in a certain state before the measurement. One could say we have selected to work only in a subspace of the Hilbert space, by projecting the system's state to the subspace defined by the sensor being in the initial eigenstate. One could further depict the action of post selection as encoding some of the noise in redundant degrees of freedom of the Hilbert space, in orthogonal subspaces to the one we work in, and throw this noise away by the act of post selection, thus throwing some of the information collected.

Intuitively, encoding the noise in a bigger redundant Hilbert space should result in more noise being separated from the actual 'pure' data. This can be done by using an error-detection or an error-correction code, and instead of correcting the noise we can just detect it and post select data fitting our desires. Although we could focus on making the operations fault-tolerant [Aharonov], or doing error correction, for the purpose of quantum sensing (and a variety of other purposes like state distillation and error

mitigation [41, Czarnik et al., Piveteau et al.]) we do not need the ability of computing endlessly - we only need one successful run. Thus it is possible to apply only error detection on the ancillas, and post selecting the results [5].

Another incentive to use error detection instead of error correction is graphically depicted in figure 4.11 of the Results Chapter. This could be explained as follows: For small gate fidelity the act of error correction can spoil the results, and sometimes destroy them entirely. The reason for that is in table 3.2. In the realm of small gate fidelity and non fault-tolerant gates, the assumption that we have at most one faulty qubit is invalid, and we have to assume it is possible to also have two faulty qubits with some, in-neglect-able probability. In this case, we do neglect the possibility of three faulty qubits.

We define logical post selection by the act of measuring the logical state's error syndrome, and post selecting only results with the trivial syndrome. In the case of the 5-qubit code, that would be the syndrome '0000'.

In this work we use the simple 5-qubit-code as our error detection (correction) code, due to two interesting attributes it exhibits:

- LPS leads to an improved scaling of the error probability, as described in the next subsection 3.4.1.
- It enables an easy logical-physical interaction, as described in the following subsection 3.4.2 .

### 3.4.1 Scaling of the Error Probability

In this subsection we dive deeper into understanding the notion of logical post selection, and analyse the new scaling of the error probability. The incentive of developing a deeper understanding appears in table 3.2, where we can see that errors in two or less qubits will result in measuring the trivial syndrome. In our error analysis we follow the explanation by Nielsen and Choung,[31] (Chap.10).

Here, we present a simple error analysis of LPS for the five qubit code. Suppose the probability of an error in one faulty qubit is  $p$ , then the probability to have at most two faulty qubit is  $(1 - p)^5 + 5p(1 - p)^4 + 10p^2(1 - p)^3$ , and so the probability that there was an error and we couldn't recognize it is  $10p^3 - 15p^4 + 6p^5$ . To improve the results using LPS we have to require  $10p^3 - 15p^4 + 6p^5 < p$  which gives us, as expected,  $0 \leq p \leq \frac{1}{2}$ .

Now, for a slightly better analysis. We assume the depolarising channel with probability  $p$  acts on the state, giving

$$\rho \rightarrow (1 - p)\rho + \frac{p}{3}(X\rho X + Y\rho Y + Z\rho Z) \quad (3.2)$$

For a simple one physical qubit case, taking a pure state  $\rho = |\psi\rangle\langle\psi|$ , we get process fidelity of

$$F = \sqrt{\langle\psi|\rho|\psi\rangle} = \sqrt{(1 - p) + \frac{p}{3}[\langle\psi|X|\psi\rangle^2 + \langle\psi|Y|\psi\rangle^2 + \langle\psi|Z|\psi\rangle^2]}$$

This expression gets the lowest fidelity for  $|\psi\rangle = |0\rangle$ , with:

$$F = \sqrt{1 - \frac{2}{3}p} = 1 - \frac{p}{3} + O(p^2)$$

Now, for the logical qubit. Assume we encode one qubit of information into  $n$  physical qubits, each goes through a depolarizing channel  $\epsilon$  with

probability  $p$ , as in equation 3.2. Then the channel's action on a state  $\rho$  becomes:

$$\begin{aligned}\varepsilon^{\otimes n}(\rho) &= (1-p)^n \rho + \sum_{j=1}^n \sum_{k=1}^3 (1-p)^{n-1} \frac{p}{3} \sigma_k^j \rho \sigma_k^j \\ &\quad + \sum_{j_1=1}^n \sum_{j_2=1}^n \sum_{k_1=1}^3 \sum_{k_2=1}^3 (1-p)^{n-2} \frac{p^2}{9} \sigma_{k_1}^{j_1} \sigma_{k_2}^{j_2} \rho \sigma_{k_2}^{j_2} \sigma_{k_1}^{j_1} + \dots\end{aligned}$$

With  $\sigma_k^j$  being the  $k$ 'th pauli operator acting on the  $j$ 'th qubit. The first element represents one faulty qubit and the second represents two faulty qubits, and the dots represent errors in more than 2 qubits. Now, after performing LPS, each element in this sum will be returned to the state  $\rho$  given  $\rho$  was in the code:

$$(R \otimes \varepsilon^{\otimes n})(\rho) = [(1-p)^n \rho + np(1-p)^{n-1} + \binom{n}{2} p^2 (1-p)^{n-2}] \rho$$

And finally, the fidelity  $F$  remains:

$$\begin{aligned}F &\geq \sqrt{(1-p)^{n-2}(1 + (n-2)p + (\frac{n(n-1)}{2} - n + 1)p^2)} \\ &= 1 - \frac{1}{12}n(n^2 - 3n + 2)p^3 + O(p^4)\end{aligned}\tag{3.3}$$

Giving a  $p^3$  dependence and confirming our intuition from table 3.2.

Error Syndrome $\langle g_1, g_2, g_3, g_4 \rangle$	Possible Cause
0000	IIII
0001	IIIXY, IYYI, IIZIX, IXIZI, IYXII, IZIIZ, XHHH
0010	IIIIX, IIXYI, IYYII, IZIXI, XIZII, YXIII, ZIIIZ
0011	IIIXZ, IIZII, IITYI, IZIIZ, XHHH, YYIII, ZXIII
0100	IIIXI, IIZIZ, IXYII, IZIIX, XHHY, YYIII, ZIXII
0101	IIHY, IIYZI, IXIYI, IZZII, XIIXI, YIXII, ZYIII
0110	IIIXX, IIXZI, IIZIY, IZIII, XIIZ, YIYII, ZIIYI
0111	IIIZZ, IIZXI, IXXII, IYIZI, XZIII, YIIYI, ZIYII
1000	IIIXY, IIXII, IXIIZ, IZIZI, XYIII, YIIIY, ZIIXI
1001	IIIZZ, IIYIX, IIZYI, IYIII, XIXII, YIIXI, ZIIIY
1010	IIYI, IIXIX, IXIY, IYZII, XIYII, YIIIZ, ZZIII
1011	IIIZY, IIYII, IXIXI, IYIIX, XIYI, YZIII, ZIIIZ
1100	IIIZX, IIXXI, IIYIZ, IXZII, IYIY, IZIYI, ZHHH
1101	IIIZY, IIIXY, IIZZI, IXIIX, IYIXI, IZYII, YIIIY
1110	IIIZI, IIYTY, IYIIZ, IZXII, XXIII, YIZII, ZIIIY
1111	IIYYY, IIXIZ, IIYXI, IXIII, XIIZI, YIIIX, ZIZII

Table 3.2: Error syndrome and possible cause for the 5 qubit code. Causes with errors in more than 2 qubits are neglected.

### 3.4.2 Hybrid Logical-Physical Entanglement

As explained earlier, some of the noise can be encoded in redundant degrees of freedom. We hope to achieve this encoding by using a logical qubit interacting with a physical qubit, and describing this interaction is

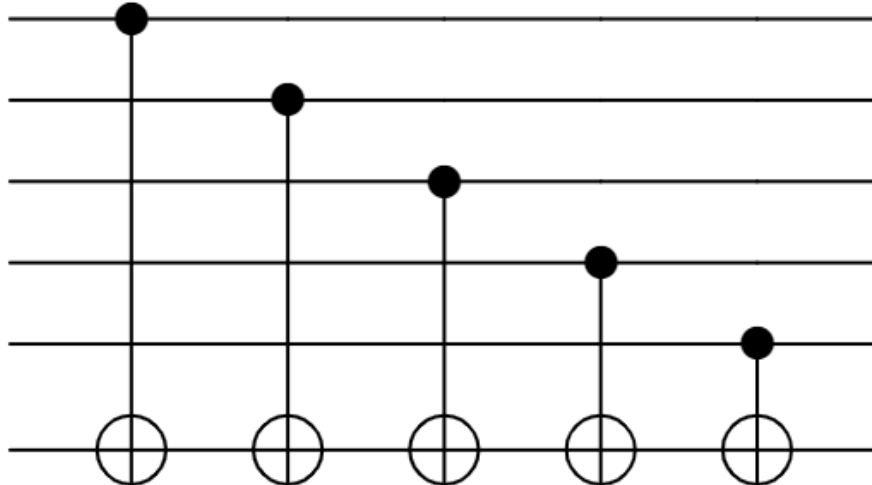
what we do in this subsection. Assumptions on the noise vulnerability of both qubits, logical and physical, will be made throughout the work, and we will make sure to point out our assumptions in each stage.

We start by remarking that any multi-qubit gate can be decomposed into single qubit gates and CNOT gates [31], and so our focus should be on understanding how to implement the CNOT gate between a logical and physical qubits, as control and target respectively. Some QECC have a nice attribute: The logical ground state,  $|0_L\rangle$ , is made up of a sum of quantum states with even number of 1's, and the logical excited state,  $|1_L\rangle$ , is made up of a sum of quantum states with odd number of 1's, as for example, for the 5-qubit code, in figure 3.4 (a). In the case of one logical layer, this attribute allows us to implement the CNOT gate in a semi-transversal manner, as in figure 3.4 (b). This can be generalized trivially for any number of logical layers, provided that the quantum code used for each layer has this attribute.

We have thus given a way of implementing logical-physical qubit interaction for the five qubit code, used in this work. In the case of quantum phase estimation implementation, the first five qubits in figure 3.4 (b) are the ancilla qubits composing the logical ancilla, and the sixth qubit (first from the bottom) is the sensor.

$$\begin{aligned}
 |0_L\rangle = & \frac{1}{4} \left[ |00000\rangle + |10010\rangle + |01001\rangle + |10100\rangle \right. \\
 & + |01010\rangle - |11011\rangle - |00110\rangle - |11000\rangle \\
 & - |11101\rangle - |00011\rangle - |11110\rangle - |01111\rangle \\
 & \left. - |10001\rangle - |01100\rangle - |10111\rangle + |00101\rangle \right] \\
 |1_L\rangle = & \frac{1}{4} \left[ |11111\rangle + |01101\rangle + |10110\rangle + |01011\rangle \right. \\
 & + |10101\rangle - |00100\rangle - |11001\rangle - |00111\rangle \\
 & - |00010\rangle - |11100\rangle - |00001\rangle - |10000\rangle \\
 & \left. - |01110\rangle - |10011\rangle - |01000\rangle + |11010\rangle \right]
 \end{aligned}$$

(a) 5-Qubit Code Basis States



(b) Logically Controlled CNOT

Figure 3.4: (a) The logical basis states for the 5-qubit code. This code has the aforementioned attribute, allowing the application of a logically-controlled CNOT gate (b) with the first 5 qubits acting as a logical qubit and the sixth qubit as the target qubit.

### Logical-Physical Interaction - Simulation Method

As mentioned earlier, each multi-qubit interaction can be reduced to single qubit gates and simple CNOT or CZ entangling gates. Thus it is interesting to ask how does the threshold value (in which logical control is better than physical control) depend on the number of entangling gates? To answer this question, we take  $T_1/T_{gate} = \infty$  for all qubits, and a varying  $T_2/T_{gate}$  for all qubits. We also take a varying number of CNOT gates, in the range [1,200]. We start with the initial state  $|++\rangle$  which is an eigenstate of the CNOT gate, where the first + in the tensor product may represent the logical qubit. For a specific number  $N_{gates}$  of CNOT gates, we apply  $N_{gates}$  CNOT gates and then apply noisy LPS. We calculate and save the fidelity of the output state and  $|++\rangle$ , and plot a three dimensional graph (figure 4.8) where one axis is the number of entangling gates, the second axis is the worst case single gate fidelity (extracted from figure 4.3), and the third is the fidelity difference between the logical and the traditional control. Note that we apply noisy syndrome extraction, so the circuit depth has a constant overhead of approximately 20 gates.

The fidelity is calculated as follows: The ideal (noiseless) state  $\rho_i$ , right before measurement, is a two qubit matrix (4x4). We define the logical state for a logical register with one sensor (6 qubits) at state  $\rho'$  as:

$$\rho = \begin{pmatrix} \langle 0_L 0 | \rho' | 0_L 0 \rangle & \langle 0_L 0 | \rho' | 0_L 1 \rangle & \langle 0_L 0 | \rho' | 1_L 0 \rangle & \langle 0_L 0 | \rho' | 1_L 1 \rangle \\ \langle 0_L 1 | \rho' | 0_L 0 \rangle & \langle 0_L 1 | \rho' | 0_L 1 \rangle & \langle 0_L 1 | \rho' | 1_L 0 \rangle & \langle 0_L 1 | \rho' | 1_L 1 \rangle \\ \langle 1_L 0 | \rho' | 0_L 0 \rangle & \langle 1_L 0 | \rho' | 0_L 1 \rangle & \langle 1_L 0 | \rho' | 1_L 0 \rangle & \langle 1_L 0 | \rho' | 1_L 1 \rangle \\ \langle 1_L 1 | \rho' | 0_L 0 \rangle & \langle 1_L 1 | \rho' | 0_L 1 \rangle & \langle 1_L 1 | \rho' | 1_L 0 \rangle & \langle 1_L 1 | \rho' | 1_L 1 \rangle \end{pmatrix} \quad (3.4)$$

Fidelity was calculated in comparison to the ideal state,  $F(\rho_i, \rho) = \text{Tr}(\sqrt{\sqrt{\rho}\rho_i\sqrt{\rho}})$ .

## 3.5 Logical Post Selection for Quantum Metrology

In the previous section we introduced the idea of Logical Post Selection and gave a way to implement an entangling gate between a physical sensor qubit and a logical ancilla qubit. In this section we demonstrate the use of LPS and this hybrid interaction for the purpose of algorithmic quantum sensing.

The field of error correction for quantum metrology is a new, exciting growing field, which suffers one major issue: It is hard to correct noise in the sensed signal without 'correcting' the signal itself. We offer an approach to possibly overcome some of that noise by encoding the ancilla instead of the sensor, letting some of the noise from the sensor be propagated to the ancilla, and using post selection to purify the system's state.

In the following we focus on two specific QPE algorithms: The Iterative Phase Estimation Algorithm (IPEA) ?? and Kitaev's Iterative Phase Estimation 1.4.3.

### 3.5.1 Gate Implementations

Looking at the gate sequence defining each of the above algorithms, we can easily deduce our focus should be on implementing the following set of gates or procedures:

- Logical state preparation.
- Logical Hadamard gate.

- Logically-controlled operator. In this work we focus, for simplicity, on single qubit  $Z$  and  $X$  rotations,  $R_z(\theta)$  and  $R_x(\theta)$  respectively.
- Logical  $R_z(\theta)$  rotation for phase kicks.
- Syndrome extraction procedures.

We will focus on the non-fault-tolerant implementations of these gates, and offer directions for making some of them fault-tolerant, meaning - implement them in such a way that errors will not spread throughout the circuit.

### Logical State Preparation

First we need to prepare the logical  $|0\rangle$  state. State preparation can be done by first preparing the  $|+\rangle^{\otimes 5}$  state by applying a transverse Hadamard gate, and then continue following the procedure depicted in figure 3.5 (a). Note that the procedure is taken from Chao and Reichardt [8] with small adjustments. For fault-tolerant state preparation, insert flags as in 3.5 (b). Under the assumption ancilla qubits are not perfect and have all the same decoherence and relaxation times, a simulation of the two methods was done and depicted in figure ?? on page ??, and it is clear that in the realm of small gate fidelity it is better to use the non fault-tolerant method. For perfect ancilla qubits we also use the non fault-tolerant method, for faster simulation times.

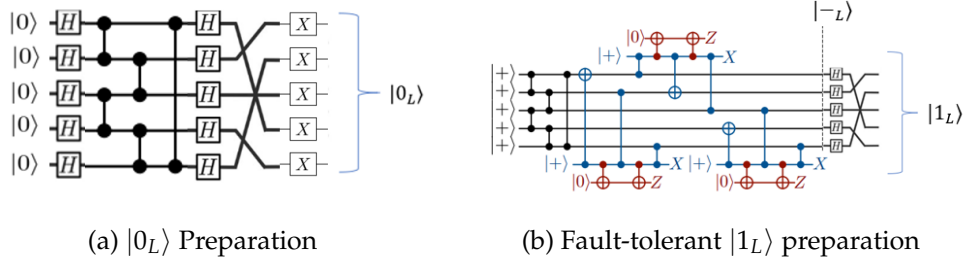


Figure 3.5: State preparation for the 5-qubit code. (a) Prepare the logical 5-qubit code ground state as appearing in section 1.5.1. (b) Flag fault tolerant preparation of the logical 5-qubit code excited state as appearing in section 1.5.1. logical ground state may be achieved by applying transverse X gate.

### Logical Hadamard

The Hadamard gate can be implemented as depicted in figure 3.6 [44]. It is a transversal application of Hadamard followed by simple qubit permutation. If the permutation is done by relabelling the qubits, the logical Hadamard is transversal and thus automatically fault tolerant.

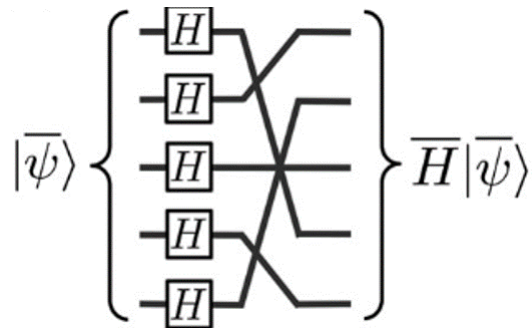


Figure 3.6: Logical Hadamard

### Logically Controlled Operator

In the case of interest, where the measured operator is a single qubit operator, the logically controlled operator can be realized as a series of CNOTs and single qubit gates, as explained by Nielsen [31]. We focus for simplicity on single qubit  $Z$  and  $X$  rotations,  $R_z(\theta)$  and  $R_x(\theta)$  respectively. We denote them  $R_p(\theta)$  with  $p \in \{X, Z\}$ . The implementation of controlled  $R_p(\theta)$  rotation is depicted in figure 3.7. We have given here a symmetric representation of the rotation to fight error echoing.

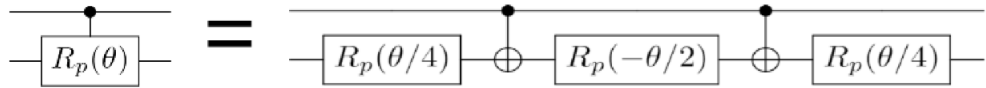


Figure 3.7: Controlled P ( $\in \{X, Z\}$ ) rotation of angle  $\theta$ . Operator is controlled by logical qubit and acted upon the sensor qubit.

The CNOT gate can be traditional or logical. In figure 3.8 I give a logical way to implement the logically controlled CNOT gadget. Whether or not it is possible to make this gadget fault-tolerant (Perhaps with using Flag Fault-Tolerance?) remains an interesting question for future work.

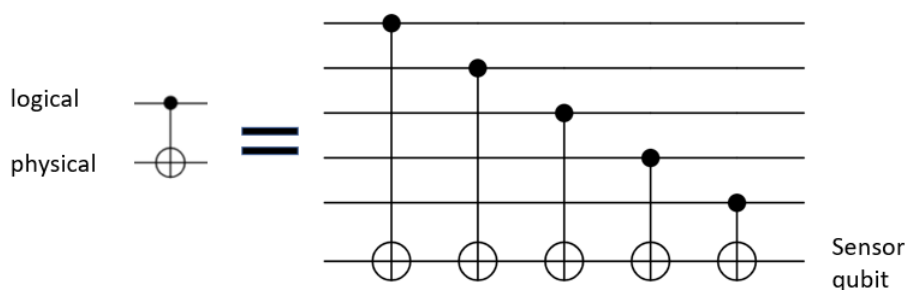


Figure 3.8: non-Fault-Tolerant Logically Controlled CNOT Gate

### Logical Z rotation

Yoder *et al.* as shown that the logical Z rotation may be implemented according to figure 3.9 [44]. Note that we use  $K = SH$ . Whether or not it is possible to make this procedure fault-tolerant (Perhaps with using Flag Fault-Tolerance?) remains an interesting question for future work.

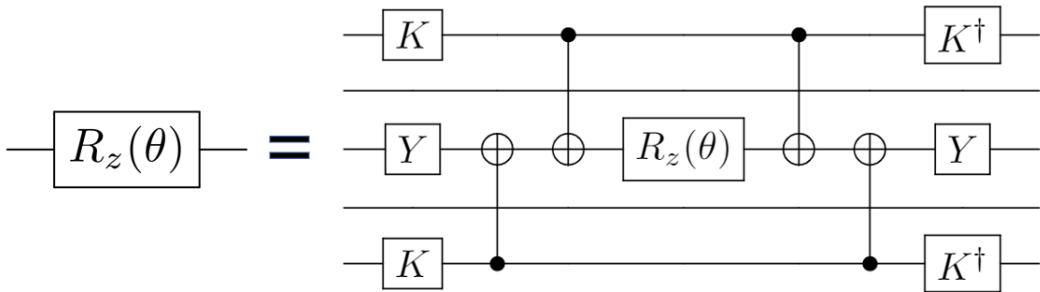


Figure 3.9: Logical  $R_z(\theta)$  implementation for the five qubit code by Yoder *et al.* Note that we use  $K = SH$ .

### Syndrome Measurement

First, note that state measurement can be done by measuring the logical Z operator, which serves as a parity check. Syndrome measurement was simulated non fault-tolerantly. Chao and Reichardt [8] give ways of measuring syndromes fault tolerantly using flags. the syndromes were extracted as in figure 3.10. Note that we use the sensor qubit as a measurement qubit, and so before the syndrome extraction we need to reset it to the ground state.

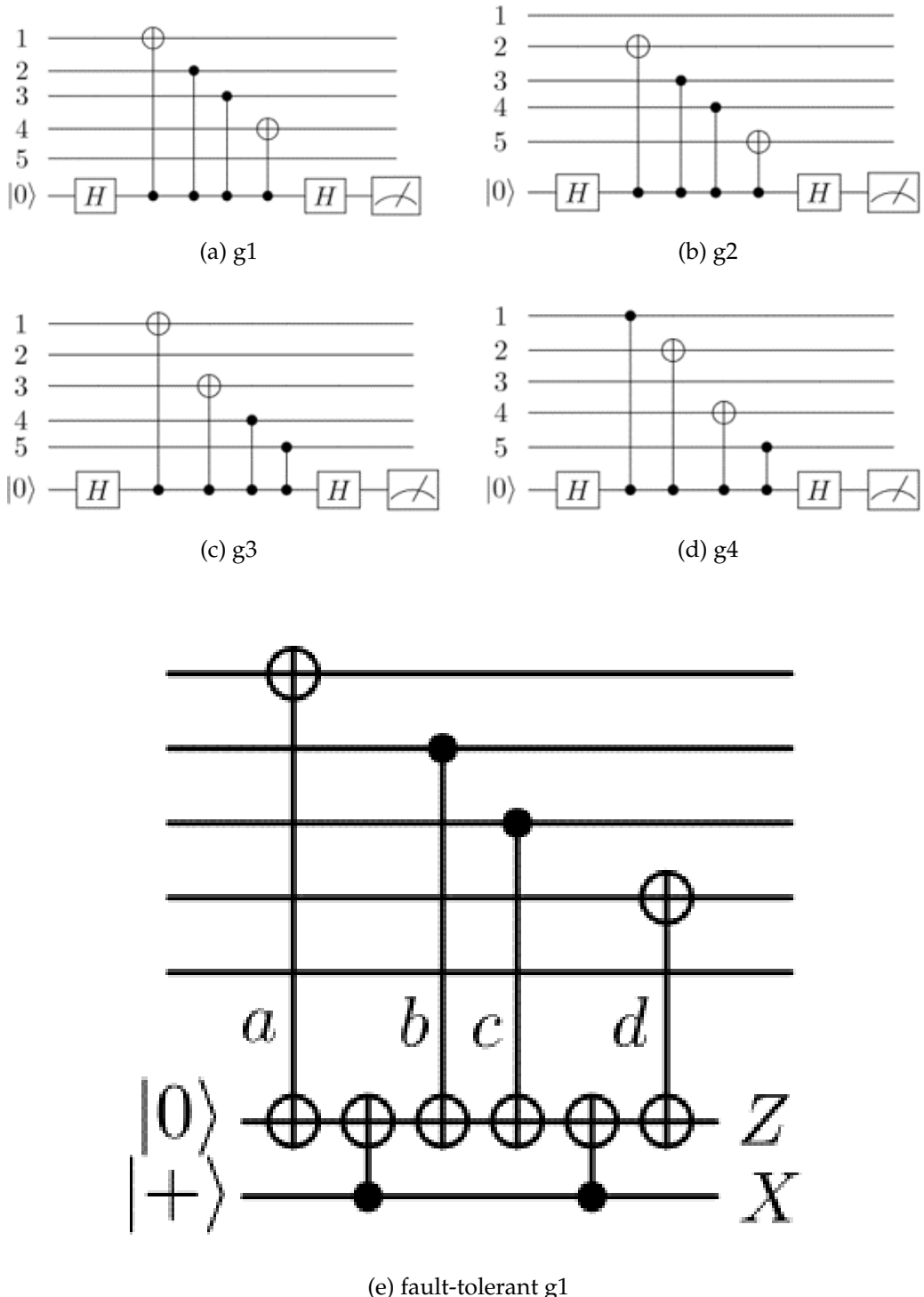


Figure 3.10: Syndrome extraction circuits for the five qubit code. (e) is a fault-tolerant example of extracting g1 syndrome from Chao and Reichardt.

### 3.5.2 LPS Simulation Methods

Up until now we have described in this Chapter how we simulate SPS ?? and how we simulate the general case of logical control 3.4.2. In this subsection we describe the simulations done in a big bulk of our research: Simulations of logical post selection for algorithmic quantum metrology, done by using Kitaev's iterative phase estimation algorithm (Kitaev's approach) and the iterative phase estimation algorithm (IPEA). The goal of those simulations is to find the circumstances in which algorithmic quantum sensing with logical ancillary qubits is better then the traditional approach, with physical ancillary qubits.

For this end we make a set of assumptions defining the rules of the game:

- All measurements are perfect, meaning there are no classical measurement errors. All errors are thus quantum.
- We study the effects of pure dephasing and relaxation independently, in each simulation we take one of  $T_2$ ,  $T_1$  to be infinite.
- We may assume 'good' qubits, meaning some qubits are much more resiliant to noise then others.
- We may assume doing SPS or not.
- We may assume that we have access to accelerated Hamiltonians, meaning we have available black boxes capable of performing controlled- $U^{2^j}$  operations for some positive integer  $j$  with high fidelity. Great study has been done by D.Aharonov on the subject of accelerated Hamiltonians [2, 6]. This can be achieved via situation-specific methods like applying a sensed magnetic field in different angles, or by

using general methods like QAQC [24], or VFF [12].

### Kitaev's Iterative Approach - With Accelerated Hamiltonians

Algorithmic quantum sensing using the quantum phase estimation algorithm is especially powerful under the assumption of accelerated Hamiltonians - having a black-box that can apply high powers of the time evolution operator with high fidelity. For our study we first assume accelerated Hamiltonians and we simulate one iteration of Kitaev's approach ?? (b), with logical post selection (LPS) and sensor post selection (SPS). We average over 10 angles uniformly distributed in the range  $[0, 2\pi)$  and calculate (after post selection) the fidelity with the state of the two-qubit quantum register after an ideal run right before the measurement (and thus assume a perfect measurement). We do that for three different algorithms:

- *Traditional* - The simple, two-qubit circuit for iterative QPE (Kitaev and IPEA). This algorithm requires 2 qubits.
- *Logical 1LPS* - Using physical sensor and one logical layer of ancilla. All non transversal gates are not fault tolerant. Logical Post Selection (LPS) happens once after the whole procedure. sensor post selection (SPS) happens once after the controlled operation. This algorithm requires 6 qubits.
- *Logical 1EC* - Same as the above, except an error correction step happens once after the syndrome measurement at the end of the iteration, adapted from table 1.2.

The results are plotted in figure ??, where we include the fidelity of the error-corrected state. Note that the error-corrected state shows a stochastic

behaviour, due to it's 'random' nature - a mistake in the syndrome extraction leads to the application of a faulty correction operator, and note that we have only one round of error correction in the circuit. In addition to the fidelity we define our 'Trace Distance' to be the distance from a perfect measurement:

$$D = \sqrt{(P_0 - P_0^{ideal})^2 + (P_1 - P_1^{ideal})^2} \quad (3.5)$$

Here we see an interesting result: there is a threshold of noise for which the logical control is better then using the traditional approach. The problem with this result is that it does not give any weight to the lost information, and one has to define a 'resource' and give the final results as a function of that resource. We follow [39] and set our resource to be the number of measurements done in one iteration to evaluate the probabilities correctly.

The relevant sizes for the problem are the ideal probability for the ideal circuit without noise  $P_i$ , the ideal probability for the noisy circuit  $P_n$  and the estimate to that probability  $\tilde{P}_n$  obtained by  $m = N(1 - li)$  successful trials, with  $li$  being the lost information obtained from equation 3.1 . We define the distance between the ideal circuit's probability and the noisy circuit's ideal probability by  $|d| = |P_n - P_i| = D/\sqrt{2}$ . Following reference [3] we demand that the error in estimating the ideal probability be confined, such that the probability that the algorithm succeeds is (by the addition rule for statistical and systematic errors)

$$Pr\left(\sqrt{|\tilde{P}_n - P_n|^2 + \frac{D^2}{2}} < \frac{2 - \sqrt{2}}{4}\right)$$

. This equals to

$$Pr\left(|\tilde{P}_n - P_n|^2 < \left(\frac{2 - \sqrt{2}}{4}\right)^2 - \frac{D^2}{2}\right)$$

So, the first conclusion is that the algorithm fails for  $T_2$  such that

$$D(T_2) > \frac{\sqrt{2} - 1}{2} \quad (3.6)$$

We conclude that the probability for the algorithm to fail (by applying Chernoff bound) is

$$\Pr(|\tilde{P}_n - P_n| \geq \sqrt{(\frac{2-\sqrt{2}}{4})^2 - \frac{D^2}{2}}) \leq 2e^{-2((\frac{2-\sqrt{2}}{4})^2 - \frac{D^2}{2})m}$$

and we demand that the probability to succeed is

$$\Pr(|\tilde{P}_n - P_n| < \sqrt{(\frac{2-\sqrt{2}}{4})^2 - \frac{D^2}{2}}) \geq 1 - \epsilon$$

This gives us a Minimum of

$$N > \frac{\ln(\frac{2}{\epsilon})}{2(1 - li(T_2))((\frac{2-\sqrt{2}}{4})^2 - \frac{(D(T_2))^2}{2})} \quad (3.7)$$

trials for the algorithm to succeed with probability of success  $p \geq 1 - \epsilon$ .

Overall we have assumed perfect measurements, accelerated hamiltonians, infinite relaxation time for all qubits, we did SPS and we assumed we have no access to good qubits.

### IPEA - Without Accelerated Hamiltonians

Our previous results show no advantage of using logical control for quantum sensing in the resource limited case, but those results are the product of a highly non-trivial assumption - that we have access to accelerated Hamiltonians. Here give up on this assumption and use the IPEA which has one huge advantage over Kitaev's iterative approach - given enough

trials, it has no condition to satisfy in order to succeed like equation 3.6. Instead, in the worst scenario it will give the output  $\phi = \pi \pm \pi$ . Meaning - This algorithm outputs a phase and a standard deviation.

Due to high simulation times we pick randomly the irrational phase  $\phi = 2\pi/\sqrt{3}$  and evaluate it for up to nine binary digits of accuracy, requiring a maximum of  $2^8 = 256$  consecutive applications of gates. Thus the maximum circuit depth we use, including syndrome extraction, is around 280 gates, approximately 10 times longer than the accelerated case.

In this part of the research we do only LPS (no SPS) and compare the traditional and the logically-assisted approaches, in three main scenarios:

- Perfect Sensor & Noisy Ancilla with Dephasing - We measure  $R_z(\frac{2\pi}{\sqrt{3}})$  with sensor qubit initialized in the excited state  $|1\rangle$ , assuming all qubits are susceptible to  $T_2$  noise with infinite  $T_1$ .
- Noisy Sensor & Perfect Ancilla with Dephasing - we measure  $R_x(\frac{2\pi}{\sqrt{3}})$  with sensor qubit initialized in the eigenstate  $|+\rangle$ , assuming perfect ancillas (with infinite  $T_1, T_2$  and allow only dephasing to occur to the sensor).
- Noisy Sensor & Perfect Ancilla with Amplitude Damping - Same as the above, but instead of infinite  $T_1$  we assume infinite pure dephasing rate  $T_2$  and allow  $T_1$  processes (which have some dephasing in them [27]).

Using IPEA here is comfortable since it gives us an assessment of the standard deviation of the phase, which is just the inverse of the extracted Fisher information [30]. We compare the standard deviation difference  $\sigma - \sigma_{ideal}$  for the traditional and the logical ancillas approaches, and we

define the standard deviation to be, in general,

$$\sigma = \frac{\sigma'}{\sqrt{N(1 - l_i)}} \quad (3.8)$$

Where  $\sigma'$  is the standard deviation of the histogram of phase results,  $N$  is the total number of trials and  $l_i$  is the lost information.

### 3.6 Measurement Errors

Now, we give an explanation of how we treat measurement errors. Suppose the probability of error in the measurement of one qubit is  $P_m$ . So for example if the state collapsed with projector  $P = IIII|0\rangle\langle 0|$ , we will get 1 in the measurement with probability  $P_m$ . The probability that there was some quantum error and yet we got ‘0000’ in the syndrome measurement is at most  $P_m P_Q$  where  $P_Q$  is the probability of a quantum error. Assuming this probability is small, we get  $P_m P_Q \ll P_m$  and so the real problem is not syndrome measurement, but the measurement of a digit at the end of the algorithm.

To overcome this **classical** error cause, we can use classical error correction techniques. Repeating the measurement (or the whole iteration) 3 times and taking majority vote, gives error with probability  $P_m^2(1 - P_m) + P_m^3 = P_m^2$ . Adding  $n$  layers of repetitions like so (overall  $3^n$  measurements) gives measurement error with probability  $P_m^{2^n}$ . In this technique, we beat measurement errors exponentially with the number of repetitions.

The above approach works fine in theory, but in practice we do care about the number of repetitions, and while we assume for simplicity that we have no measurement errors this problem remains an interesting question for future work.

# 4 Results

## 4.1 Sanity Checks for the Simulation

In this Chapter we show and analyze our results to the experiments (simulations) described in the last Chapter. First things first, in the next two subsections we show two sanity checks done to make sure the simulation acts right, in addition to the gate sanity checks that are plotted in figure A.3 of the appendices. In the third subsection of this section we describe our map from  $T_1$  and  $T_2$  of qubits to the worst-case gate fidelity.

### 4.1.1 $T_1$ & $T_2$ Extractions

Our simulation of decoherence is based on Krauss operators, and trotterization. Here we do  $T_2$  relaxation on the state  $|+\rangle\langle+| = \frac{1}{2}(\begin{smallmatrix} 1 & 1 \\ 1 & 1 \end{smallmatrix})$ , and expect to see that the state evolves under dephasing as

$$\rho(t) = \frac{1}{2} \left( \begin{smallmatrix} 1 & e^{-t/T_2} \\ e^{-t/T_2} & 1 \end{smallmatrix} \right) \quad (4.1)$$

We plot (fig.4.1 (a)) the coherence and see how close is the graph of  $\rho_{10}(t)$  to  $e^{-t/T_2}$ . Next we check our amplitude damping on the state  $|+\rangle\langle+| = \frac{1}{2}(\begin{smallmatrix} 1 & 1 \\ 1 & 1 \end{smallmatrix})$ , and we expect to see that the state evolves under amplitude damp-

ing as

$$\rho(t) = \frac{1}{2} \begin{pmatrix} 2 - e^{-t/T_1} & e^{-t/2T_1} \\ e^{-t/2T_2} & e^{-t/T_1} \end{pmatrix} \quad (4.2)$$

We plot (fig.4.1 (b,c,d)) all elements of the density matrix to see that they are well-behaved. Overall the decoherence simulation is as expected and plotted in figure 4.1

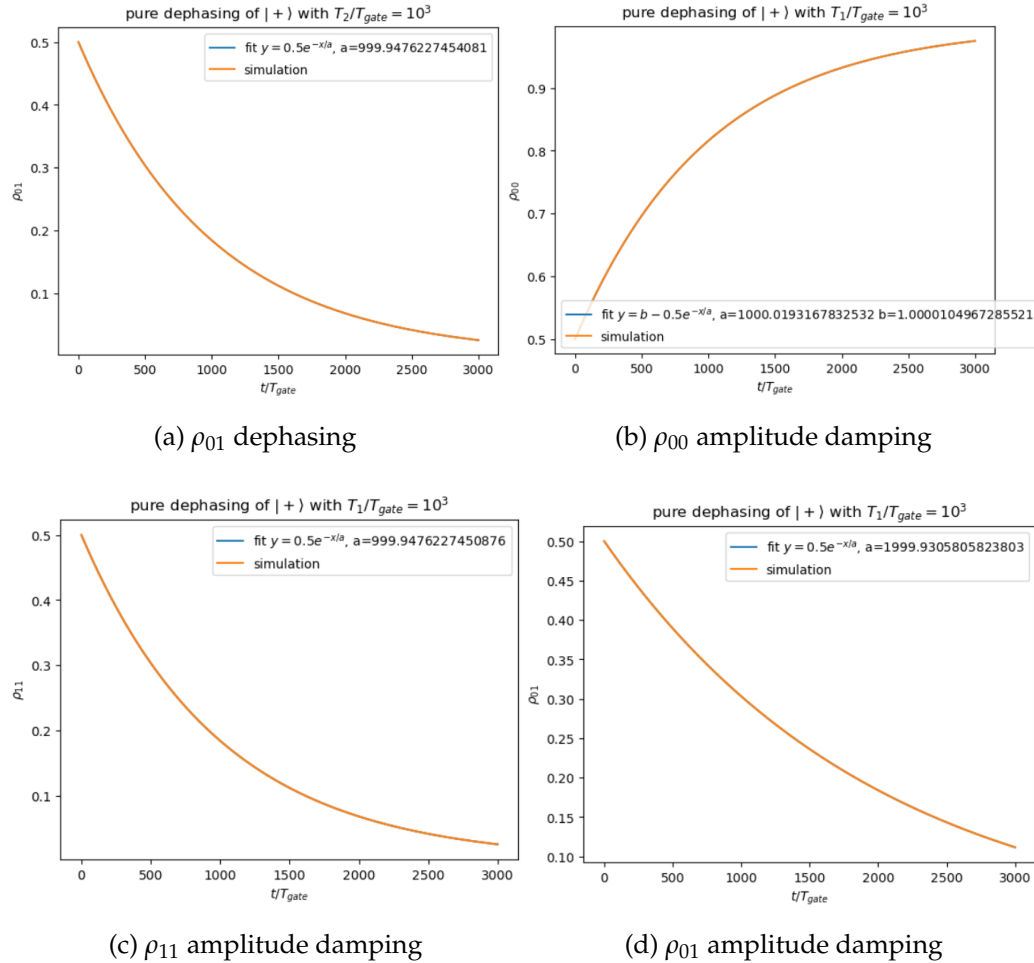


Figure 4.1: Relaxation for three decoherence times. Fit and simulation are the same.

### 4.1.2 Ramsey Experiment

. Another sanity check we do is implementing the Ramsey experiment as described in the introduction, 1, but in the presence of  $T_2$  noise. We do that for energy splitting  $\omega_0 T_{gate} = \pi/20$  and noise  $T_2/T_{gate} = 500$  and expect to measure the excited state  $|1\rangle$  with probability:

$$P(1) = \frac{1}{2}(1 + e^{-\frac{t}{T_2}} \sin \omega_0 t) \quad (4.3)$$

We collect data and perform a fit to the above probability. We expect the envelope to be  $\frac{1}{2}(1 \pm e^{-\frac{t}{T_2}})$  with  $T_2$  being approximately 500 and the data to oscillate with angular velocity of approximately  $\pi/20 = 0.157$ . The data and fits are plotted in figure 4.2 and act as expected, meaning our simulation is built properly.

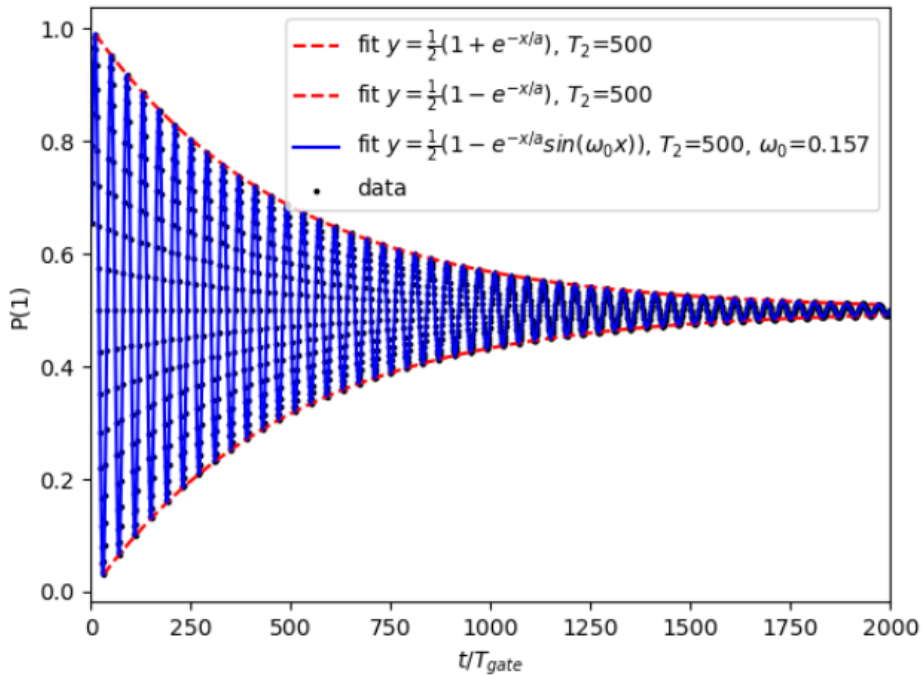


Figure 4.2: Simulation of Ramsey experiment with  $T_{gate}\omega_0 = \pi/20$  and  $T_2/T_{gate} = 500$ . Probability develops as equation 4.3.

### 4.1.3 From Decoherence to Gate Fidelity

For our study, we need a way to speak in the language of gate fidelity instead of in terms of  $T_2/T_{gate}$ ,  $T_1/T_{gate}$  where  $T_{gate}$  is the time required to apply the average gate. We study the effect of dephasing and amplitude damping independently, and so we create a map between the coherence times to the worst case gate fidelity, both for a single qubit and a two-qubit gates. For **dephasing** we set the qubit(s) in the (tensor product) state  $| + (+) \rangle$  and let them dephase for a varying time, and we then calculate the fidelity according to  $F = \sqrt{\langle +(+)|\rho| + (+)\rangle}$  assuming the end up in the density matrix state  $\rho$ . For **amplitude damping** we apply the same procedure, starting from the state  $|1(1)\rangle$  and calculating the worst case gate fidelity by  $F = \sqrt{\langle 1(1)|\rho|1(1)\rangle}$ . Both maps are available in figure 4.3.

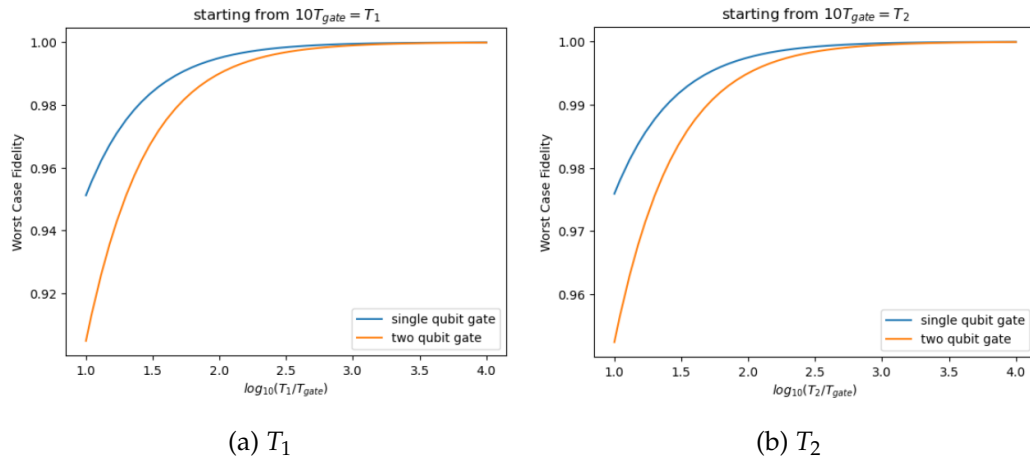


Figure 4.3: (a) ((b)) Maps from coherence times to worst case gate fidelity for single and two-qubit gates, extracted by putting the qubits in their most vonurable state to dephasing (amplitude damping) and letting them decohere.

## 4.2 Sensor Post Selection for Quantum Sensing

As discussed in section 3.3 post selection can sometimes be used to enhance the sensitivity of a quantum sensor. In this section we check whether or not this is the case for Kitaev's iterative approach of quantum phase estimation, for the simple sensor post selection schemes of figure 3.3.

Throughout this work we separate two scenarios:

- **Target: Accuracy** - In the presence decoherence, quantum phase estimation will converge (given an infinite amount of trials) to measurement probabilities  $P_0, P_1$  different from the ideal. In some cases we may be interested in getting this systematic error as low as possible, and we wouldn't care about how much information we have lost.
- **Resource: Minimal Number of Trials** - In other, more common scenarios of quantum sensing, the lost information and number of trials does play a role, and a strong evidence for that is the fact that sensitivity is often defined per root Hertz.

### 4.2.1 Target: Accuracy

In some cases when we are interested in measuring something, the number of measurements required is of no interest, and we aim to be as accurate as possible measuring the observable.

A simulation has been done as described in section 3.3.2, and the results are depicted in figure 4.4. As we can see and as expected, SPS helps with the cost of losing information. A weird phenomenon I cant explain right now is the existence of the threshold in which Single SPS is better than

Multiple SPS. And yet, the two methods perform much better than the traditional approach. Another interesting think to notice is the existence of a threshold for the trace distance, which represents the actual information that can be extracted from the state after measurements. This quantity is better for estimating algorithmic sensing performance and so in the next subsection we continue working with this quantity.

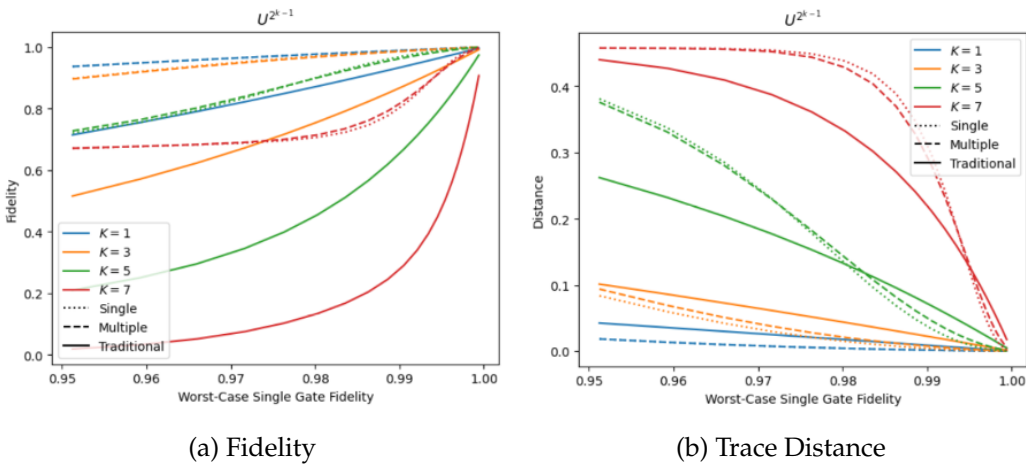


Figure 4.4: Kitaev Iterative QPE as in figure 3.3, without Hamiltonian acceleration. (a) Fidelity of the entire algorithm, (b) Trace Distance ( $\sqrt{\sum_i d_i^2}$  with  $d_i = \rho_{ii} - \rho'^{ii}$ ,  $\rho$  is noisy density matrix and  $\rho'$  is ideal density matrix) for the entire algorithm, (c) lost information for the entire algorithm.

### 4.2.2 Resource: Minimal Number of Trials

In this subsection our resource is the minimal number of trials required for Kitaev's algorithm ( $K = S$  for taking the worst case) to not fail according to equation 3.7, which is valid to any run of Kitaev's phase estimation with noise and lost information. Results are depicted in figure 4.5.

For  $K = 1$  we see no advantage for using SPS, and for any  $K$  higher the per-

formance in terms of the defined resource is getting worse and worse, as expected due to the high lost information caused by the big circuit depth.

To conclude, Sensor Post Selection as defined earlier does not help us in the common sensing scenarios but rather only in those we aim for accuracy at the expanse of measurement time.

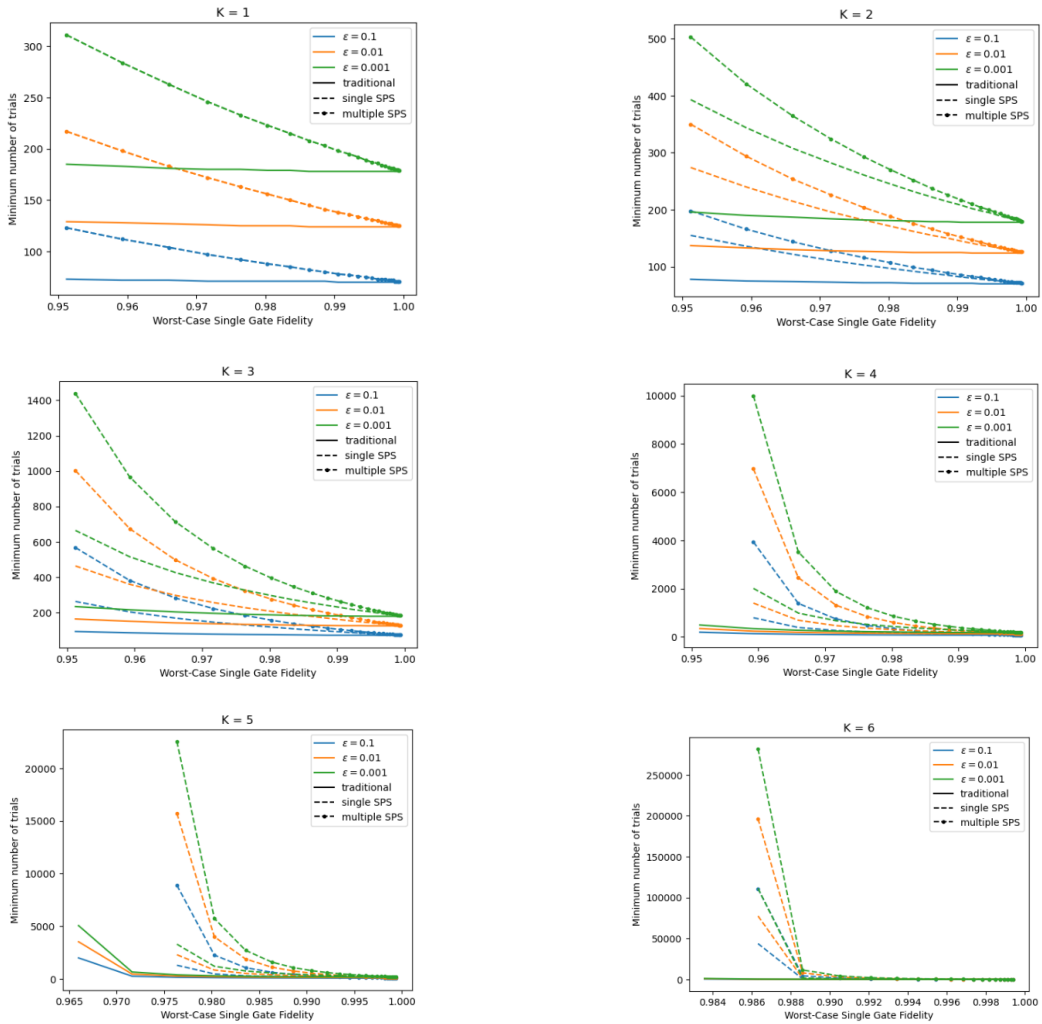


Figure 4.5: Minimal Number of Trials that is required for Kitaev's algorithm to work according to equation 3.7 is plotted for each value of  $K$  from 1 to 6, where we raise the measured operator to the power  $2^{K-1}$ .

## 4.3 Logical-Physical Interaction - General Numeric Exploration

In the previous section we have explored the use of sensor post selection for algorithmic quantum sensing. We saw that for some needs it might help and for others it can only harm. This section and the next focuses on mapping the world of logical post selection in the presence of noise, finding scenarios in which it might be helpful to use logical post selection and pointing at the ones where it is not.

In this section we require insights on the general use of logical-physical interaction, in terms of the circuit's depth (or it's number of entangling gates,  $N_{gates}$ ) and the qubit's decoherence time  $T_2$ , which translates to worst-case gate fidelity as described in section 4.1.3. A simulation has been performed as described in section 3.4.2.

So, for what number of entangling gates does the logical control contribute? does this number even exist? Picking a constant  $T_2/T_{gate}$  ratio we can depict (fig.4.6 (c)) the fidelity as a function of the number of entangling gates. We can see that for each gate fidelity, it is always better to use traditional CNOT gate when we have to apply only one such gate. But there is a range of number of gates in which it is better to use logical control (fig.4.6 (c)). This range stops at some point, in which the gate overhead is not profitable. The cost, the amount of lost information, is large, and depicted in fig.4.6 (b). Looking at fig.4.6 (c), we suspect that for infinitely good gates, using logical control is better for infinitely deep circuits.

A similar graph is extracted for constant number of CNOT gates  $N_{gates}$ , and varying  $T_2/T_{gate}$  ratio, and depicted in figure 4.7 (c). We can see that

for each number of gates, there is a threshold of worst case single gate fidelity for which the logical gadget is better than the traditional approach. This threshold was extracted and depicted in fig.4.7 (a), and we can see it extracts the same graph as in fig.4.6 (a). Here as well, the cost (lost information) is high and depicted in figure 4.7 (b).

Finally, a three dimensional view of the above is depicted in figure 4.8. Although this simulation is done for varying  $T_2$ , we expect similar behaviour for  $T_1$  noise. We remind that these results were obtained with gate overhead of about 20 gates for syndrome extraction, and that they were obtained for both noisy logical and physical qubits, and thus we expect the following limit behaviour:

- Noisy Physical & Perfect Logical - logical control will always be better starting from a certain circuit depth.
- Perfect Physical & Noisy Logical - logical control will never improve the fidelity. Adding noisy sources shouldn't help, intuitively.

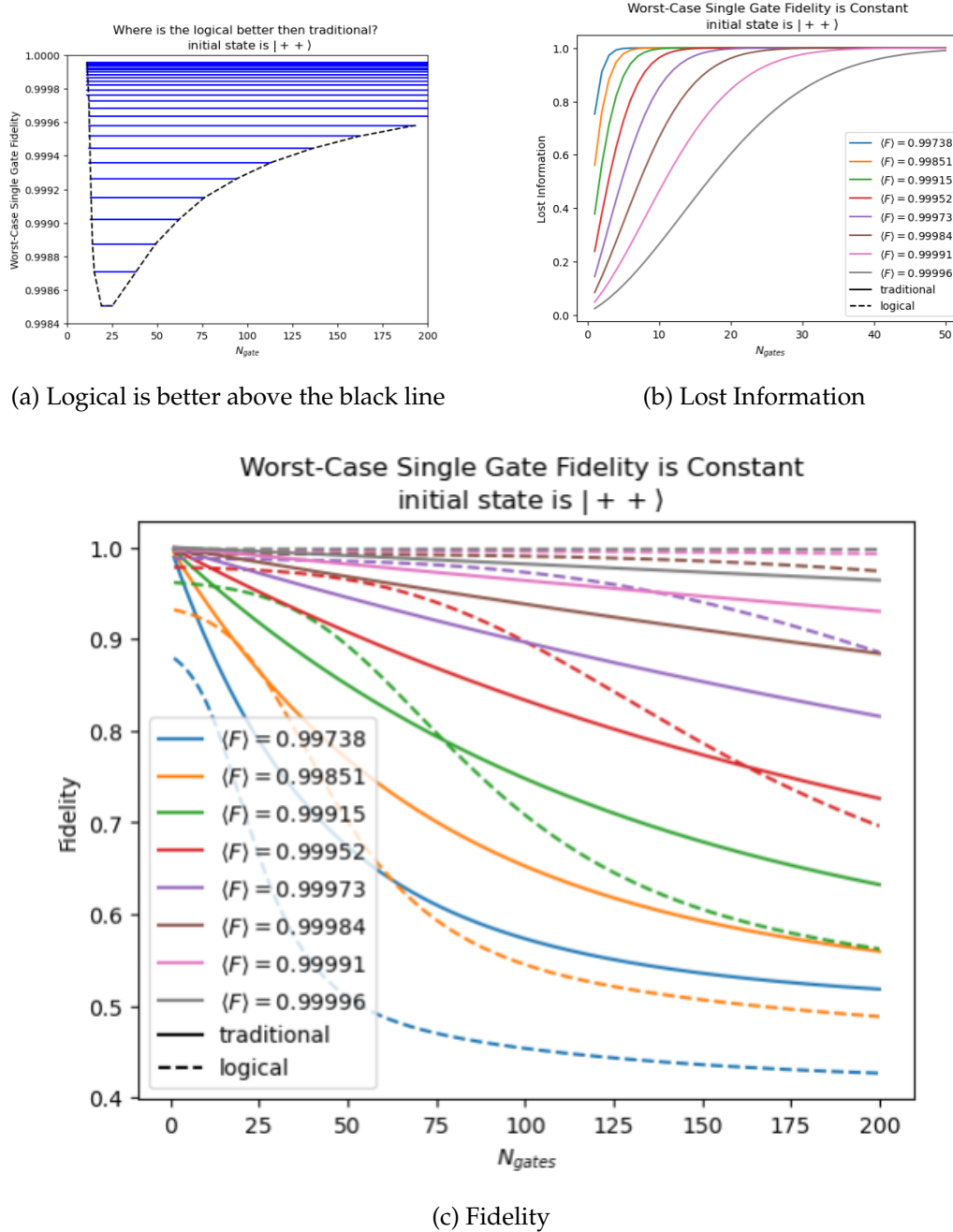


Figure 4.6: Simulation of logical CNOT gate compared to the traditional CNOT gate, for a varying number  $N_{\text{gates}}$  of CNOT gates and constant  $T_2/T_{\text{gate}}$  ratio.

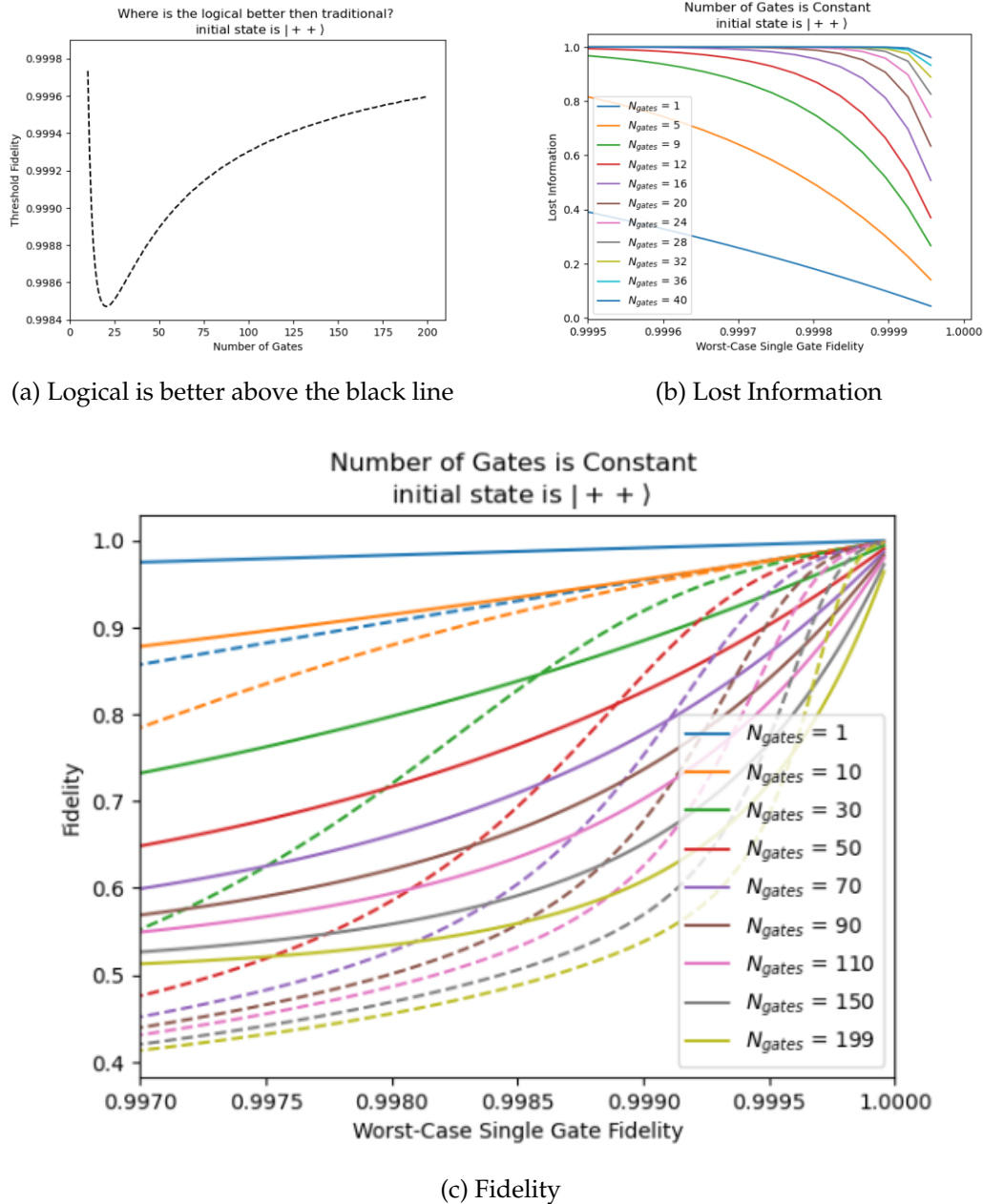


Figure 4.7: Simulation of logical CNOT gate compared to the traditional CNOT gate, for a varying  $T_2/T_{gate}$  ratio and a constant number  $N_{gates}$  of CNOT gates.

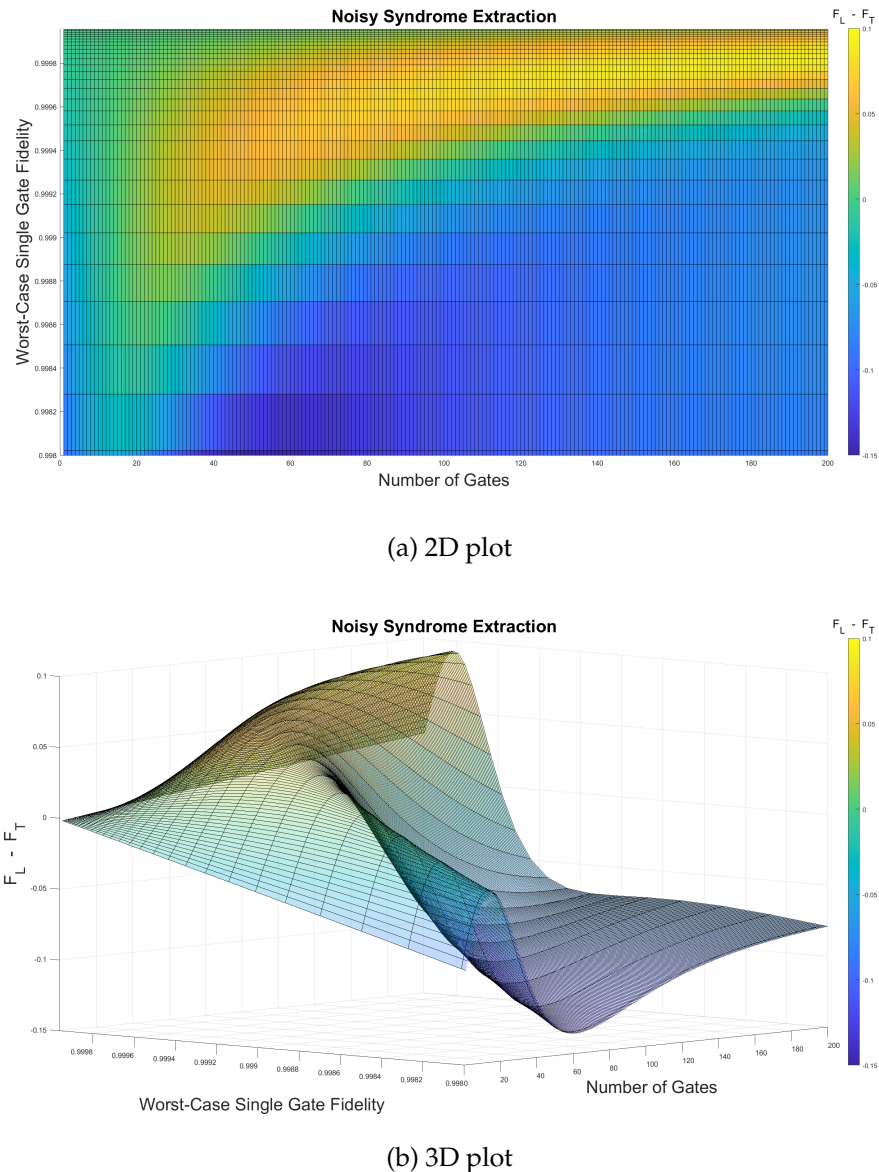


Figure 4.8: Simulation of logical CNOT gate compared to the traditional CNOT gate, for a varying number  $N_{gates}$  of CNOT gates and a varying  $T_2/T_{gate}$  ratio.

## 4.4 Logical Post Selection for Quantum Metrology

In the last section we have numerically explored the behaviour of logical control and logical post selection under the change in circuit depth and gate fidelity, taking both the logical qubit (ancilla system) and the physical qubit (sensor) to be noisy. We got an interesting result: for each gate fidelity, there is a range of circuit depth's where introducing logical ancillary system improves the fidelity of our circuit under the presence of noise which causes a systematic error in the system's state.

In this section we demonstrate a version of this result in the case of algorithmic quantum sensing. We seek to find circumstances in which using logical acilla may improve sensing results, and to point on the situations where it wouldn't. In the following subsection we briefly show that for our cause, of sensing with accuracy, it will always be better to use the non-fault-tolerant implementation of state preparation. Then, in the two subsequent subsections we separate our research to two main scenarios: having access to accelerated Hamiltonians, and not having it. Observing the improved scaling of the error probability for the Kitaev circuit with  $K = I$  is made possible due to the natural transversality of the circuit.

### 4.4.1 Gate Selection

Here we briefly show two simulations of the state preparation procedure - comparing both non fault-tolerant and faulty-tolerant implementations, with and without logical post selection on the result. The simulations are

depicted in figure 4.9, and we can easily see that in no circumstances it is better to use the fault-tolerant implementation if we are interested in maximizing the fidelity. The fault-tolerant implementation is of importance only for long computations where it is likely an error occurred before the entangling CZ gates, to stop the error from propagating, in this case we deal with big circuit depth's in which the depth of state preparation is negligible, thus allowing us to neglect errors occurring at this stage.

Note that we simulate both for only flag measurements and flag measurements along with logical post selection. Both scenarios point us towards the non fault-tolerant implementation.

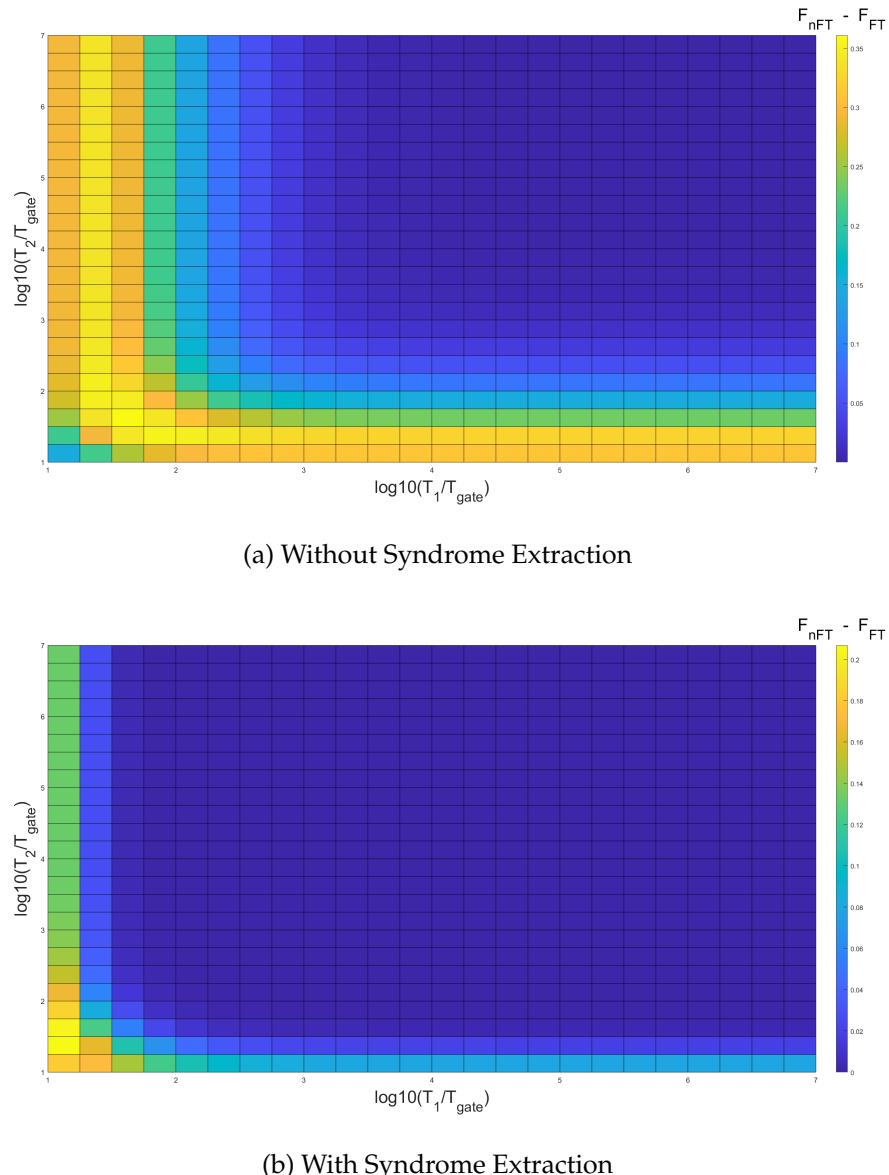


Figure 4.9: Mapping the fidelity difference between the the non fault tolerant and the fault tolerant implementations of state preparation, 3.5

#### 4.4.2 Kitaev's Approach - with Accelerated Hamiltonians

As mentioned in section 3.5.2, algorithmic quantum sensing is especially powerful under the assumption of accelerated Hamiltonians. We state again our assumptions for this section:

- All measurements are perfect
- There is no energy relaxation, only dephasing:  $T_1 \approx \infty$
- Sensor post selection is being used
- We have access to accelerated Hamiltonians
- We assume no good qubits - all qubits decohere

Although we assume no good gubits, we measure here the operator  $R_z(\theta)$  and we put the sensor qubit in its ground state,  $|0\rangle$ . Dephasing does not affect this state, and we assumed no energy relaxation, so in practice we assume a perfect sensor and noisy ancilla. Thus, intuitively, we expect no improvement whatsoever. Our only hope is the non intuitive nature of quantum mechanics.

Data collection has been made as described in section 3.5.2 for Kitaev's approach. As in section 4.2 we separate our results to two scenarios, caring of accuracy for the following part or efficiency for the subsequent one.

##### **Target: Accuracy**

Two interesting phenomena occur in figure 4.11:

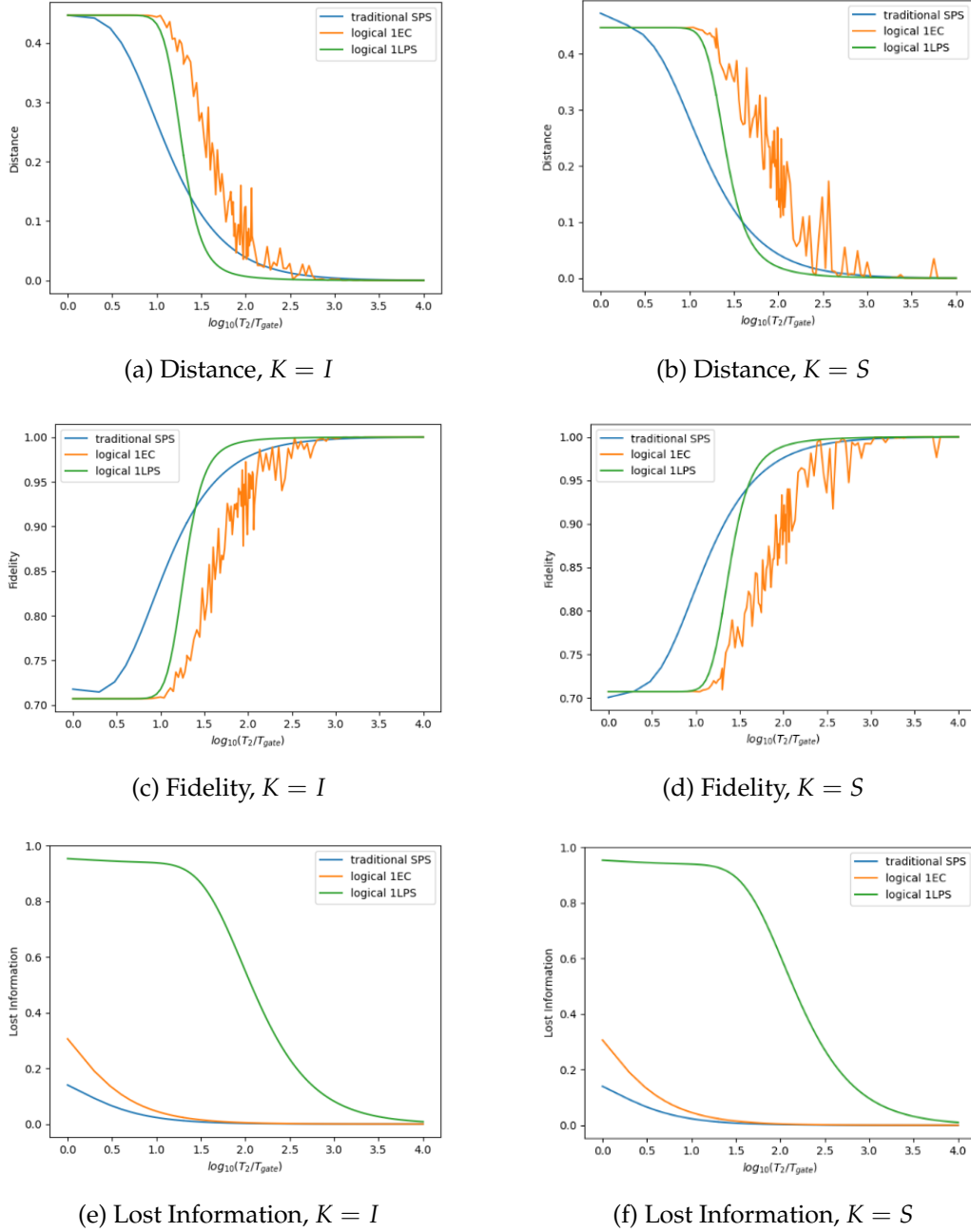


Figure 4.10: Simulation of the logical and traditional Kitaev circuits, averaged over 10 angles evenly distributed in the range  $[0, 2\pi)$ . Simulation is done for decay time of  $T_1 = \infty$ , and eigenvector  $|\psi\rangle = |0\rangle$ .

First, counter intuitively, we get a threshold for which logical control is better than physical control. This is counter intuitive because only the ancillas are noisy. Apparently, there are circumstances in which it is better to use five noisy ancillas than only one noisy ancilla. The thresholds are summarised in table 4.1

Fidelity	$T_2/T_{gate}$	Worst-Case Single Gate Fidelity	Worst-Case Entangling Gate Fidelity
$K = I$	24	0.99	0.98
$K = S$	40	0.994	0.987

Table 4.1: Thresholds for Accelerated Hamiltonian from the data of figure 4.11

Surprisingly, these thresholds are well below [22] the achievements of today's state of the art technology! Thus, for the purpose of accurate sensing, with infinite sensing time, using logical post selection is the better approach for the NISQ era.

The second interesting we can see in these graphs is that the error-corrected algorithm is stochastic. Earlier we explained it is the result of a faulty error detection. This random faulty detection projects the system's state to one with 100% error, and then applies a faulty 'correction operator', which might make the state even further than the ideal. This behaviour is not seen when using logical post selection, because in this scenario we project to a state which includes no error at all.

## Resource: Minimal Number of Trials

Here we use the same procedure as in section 4.2.2, plotting the minimal number of trials needed for the algorithm to work correctly. Two equations are of great importance here: equation 3.6 giving the  $T_2$  threshold for which the algorithm fails entirely, and equation 3.7 giving the minimal number of trials required for the algorithm to work, given  $T_2$  is below the threshold determined by equation 3.6.

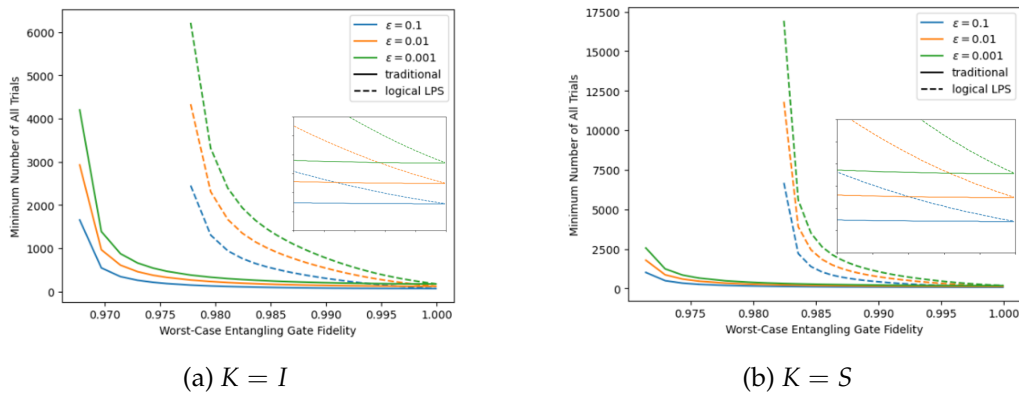


Figure 4.11: Minimal number of trials required for Kitaev’s algorithm to work under  $T_2$  noise and  $R_z$  measurement. Algorithm fails according to equation 3.6 below the plotted fidelities.

As in the sensor post selection case, logical post selection here only spoils the results due to the high percentage of information lost. The following part of our study will focus on finding the circumstances in which logical post selection is helpful even in the resource limited scenarios.

### Confirming New Error Probability Scaling

Going back a few steps to section 3.4.1, Kitaev's phase estimation circuit with  $K = I$  is almost fault-tolerant - the only non fault tolerant part of it is the first one, the state preparation. Thus we can use this circuit to approximate a fit to the scaling of the error probability after logical post selection. We do logical post selection after the whole iteration, and thus we need to consider the error probability as the probability a single error occurred in a single qubit throughout the whole iteration. Due to the circuit's transversality this error will not propagate to other qubits. We extract the error probability according to

$$P_{error} = 1 - F^2 \quad (4.4)$$

With  $F$  being the calculated fidelity of figure 4.11. We see in figure 4.12 that indeed the best approximation to the scaling is not a forth or a second degree polinomial, but a third degree polinomial - as predicted by our calculations.

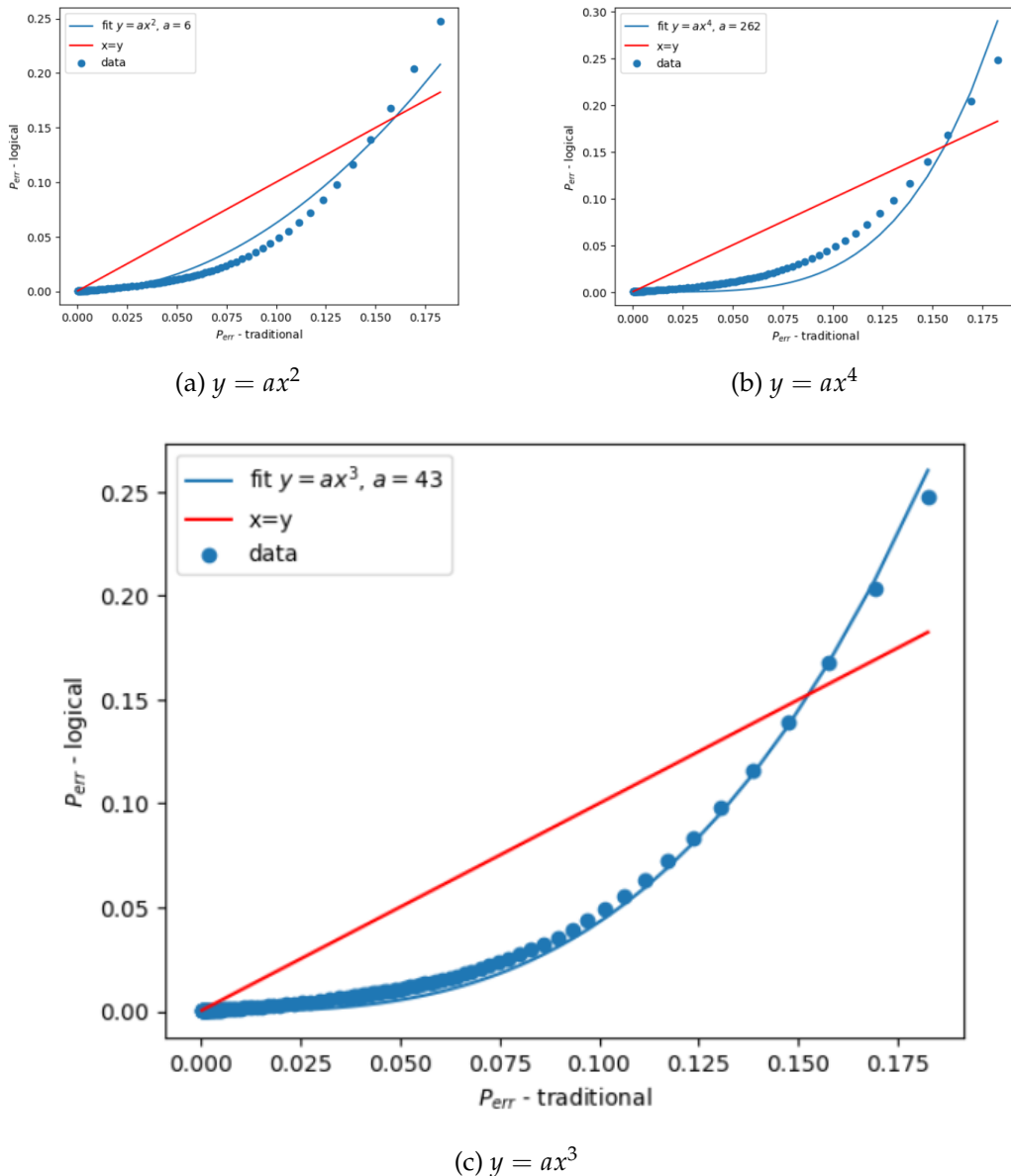


Figure 4.12: Confirming the error probability as predicted by equation 3.3.  
Error probability extracted from fidelity according to equation 4.4.

### 4.4.3 IPEA - without Accelerated Hamiltonians

Up until now we had a strong assumption on the rules of the game - we had access to accelerated Hamiltonians. From this point forward, we give up on that assumption. Here we choose to work with the Iterative Phase Estimation Algorithm (IPEA), due to it's advantage over Kitaev's approach - it can not fail. the IPEA will output two numbers - the estimation for the phase, and the standard deviation (the error) of that estimation. We note that one iteration of IPEA is not that different then one iteration of Kitaev's algorithm - the only difference is the location of the phase kick within the circuit.

Estimating whether or not logical post selection is better then the traditional approach using this algorithm is optimal since here we consider all required iterations to estimate the phase up to some precision, in contrast to the previous work that compared only one iteration. This was possible due to the accelerated Hamiltonian, making all iterations look the same after averaging on different phases.

We simulate according to section 3.5.2, and state again our assumptions in table 4.2 on this simulation according to the results in figures 4.13, 4.14, 4.15.

We see in figure 4.13 that giving up the assumption of accelerated Hamiltonians is not enough, and we need to further assume access to 'Good' qubits - qubits with long coherence and relaxation times. We do that and the amazing results are plotted in figure 4.14, showing an absolute win for the logical method for circuit depths greater then about 50 gates, and for some fidelity threshold. We check the same situation for the more vulnerable case (figure 4.15) with  $T_1$  from initial sensor state  $|+\rangle$  which exhibits

both energy relaxation and dephasing processes. In this scenario as well we see a win for the logical algorithm, for a certain range of gate fidelities and circuit depths. A similar scenario, where the sensor is put in the excited state and is susceptible to  $T_1$  noise, with perfect ancillas, measuring  $R_z(\frac{2\pi}{\sqrt{3}})$  is depicted in figure 4.16. In both scenarios we see a threshold of approximately 0.998 worst case single gate fidelity.

Figure 4.13	Figure 4.14	Figure 4.15	Figure 4.16
Perfect Measurements	Perfect Measurements	Perfect Measurements	Perfect Measurements
$T_1 \approx \infty$	$T_1^{sensor} \approx \infty,$ Perfect Ancillas	$T_2^{sensor} \approx \infty,$ Perfect Ancillas	$T_2^{sensor} \approx \infty,$ Perfect Ancillas
No SPS	No SPS	No SPS	No SPS
No Accelerated Hamiltonian	No Accelerated Hamiltonian	No Accelerated Hamiltonian	No Accelerated Hamiltonian
$\rho_0 =  1\rangle$	$\rho_0 =  +\rangle$	$\rho_0 =  +\rangle$	$\rho_0 =  1\rangle$

Table 4.2: Assumptions for the simulations of this section

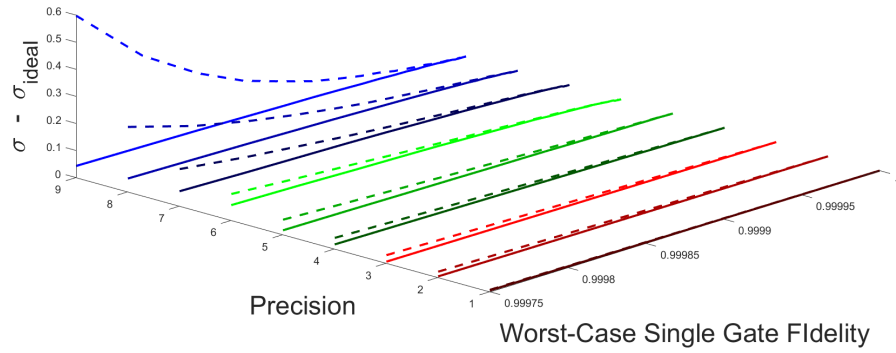
**Good Sensor & Noisy Ancilla**

Figure 4.13: Measuring  $R_z(\frac{2\pi}{\sqrt{3}})$  with  $T_1 \approx \infty$  and noisy ancilla, with the Iterative Phase Estimation Algorithm. Dotted line is the logical control, and continuous line is traditional control.

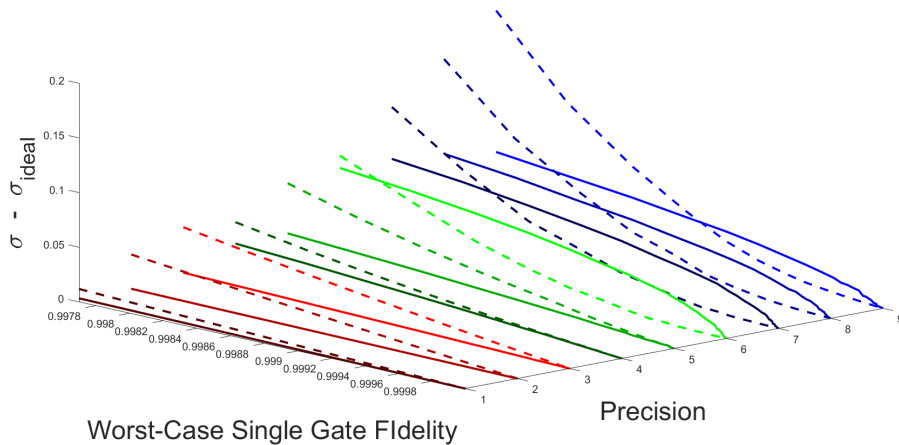
**Noisy Sensor & Good Ancilla &  $T_2$** 

Figure 4.14: Measuring  $R_x(\frac{2\pi}{\sqrt{3}})$  with dephasing sensor and perfect ancilla, with the Iterative Phase Estimation Algorithm. Dotted line is the logical control, and continuous line is traditional control.

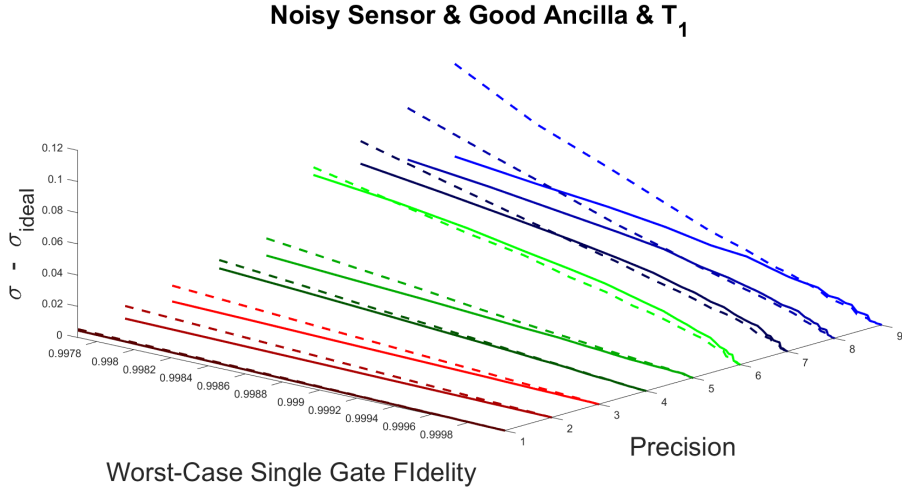


Figure 4.15: Measuring  $R_x(\frac{2\pi}{\sqrt{3}})$  with relaxing sensor ( $T_1$  noise according to section ) and perfect ancilla, with the Iterative Phase Estimation Algorithm. Dotted line is the logical control, and continues line is traditional control.

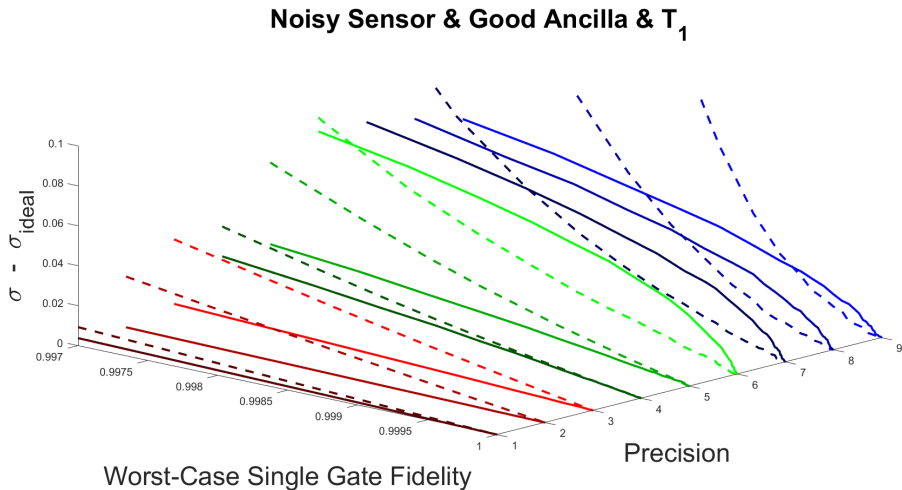


Figure 4.16: Measuring  $R_z(\frac{2\pi}{\sqrt{3}})$  with relaxing sensor ( $T_1$  noise according to section ) and perfect ancilla, with the Iterative Phase Estimation Algorithm. Dotted line is the logical control, and continues line is traditional control.

## 5 Conclusion & Outlook

We have introduced the concept of logical-physical qubit interaction and found when it is beneficial to use this kind of interaction, as a function of the number of entangling gates and the worst case single gate fidelity, under the presence of dephasing and amplitude damping being the most significant causes of error [10, 45]. We have used our idea to show an improvement for algorithmic quantum sensing, by encoding the noise into a bigger Hilbert space and post selecting the purified state. Although the gate fidelities needed for the method to contribute to Heisenberg-limit scaling are far beyond the reach of today's state-of-the-art technology, we have witnessed situations in which using logical post selection leads to more precise measurements. The concept of hybrid logical-physical interaction is an exciting and wide new frontier. We think the concept of logical control and logical post selection can be efficient in a big number of algorithms and purposes, especially ones that require a long-lived ancilla qubit like state distillation, error mitigation and algorithmic sensing [Czarnik et al., Piveteau et al.]. The most significant drawback of the method is the lost information due to post selection, and recent studies show promise to discover a method of simulating without the need for post selection [20]. This new idea opens a wide set of questions to be

asked, like what is the way to implement a CNOT between a logical and physical qubits with minimum error or error propagation? Can this interaction be done in a fault-tolerant manner? We have defined an attribute of quantum error correction codes that enables this kind of interaction. What other attributes are there, and how do they project on the topology of the interaction or on the general structure of these QECC? Can it be implemented with today's most promising codes, the surface codes [16]? And although it cannot be made universal by transversality [46], can it be made fault-tolerant using flag fault-tolerance? [8, 9, 35, Tansuwannont et al.].

# A Code Guide

## A.1 About

The simulation of quantum circuit comprising of individual qubits is a subject under study. A tool for simulating quantum circuits with decoherence (energy relaxation and dephasing) is hard to find, especially with precise control over the qubit's decoherence times  $T_1$ , related to energy relaxation, and  $T_2$ , related to dephasing. This is a documentation on the basic tool written for my thesis research, with a few examples on how to use it. This package includes the basic simulation tool for noisy or ideal circuits, and notebooks that re-create the results of my research. The documentations includes some basic examples of how to use the tool.

## A.2 Installation

### A.2.1 required packages

- Numpy
- QisKit (will not be required in future work)

- QuTiP
- SciPy

## A.2.2 Download

All relevant code is open for use in this GitHub repository or in the following url: <https://github.com/nadavcarmel40/thesis>.

To install and use the package, just install QuTiP (<https://qutip.org/docs/latest/installation.html>) by following the instructions on the above web page.

The basic tool enabling the simulations can be found under the ‘simulators’ folder in the attached GitHub repository. ‘BigStepSimulator’ is a state-vector simulator and ‘SmallStepSimulator’ is a density matrix simulator. The state vector simulator is fast and can simulate quantum circuits without noise, and the density matrix simulator is slower and can simulate noisy circuits.

## A.3 The Simulators

The basic tools created for my project are the simulators. They are constructed with the same user interface, so this documentation will show examples with the density matrix simulator but is relevant for both.

### A.3.1 Creating a Quantum Register

The first and most basic step of every simulation is the creation of the underlying quantum register. This subsection is a walk-through of how to create this register.

Here we will introduce the set of parameters that define the quantum register:

- The register is built from  $N$  qubits, that can interact and be entangled with each other.
- The register starts from some state (which is a density matrix - a positive semi-definite hermitian matrix with trace one) in the  $N$ -qubit Hilbert-Space,  $\rho_0 \in M_{2^N, 2^N}(\mathbb{C})$ .
- Each qubit  $q$  has the amplitude-damping time  $T_1^q$ . If all qubits have the same  $T_1$ , we can just pass the parameter  $T1$ . Else, we set  $T1$  to some unimportant constant and pass the Python list of amplitude damping times, ordered as are the qubits, as the parameter  $T1s = [T_1^0, \dots, T_1^N]$ .
- Each qubit  $q$  has the pure dephasing time  $T_2^q$ . If all qubits have the same  $T_2$ , we can just pass the parameter  $T2$ . Else, we set  $T2$  to some unimportant constant and pass the Python list of pure dephasing times, ordered as are the qubits, as the parameter  $T2s = [T_2^0, \dots, T_2^N]$ .
- The simulation works with finite size time steps, each of length  $dt$ . Default is  $10^{-4}T_1$  assuming all qubits have the same  $T_1$ .
- Another important parameter is the time it takes to apply a single

gate,  $T_{gate}$ . We usually take this time to be '1' in arbitrary units, and work in the units of this time. default is  $20 * dt$ .

- The last parameter required to define a quantum register is a list of all of the qubit's frequencies. Default is 6[GHZ] for all qubits, and this essentially has no impact on the simulation results. The difference is whether or not to work in the qubit's rotating frame.

So, if we want to create a quantum register, we first need to import the relevant classes:

```
from qutip import *
from simulators.BigStepSimulation import \
    EfficientQuantumRegister
from simulators.SmallStepSimulation import \
    InCoherentQuantumRegister
```

And to create a register comprised of  $N = 2$  qubits starting from the state  $\rho_0 = | + 1 \rangle$  with  $T_{gate} = 1$ ,  $T_1/T_{gate} = 10^3$  and  $T_2/T_{gate} = 10^4$  for both qubits, with  $dt = T_{gate}/20$ , we can run the following code block:

```
plus = 1/np.sqrt(2)*(fock_dm(2,0) + fock_dm(2,1))
rho0 = tensor([plus, fock_dm(2,1)])
register = InCoherentQuantumRegister(2, rho0, 1e3, 1e4, \
    Tgate=1, dt=1/20)
```

Or if we want to initialize the register such that qubit 2 has different lifetimes from qubit 1, we can initialize it like so:

```

T1s = [1e3,2e3]
T2s = [1e4,3e4]
qr = InCoherentQuantumRegister(2,rho0,None,None,T1s=T1s,\ 
                                T2s=T2s,Tgate=1,dt=1/20)

```

We can also control all decoherence related parameters of the register via the function 'setError(self, dephase=True, amplitude\_damp=True, T1s=None, T2s=None)'. It enables us to switch  $T_1, T_2$  processes on and off, and updates the qubit's lifetimes. For example, if we want to switch amplitude damping off, we can just run:

```
qr.setError(amplitude_damp=False)
```

Some important and useful attributes of the quantum register are:

- self.state - The state of the register. Can be accessed any time.
- self.qI - The identity matrix of the register
- self.dt, self.Tgate - The times defining how big are the time steps of the simulation. Can be changed, for example, before and after the activation of some gates if one wants to make them last a different amount of time, or have better or worse trotterization.
- self.dephase, self.amplitude\_damp - Boolean values that can be changed if we want to switch  $T_1, T_2$  processes on and off.
- self.Sx, self.Sy, self.Sz - Lists of the Pauli operators acting on the register's qubits. For example, self.Sx[q] is the Pauli-X operator acting on the qubit 'q'.

### A.3.2 Simulating a Quantum Circuit

Now, we can run a simple quantum circuit on the quantum register we have just created. All quantum circuits are passed to the register as a list of commands, each command is a physical command acting on a physical qubit. The list of commands is built in a logical way and can be understood easily by looking at figure 3.2, describing a general simulation of gates.

The commands is a list containing all big time steps T, in each one a number of different gates can be acted upon the register. Each of these lists is a list itself, containing all gates acting at that moment. Each gate can be represented as a tuple object, in the form ('c',q<sub>1</sub>,q<sub>2</sub>,operator).

'c' is the command. It can be one of the Strings:

$$C \in \{i, X, Y, Z, H, CNOT, CZ, Rx, Ry, Rz, SingleQubitOperator, m\}$$

Note that every controlled operator can be constructed as a series of CNOTs and single qubit gates be Nielsen and Chaung.

'q<sub>1</sub>' is the qubit the operator is acted upon.

'q<sub>2</sub>' is the control qubit in a two-qubit gate (Else, None).

'operator' is some extra information needed for the gate. It can be:

- None for defined gates (H,X,Y,Z,CNOT,CZ).
- Angle for Rotations (Rx,Ry,Rz) in Radians.
- Number of gates to wait (int) for the identity gate 'c'='i'.
- A 2x2 Numpy or QuTiP matrix for general single qubit operator.

For example, creating a quantum register of two qubits starting in the |00⟩ state, and creating the bell state A.1, can be simulated using the simple code block:

```

T1s = [1e3,2e3]
T2s = [1e4,3e4]
rho0 = tensor([fock_dm(2,0),fock_dm(2,0)])
qr = InCoherentQuantumRegister(2,rho0,None,None,T1s=T1s \
, T2s=T2s, Tgate=1, dt=1/20)
qr.run([(H,0,None,None)],[(CNOT,1,0,None)])

```

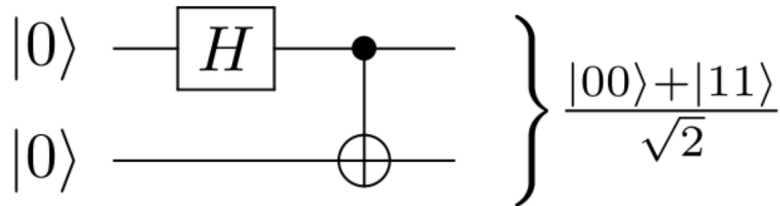


Figure A.1: The Bell State

### A.3.3 Visualizing The State History of a Qubit

Here we will show two sanity checks for the simulation, confirming that the decoherence is correct and that all defined gates act as we expect them to. For this purpose we will simulate a noisy register of only one qubit, and we will introduce some new attributes of the quantum register.

#### Confirming Decoherence

Here we do  $T_2$  relaxation on the state  $|+\rangle\langle+| = \frac{1}{2} \begin{pmatrix} 1 & 1 \\ 1 & 1 \end{pmatrix}$ , and expect to see that the state evolves as  $\rho(t) = \frac{1}{2} \begin{pmatrix} 1 & e^{-t/T_2} \\ e^{-t/T_2} & 1 \end{pmatrix}$ . we plot (fig.A.2 (a)) the coherence and see how close is the graph of  $\rho_{10}(t)$  to  $e^{-t/T_2}$ .

The simulation is done by executing the code block below. A similar code, setting 'dephase'=False and 'amplitude\_damp'=True can simulate energy relaxation on the state  $|+\rangle\langle+| = \frac{1}{2}(\begin{smallmatrix} 1 & 1 \\ 1 & 1 \end{smallmatrix})$ , and we expect to see that the state evolves as  $\rho(t) = \frac{1}{2}(\begin{smallmatrix} 2-e^{-t/T_1} & e^{-t/2T_1} \\ e^{-t/2T_2} & e^{-t/T_1} \end{smallmatrix})$ . We plot (fig.A.2 (b,c,d)) all elements of the density matrix to see that they are well-behaved. Overall the decoherence simulation is as expected and plotted in figure A.2

```
def get_rho_from_bloch(x,y,z):
    """
    (x,y,z) is point in bloch sphere.
    returns density matrix
    """
    return 0.5*qeye(2) + x/2*sigmax() + y/2*sigmay() \
        + z/2 * sigmaz()

import matplotlib.pyplot as plt
from scipy.optimize import curve_fit

plus = 1/np.sqrt(2)*(basis(2,0)+basis(2,1))
T2 = 1000
qubit = InCoherentQuantumRegister(1,plus*plus.dag())\
    , T1=1, T2 = T2, Tgate=1, dt = 1/20)
qubit.setError(dephase = True, amplitude_damp=False)
qubit.setCollectData(data = True, bloch=True)
qubit.run([[('i', 0, None, 3000)]])
xs, ys, zs = qubit.history[0][0], qubit.history[0][1], \
```

```

        qubit.history[0][2]
time = qubit.times
print('constructing coherence')
coherence = []
for i in range(len(xs)):
    rho = get_rho_from_bloch(xs[i], ys[i], zs[i])
    coherence.append(rho[0,1])

def func(x,a):
    return 1/2*np.exp(-x/a)
popt, pcov = curve_fit(func, time, coherence)
print(popt)
plt.plot(np.array(time), func(np.array(time),*popt), \
         label = 'fit $y=0.5e^{-x/a}$, $a=' + str(popt[0]))
plt.style.use('default')
plt.title('pure dephasing of $|+\rangle$ with \
           $T_2/T_{gate}=10^3$')
plt.xlabel('$t/T_{gate}$')
plt.ylabel('$|\rho_{01}|$')
plt.plot(time, coherence, label='simulation')
plt.legend()
plt.show()

```

So, what's new in that code?

- self.setCollectData() - Gets the two boolean parameters 'data' and 'bloch' (with default values False). 'data' controls the collection 'self.history' and 'self.purities'. 'bloch' controlles the

collection of bloch sphere figures for each qubit, 'self.blochs' and 'self.bloch3ds'.

- self.history - List of lists. Each list is of the form [xs,ys,zs] such that (xs[i],ys[i],zs[i]) is the position of the qubit's state on bloch sphere in time  $i * dt$ .
- self.purities - If the register has  $N$  qubits, then this is a list of length  $N + 1$ . the first  $N$  elements are lists such as the  $i$ 'th list contains the purity as a function of time  $dt$  of the  $i$ 'th qubit, and the last list (in place  $N + 1$ ) is the purity of the entire register as a function of time. Purity is calculated as  $Tr(\rho^2)$ .
- self.blochs - A list of QuTiP's bloch spheres, one for each qubit, with the qubit's trajectory.
- self.bloch3ds - A three dimentional version of the above.
- self.times - a list of  $dt$  times the qubit had lived through.

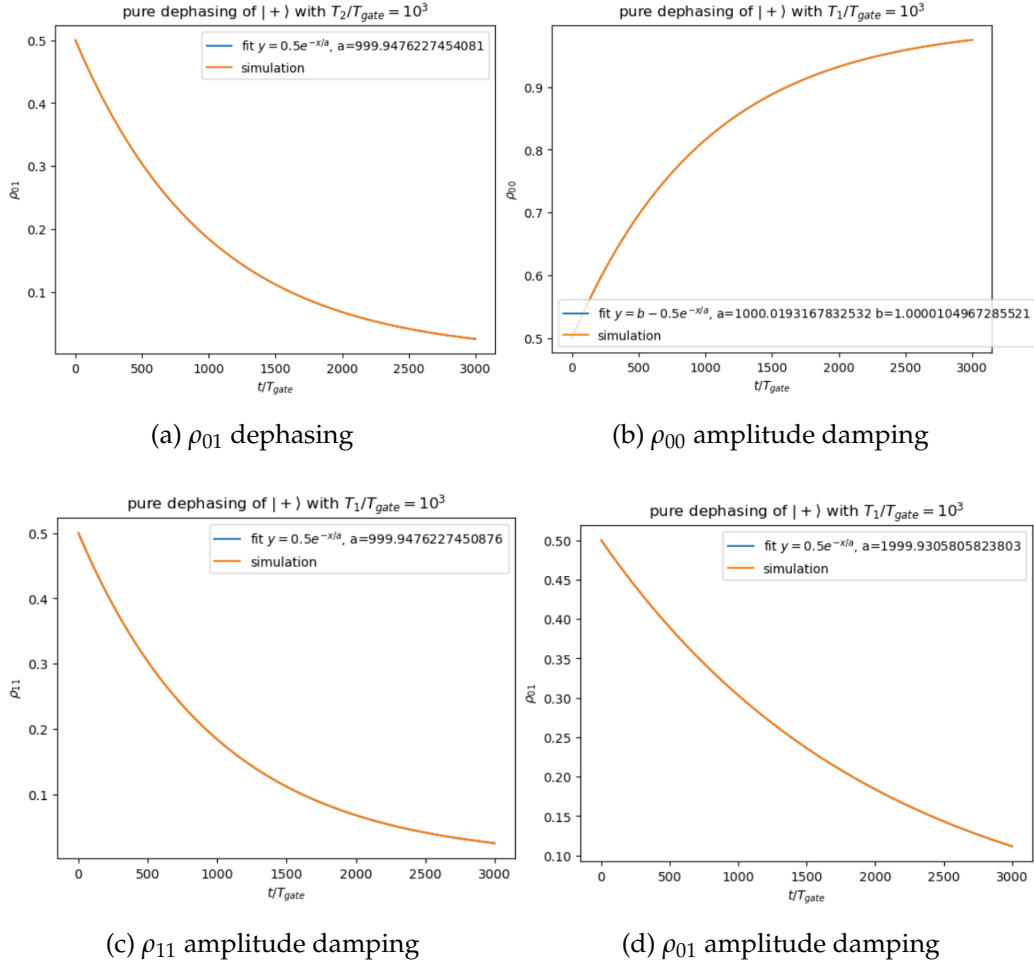


Figure A.2: Relaxation for three decoherence times. Fit and simulation are the same.

### Confirming Defined Gates

Here we show the action of all previously defined gates on one (or two) qubits, on the Bloch Sphere. One can reproduce these figures by running the code blocks similar to the one below:

```
qubit.setCollectData(data = True, bloch=False)
qubit.run([(('Rz', 0, None, np.pi / 4)])]
bloch = Bloch()
bloch.add_points([qubit.history[0][0], \
                  qubit.history[0][1], qubit.history[0][2]])
bloch.show()
```

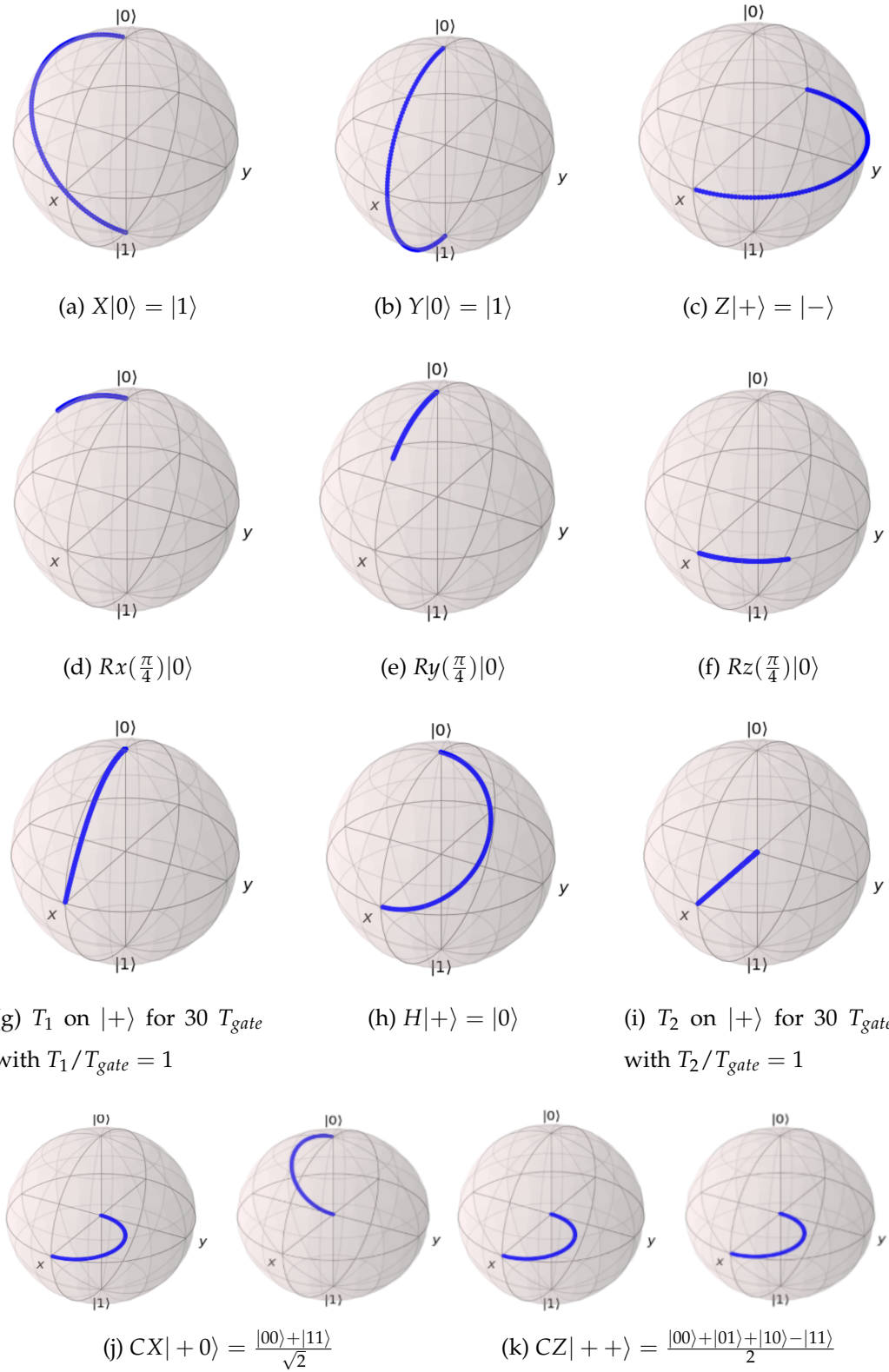


Figure A.3: All Defined Gates

# Bibliography

- [Aharonov] Aharonov, D. Fault-Tolerant Quantum Computation With Constant Error. pages 1–18.
- [2] Aharonov, Y. and Popescu, S. (2002). Measuring Energy, Estimating Hamiltonians, and the Time-Energy Uncertainty Relation. Technical report.
- [3] Ahmadi, H. and Chiang, C.-F. (2010). Quantum Phase Estimation with Arbitrary Constant-precision Phase Shift Operators.
- [4] Arrad, G., Vinkler, Y., Aharonov, D., and Retzker, A. (2013). Increasing sensing resolution with error correction.
- [5] Arvidsson-Shukur, D. R., Yunger Halpern, N., Lepage, H. V., Lasek, A. A., Barnes, C. H., and Lloyd, S. (2020). Quantum advantage in postselected metrology. *Nature Communications*, 11(1):1–7.
- [6] Atia, Y. and Aharonov, D. (2017). Fast-forwarding of Hamiltonians and exponentially precise measurements. *Nature Communications*, 8(1).
- [7] Cappellaro, P., Layden, D., Jiang, L., Zhou, S., Zhang, M., and Preskill, J. (2019). Error-corrected quantum sensing. page 51.

- [8] Chao, R. and Reichardt, B. W. (2017). Fault-tolerant quantum computation with few qubits.
- [9] Chao, R. and Reichardt, B. W. (2019). Flag fault-tolerant error correction for any stabilizer code.
- [10] Chapeau-Blondeau, F. and Belin, E. (2020). Fourier-transform quantum phase estimation with quantum phase noise. *Signal Processing*, 170(March):1–24.
- [11] Cheng, S., Cao, C., Zhang, C., Liu, Y., Hou, S.-Y., Xu, P., and Zeng, B. (2020). Simulating Noisy Quantum Circuits with Matrix Product Density Operators.
- [12] Cîrstoiu, C., Holmes, Z., Iosue, J., Cincio, L., Coles, P. J., and Sornborger, A. (2020). Variational fast forwarding for quantum simulation beyond the coherence time. *npj Quantum Information*, 6(1).
- [13] Cruz, P. M. Q., Catarina, G., and Gautier, R. (2020). Optimizing quantum phase estimation for the simulation of Hamiltonian eigenstates. pages 1–16.
- [Czarnik et al.] Czarnik, P., Arrasmith, A., Cincio, L., and Coles, P. J. Qubit-efficient exponential suppression of errors.
- [15] Degen, C. L., Reinhard, F., and Cappellaro, P. (2016). Quantum sensing.
- [16] Dennis, E., Kitaev, A., Landahl, A., and Preskill, J. (2002). Topological quantum memory. *Journal of Mathematical Physics*, 43(9):4452–4505.

- [17] Dobšíček, M., Johansson, G., Shumeiko, V., and Wendin, G. (2007). Arbitrary accuracy iterative quantum phase estimation algorithm using a single ancillary qubit: A two-qubit benchmark. *Physical Review A - Atomic, Molecular, and Optical Physics*, 76(3).
- [18] Garc, I. and Shepelyansky, D. L. (2007). Quantum phase estimation algorithm in presence of static imperfections. (Section 4).
- [19] Herrera-Martí, D. A., Gefen, T., Aharonov, D., Katz, N., and Retzker, A. (2014). Quantum Error-Correction-Enhanced Magnetometer Overcoming the Limit Imposed by Relaxation.
- [20] Ippoliti, M. and Khemani, V. (2021). Postselection-Free Entanglement Dynamics via Spacetime Duality. *Physical Review Letters*, 126(6):60501.
- [Kais] Kais, S. A Universal Quantum Circuit Scheme For Finding Complex Eigenvalues.
- [22] Kandala, A., Wei, K. X., Srinivasan, S., Magesan, E., Carnevale, S., Keefe, G. A., Klaus, D., Dial, O., and McKay, D. C. (2020). Demonstration of a High-Fidelity CNOT for Fixed-Frequency Transmons with Engineered ZZ Suppression.
- [23] Kapourniotis, T. and Datta, A. (2019). Fault-tolerant quantum metrology. *Physical Review A*, 100(2).
- [24] Khatri, S., LaRose, R., Poremba, A., Cincio, L., Sornborger, A. T., and Coles, P. J. (2018). Quantum-assisted quantum compiling.
- [25] Kitaev, A. Y. (1995). Quantum measurements and the Abelian Stabilizer Problem. pages 1–22.

- [26] Koch, J., Yu, T. M., Gambetta, J., Houck, A. A., Schuster, D. I., Majer, J., Blais, A., Devoret, M. H., Girvin, S. M., and Schoelkopf, R. J. (2007). Charge-insensitive qubit design derived from the Cooper pair box. *Physical Review A - Atomic, Molecular, and Optical Physics*, 76(4):1–21.
  - [27] Krantz, P., Kjaergaard, M., Yan, F., Orlando, T. P., Gustavsson, S., and Oliver, W. D. (2019). A quantum engineer’s guide to superconducting qubits. *Applied Physics Reviews*, 6(2):1–66.
  - [28] Layden, D. and Cappellaro, P. (2018). Spatial noise filtering through error correction for quantum sensing. *npj Quantum Information*, 4(1).
  - [29] Ma, Z., Gokhale, P., Zheng, T.-X., Zhou, S., Yu, X., Jiang, L., Maurer, P., and Chong, F. T. (2020). Adaptive Circuit Learning for Quantum Metrology.
  - [30] Meyer, J. J. (2021). Fisher Information in Noisy Intermediate-Scale Quantum Applications.
  - [31] Nielsen, M. A. and Chuang, I. L. (2010). *Quantum computation and quantum information*. Cambridge University Press.
  - [32] O’Brien, T. E., Tarasinski, B., and Terhal, B. M. (2018). Quantum phase estimation of multiple eigenvalues for small-scale (noisy) experiments.
- [Piveteau et al.] Piveteau, C., Sutter, D., Bravyi, S., Gambetta, J. M., and Temme, K. Error mitigation for universal gates on encoded qubits. pages 1–15.

- [34] Preskill, J. (2018). Lecture Notes for Ph219 / CS219 : Quantum Information Chapter 3. (October).
- [35] Reichardt, B. W. (2018). Fault-tolerant quantum error correction for Steane's seven-qubit color code with few or no extra qubits.
- [36] Reiter, F., Sørensen, A. S., Zoller, P., and Muschik, C. A. (2017). Dissipative quantum error correction and application to quantum sensing with trapped ions. *Nature Communications*, 8(1).
- [Santagati et al.] Santagati, R., Wang, J., Gentile, A. A., Paesani, S., Wiebe, N., McClean, J. R., Shadbolt, P. J., Bonneau, D., Silverstone, J. W., Tew, D. P., Zhou, X., and Thompson, M. G. Witnessing eigenstates for quantum simulation of Hamiltonian spectra.
- [38] Steck, D. A. (2012). Quantum and Atom Optics, Lecture Notes. page 843.
- [39] Takita, M., Inoue, K., Lekuch, S., Minev, Z. K., Chow, J. M., and Gambetta, J. M. (2021). Exploiting dynamic quantum circuits in a quantum algorithm with superconducting qubits.
- [Tansuwannont et al.] Tansuwannont, T., Chamberland, C., and Leung, D. Flag fault-tolerant error correction, measurement, and quantum computation for cyclic CSS codes. Technical report.
- [41] Temme, K., Bravyi, S., and Gambetta, J. M. (2017). Error Mitigation for Short-Depth Quantum Circuits. *Physical Review Letters*, 119(18):1–5.
- [Unden et al.] Unden, T., Balasubramanian, P., Louzon, D., Vinkler, Y., Plenio, M. B., Markham, M., Twitchen, D., Lovchinsky, I.,

- Sushkov, A. O., Lukin, M. D., Retzker, A., Naydenov, B., McGuinness, L. P., and Jelezko, F. Quantum metrology enhanced by repetitive quantum error correction. Technical report.
- [43] Vool, U. and Devoret, M. (2017). Introduction to quantum electromagnetic circuits. *International Journal of Circuit Theory and Applications*, 45(7):897–934.
- [44] Yoder, T. J., Takagi, R., and Chuang, I. L. (2016). Universal fault-tolerant gates on concatenated stabilizer codes. *Physical Review X*, 6(3).
- [45] Yu, A. and Chernyavskiy, A. Y. (2021). Proceedings of spie. (March 2019).
- [46] Zeng, B., Cross, A., and Chuang, I. L. (2011). Transversality versus universality for additive quantum codes. *IEEE Transactions on Information Theory*, 57(9):6272–6284.
- [47] Zhou, S., Zhang, M., Preskill, J., and Jiang, L. (2018). Achieving the Heisenberg limit in quantum metrology using quantum error correction.
- [48] Zhou, S., Zou, C. L., and Jiang, L. (2020). Saturating the quantum Cramér-Rao bound using LOCC. *Quantum Science and Technology*, 5(2):36–38.